Adaptive Manual Control

Detection of Human Adaptation to Sudden Changes in Controlled Element Dynamics

Master of Science Thesis Report

Nora Jakimovska

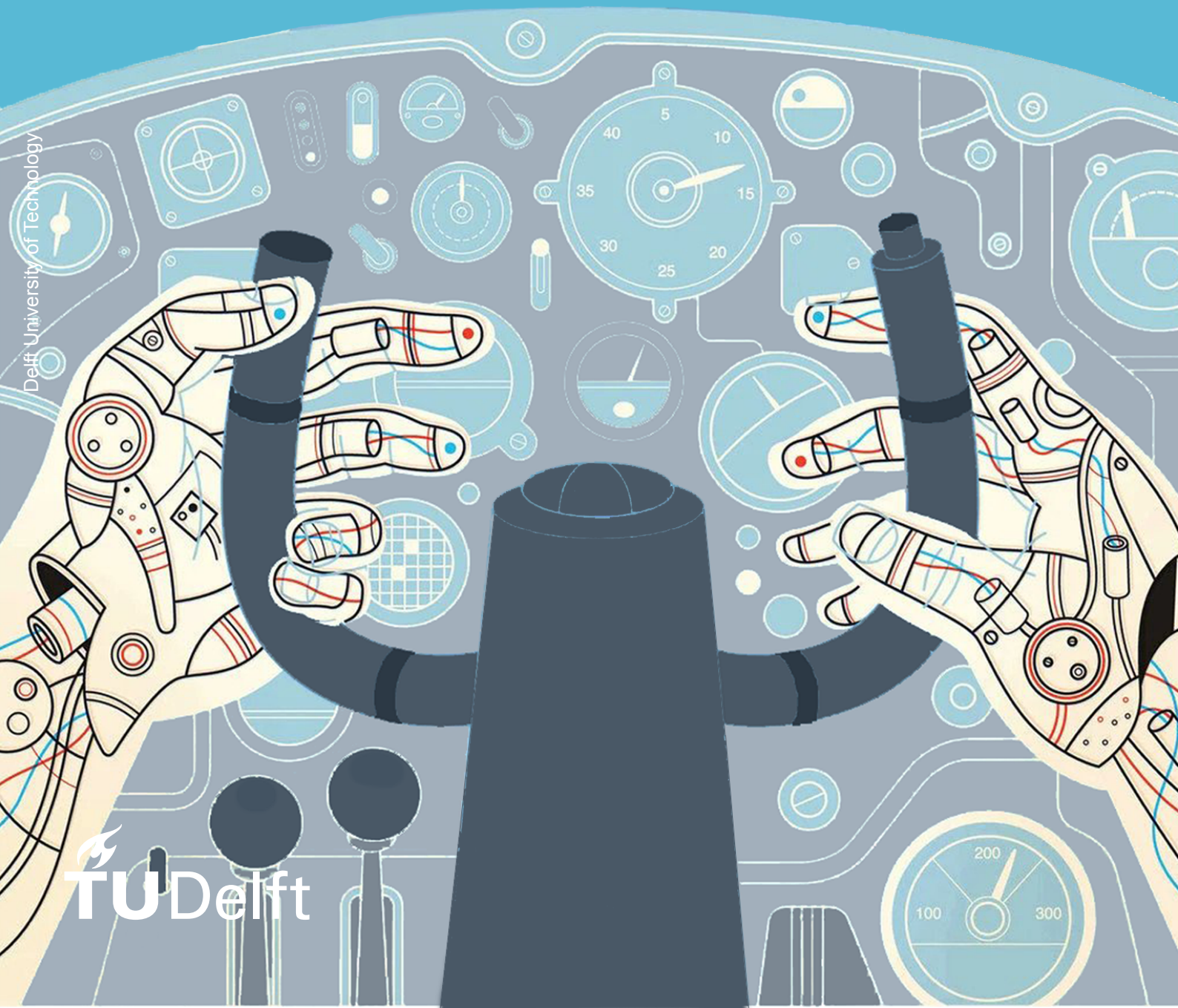

Delft University of Technology

TU Delft

Adaptive Manual Control

Detection of Human Adaptation to Sudden Changes in Controlled Element Dynamics

MSc Thesis

Nora Jakimovska

to obtain the degree of Master of Science
Faculty of Aerospace Engineering - Delft University of Technology

Supervisors:	Prof. Dr Ir. M. Mulder
	Dr ir M.M. van Paassen
	Dr. ir. D.M. Pool
Institution:	Delft University of Technology
Place:	Faculty of Aerospace Engineering, Delft

July 11, 2022

Cover Image: Adapted from Planes Without Pilots
by Harry Campbell
(https://www.nytimes.com/2015/04/07/science/planes-without-pilots.html)

TU Delft

Preface

This thesis project marks the end of my studies at TU Delft. I am grateful to have had this opportunity as it has been the most memorable experience of my life.

I would like to thank my supervisors Daan, Max and Rene for their guidance, feedback and quality support during the whole thesis project. It is remarkable how much time you invest in all your students, I am really grateful for that. I have learned a lot from all of you, and I feel privileged to have been supervised by you.

I also want to thank my mother and sister, for their unconditional love and support through all these years. Especially my mother who has encouraged me to strive for my ambitions in life, regardless of whether that was to be a professional tennis player or an aerospace engineer. Everything I have achieved is thanks to you and your sacrifices.

Lastly, I would like to thank my boyfriend, Jorge, for his love and support. You have always been by my side, and without you I would not been able to accomplish what I have so far. You encouraged me to become a better person and to not give up in difficult moments. Seven years ago, we started our studies together and now we are both closing this chapter together. Honestly, I could not have asked for a better person to spend these years with and I cannot wait to see what the next chapter of our lives holds.

Nora Jakimovska
Delft, July 2022

Contents

List of Figures

List of Tables

Nomenclature

Symbols

	Description	Unit
A_t	Amplitude of the tth sine of the forcing function	[rad]
C	Target forcing function signal	[rad]
e	Error	[rad]/[deg]
$\dot{e}/\frac{de}{dt}$	Error rate	[-/sec]
f_t	Target forcing function signal	[rad]
G	Maximum rate of change	[sec^{-1}]
G_{nm}	Neuromuscular dynamics	[-]
j	Imaginary number	[-]
K_p	Position gain	[-]
K_r	Rate gain	[-]
M	Output of vehicle or maximum rate of change	[-]
$\dot{M}$	Output rate of vehicle	[-/sec]
T_I	Pilot lag time constant	[sec]
T_L	Pilot lead time constant	[sec]
T_m	Measurement time	[sec]
t	Time	[sec]
t_c	Time of change in CE dynamics	[sec]
t_s	Small time value	[sec]
u	Control output	[rad]
u_e	Model control output	[rad]
u_m	Human operator control output	[rad]
Y_c	Controlled dynamics transfer function	[-]
Y_{OL}	Pilot–vehicle open-loop response	[-]
Y_p	Human operator transfer function	[-]
Δ	Change/ Difference	[-]
Δ_ϵ	Discrepancy	[-/s]
δ_{human}	Human operator control output	[rad]
δ_{model}	Model control output	[rad]
ζ	Neuromuscular damping ratio	[-]
σ	Standard deviation	[-]
τ_e	Human operator time delay	[sec]
Θ	Parameter estimation vector	[-]
ϕ_m	Phase margin	[rad/s]
ϕ_t	Phase of the tth sine of the forcing function	[rad]
ω	Frequency	[rad]
ω_b	Time-varying pole of the controlled element	[sec^{-1}]
ω_c	Crossover frequency	[rad]
ω_{nms}	Neuromuscular frequency	[rad]
ω_t	Frequency of the tth sine of the forcing function	[rad]

Abbreviations

APC Aircraft-pilot coupling

CNS Central Nervous System

CE Controlled Element

HC Human controller

HO Human operator

LOC Loss of control

OCM Optimal Control Model

PIO Pilot-induced oscillations

PVS Pilot-vehicle system

RMS Root mean square

VAR Variance Accounted For

Part I

Scientific Article

Modeling Human Adaptive Behaviour for a Pursuit Tracking Task

Author: N. Jakimovska
Supervisors: M. Mulder, M.M. van Paassen and D.M. Pool
Control and Simulation Section, Faculty of Aerospace Engineering
Delft University of Technology, The Netherlands

***Abstract*—In aviation, loss of control incidents are one of the most significant contributors to fatal accidents. To investigate these events, it is important to understand the pilot's control behavior in response to sudden changes in the vehicle dynamics. A previously proposed model, which predicts human adaptive behaviour in pursuit tracking tasks, was replicated. However, this model has not been validated using experimental data and it does not incorporate an inherent human time-delay. To improve the framework of the model and determine its validity for the prediction of time-varying human control behaviour, data from a previous experiment was used. The experiment involved a tracking task with a transition in controlled system dynamics from a single to a double integrator and vice-versa. The model relies on a triggering function, which compares the tracking performance to a nominal state. When triggered, control behaviour is adjusted through adaptive rules, which determine new gain settings for the model. Experimental data from steady-state system tracking was used to parameterize the model, where the human operator gains were estimated for each participant. Investigation into the steady-state system allowed for improvement of the adaptive logic in the model. The results for single to double integrator transitions, showed that the model can capture the transient control behaviour of participants. However, the adaptive logic of the model only triggers for participants that can follow the target signal with crossover frequency larger than 0.9 rad/s in the pre-transition phase. The model was not able to capture the change in control behaviour for transitions from double to single integrator; where the adaptive logic was not triggered due to transitioning to a more easily controlled system. Further investigation is required on whether the triggering mechanism can be improved, enabling more accurate prediction of the human adaptive behaviour. This project resulted in a more representative model of the human adaptive behaviour; validated using experimental data.**

NOMENCLATURE

A_n	Amplitude of the nth sine of the forcing function [rad]
C	Target forcing function signal [rad]
e	Pitch attitude error signal [rad]
f_t	Target forcing function signal [rad]
G	Maximum rate of change [s^{-1}]
G_{nm}(s)	Neuromuscular dynamics transfer function [-]
$H(s)$	Transfer function of second-order low-pass filter on x signal [-]
$H_c(s)$	Controlled dynamics transfer function [-]
H_{del}(s)	Human operator delay transfer function [-]
$J(s)$	Transfer function of second-order low-pass filter on adaptive gains [-]
K	Number of samples [-]
K_{a_p}	Adaptation constant for K_p gain [-]
K_{a_r}	Adaptation constant for K_r gain [-]
k_c(t)	Time varying gain of the controlled element [-]
K_p	Outer-loop position gain [-]
$K_{trigger}$	Triggering logic of model [-]
K_r	Inner-loop rate gain [-]
M	Output of system [rad] or maximum rate of change [s]
$\dot{M}$	Output rate of system [-/s]
N	Number of tracking axis [-]
n	Sinusoid index [-]
R	Input of outer-loop signal
rms	Root Mean Square [-]
t	Time [s]
t_c	Time of change in controlled element [s]
T_m	Measurement time [s]
T_r	Reaction time [s]
t_s	Small time value [s]
u	Human operator control output signal [rad]
u_h	Measured control output [rad]
u_m	Model control output [rad]
VAF	Variance accounted for [%]
x	Signal proportional to error-rate [rad^2]
X_n	Signal representing strength of adaptation [-]
Y_c	Controlled dynamics transfer function [-]
Y_p	Human operator transfer function [-]
ΔK_p	Change of outer-loop gain K_p [-]
ΔK_r	Change of inner-loop gain K_r [-]
ζ_{lp}	Low-pass filter damping ratio [-]
ζ_{nm}	Neuromuscular damping ratio [-]
Θ	Parameter vector [-]
τ_e	Effective time-delay [s]
ϕ_m	Phase margin [deg]
ϕ_t	Phase of the tth sine of the forcing function [rad]
$\omega_b(t)$	Time-varying pole of the controlled element [-]
ω_c	Crossover frequency [rad/s]
ω_{lp}	Low-pass filter frequency [rad/s]
ω_m	Fundamental measurement frequency [rad/s]
ω_n	Frequency of the nth sine of the forcing function [rad/s]
ω_{nm}	Neuromuscular frequency [rad/s]

I. Introduction

In order to improve our understanding of the human adaptive behaviour, it is of importance to investigate time-varying systems. One such instance of time-varying systems are Loss of control (LOC) incidents; one of the most significant contributors to fatal accidents [1]. Humans have unique adaptive behavior abilities which allows them to lessen the effect of these incidents thereby becoming essential elements of many control systems [2]. In fact, the human capability to quickly detect failures and adapt is one of the main reasons that vehicles are not fully autonomous [3] [4]. In order to investigate these events, it is important to understand human control behaviour in response to sudden changes in vehicle dynamics. Modeling human's adaptive behaviour can not only improve automation, but may improve training procedures and in turn increase safety in aviation.

Throughout the years research has been conducted in the field of manual control, helping us to understand and describe how humans control vehicles through the use of mathematical models [5]. An example of such models is the crossover model, developed by McRuer and Jex, which has served as the basis for understanding human control behaviour [6]. The limitation of this model is that it can only describe human control behaviour in controlling steady-state systems.

Furthermore, current state-of-the art cybernetics theory is restricted to compensatory feedback control, limiting the human to react on only the statistical characteristics of the error [5]. However, in order to study the adaptive human behaviour, more efforts are needed to model the human response using more realistic displays, such as pursuit and preview [7]. A consensus on a mathematical model which captures human behaviour in a pursuit tracking task has not been reached.

In the past, some research has been carried out focusing on creating qualitative and quantitative mathematical models, which make a *prediction* on how the human pilot would adapt to changes in the vehicle dynamics [8] [9] [10] [11]. This is contrary to other models which are used for *identification* of human time-varying dynamics from measured data.

One of the first reported experiments on the adaptive human behaviour was performed by Young *et al.* in 1964 [12]. In this experiment, adaptive human behaviour was investigated following sudden changes in the Controlled Element (CE) dynamics for a compensatory tracking task. They concluded that the adaptation process should be considered in three phases. The first phase, *detection*, is where the operator recognizes a change in the CE dynamics. During the second phase, *identification*, the operator identifies the nature of the change to determine a new control strategy. Lastly, in the third phase, *modification*, the operator adjusts their dynamics to the new CE dynamics.

Furthermore, many mathematical models of adaptive human behaviour are based on the idea that the humans have a reference model of the controlled system, known as an internal model. This enables humans to detect when a change in the controlled system has occurred from off-nominal tracking errors and error rates for a compensatory tracking task, and output rates for a pursuit tracking task. Detection triggers the human operator to adjust their control strategy to more appropriate settings for the new CE dynamics.

One promising model of the adaptive human operator for a pursuit tracking task was developed by Ronald Hess [13] [14] [11]. This model is rule-based and the adaptive logic was heuristically developed. It is one of the latest models developed in the field of manual control; with it having several advantages over other models. For instance, incorporating the phases of adaptation [13] and implementing multi-axis tracking [11], making it more versatile relative to the other models. However, a limitation of this model is that the inherent human time-delay is not present. Additionally, until now, the model has not been verified with experiment data.

The aim of this research is to improve the framework of Hess' model, and validate it using experimental data. This was accomplished by initially replicating the original model. Then, the model was extended to include a fixed time-delay. Additionally, the model was simplified by removing a superfluous filter and a limiter. As the original model was empirically developed and ad-hoc in nature, an analysis of the key model parameters in the adaptive logic was required. The model was tuned to cope with the steady-state cases, which included a sensitivity analysis on how changes in the human operator gains lead to changes in performance and control activity. This allowed for modifications to be made to the adaptive rules used for changing the human operator gains in the time-varying cases. An additional sensitivity analysis was carried out to investigate the changes in the relevant key model parameters of the modified model. Lastly, experimental data were used from a previous experiment to determine the validity of the modified model for prediction of time-varying human control adaptations. This was done by calculating the quality-of-fit between the experimental data and model output.

The structure of this paper is as follows: Section II presents a detailed description of the modified Hess model and how it compares to the original model. Additionally, it provides the results from replicating the original model; this was done in order to get a better understanding of the model pre-modification. In Section III, the set-up of the experiment is detailed and the steps used to analyse the modified model are presented. In Section IV the steady-state analysis is conducted, providing more insight on how the model behaves in time-varying conditions. The sensitivity analysis of the modified model is presented in Section V, where the key model parameters are determined. The results of the modified model validation are presented in Section VI. Following that, the discussion of the results is given in Section VII. Lastly, the conclusions are provided in Section VIII.

II. Hess adaptive pilot model

Section II-A describes the original model and how it differs from the modified model used in this paper and and the reasoning behind these modifications. Section II-B shows the results from replicating the original model as described in [11]. This allows for better understanding of the model and a verification that the original model was correctly implemented.

A. Description of Modified Hess adaptive pilot model

Figure 1 shows the structure of the model, composed of three main parts, the *human operator*, the *controlled dynamics* (Y_c) and the *adaptive logic*. One limitation of the model is that it does not have a remnant, which is supposed to account for control non-linearities and noise [6]. In Figure 1, the block which is added to the model is displayed in red, while dashed-outline block is removed in the modified model.

1) Human Operator: There are several blocks which make up the model of the *human operator*. These blocks include the gains of the controller, K_p and K_r, which are the outer-loop and inner-loop gains, respectively. The gain K_p controls the position, while the inner-loop gain K_r controls the rate. Therefore, K_p influences how large the human control output is, while K_r influences the magnitude of its rate of change. Additionally, the human operator's neuromuscular system, representing the human operator's limb and the interaction with the manipulator, is given by:

$$G_{nm}(s) = \frac{\omega_{nm}^2}{s^2 + 2\zeta_{nm}\omega_{nm}s + \omega_{nm}^2}, \tag{1}$$

where ω_{nm} = 10 rad/s and ζ_{nm} = 0.707 [-] [11].

Furthermore, in the original model described by Hess, the use of a time-delay was omitted, with the reasoning not reported [11]. As time delays are inherent to human behaviour, it was decided to include it in the model, as evident through the H_{del} block shown in red in Figure 1. The time delay is represented using $H_{del}(s) = e^{-\tau_e s}$. In order to understand the effects of introducing time delay in the model, a sensitivity analysis was performed, described in Section V. In this model, the neuromuscular system uses constant values not only over time, but also for all human operators. While this is a limitation, previous studies have shown that neuromuscular frequency and damping can be considered as constant parameters in the time-varying human model [15]. The effective time-delay τ_e is also taken as a constant. This constrains the model, as each human is different and controls differently, especially when controlling various system dynamics.

2) Controlled Dynamics: The limiter element represents the physical limits in the actuator of the control stick. Hess argues that this makes the model more realistic. However, in the design of simulations and experiments it should be taken into account that this limit is not reached, thus the limiter is not used in the modified model. The controlled element dynamics is represented by the block $Y_c s$ and gives the output rate $\dot{M}$. Then, an integrator is used to get the output of the model M.

3) Adaptive Logic: The adaptation of the human operator is represented through the *Adaptive Logic* which is divided into two sequential steps, namely: Triggering and Adaptation.

The first step, Triggering, is when the human operator detects that a change in the controlled element dynamics has occurred. For this, Hess' model assumes that the human operator perceives a signal proportional to the error-rate using the output rate $\dot{M}$. In mathematical terms, this is denoted as signal x which is based on the sign and magnitude of the error signal in the inner-loop and is calculated using:

$$x(t) = \text{sgn}\{|R| - |\dot{M}|\} \cdot [|R| - |\dot{M}|]^2 \tag{2}$$

Then, the x signal is filtered using a second-order low-pass filter which introduces smoothing and lag in the human adaptation process. In the frequency domain it is defined as:

$$X_{filtered}(s) = X(s) \cdot H(s), \tag{3}$$

where the filter is given by:

$$H(s) = \frac{\omega_{lp}^2}{s^2 + 2\zeta_{lp}\omega_{lp}s + \omega_{lp}^2} \tag{4}$$

In the original model provided by Hess [11], ζ_{lp} = 1 [-] and ω_{lp} = 1.5 rad/s. In this paper, the influence of this filter and its parameters, are determined through a sensitivity analysis as detailed in Section V.

Adaptation only occurs if the trigger logic is activated, which is determined through the following logical function:

$$K_{trigger} = \begin{cases} 1 & \text{if } \sqrt{|x|} \geq 3 \cdot \text{rms}[\sqrt{|x|}] \\ 0 & \text{else} \end{cases} \tag{5}$$

In this equation, the square root of x, ($\sqrt{|x|}$), is used because the square of the inner-loop error signal is used to obtain x as evident from Equation (2). Moreover, the expression $3 \cdot \text{rms}[\sqrt{|x|}]$ represents the acceptability limit, which is what the human operator accepts as a nominal state. The factor of 3 defines the lower limit of a trigger; the threshold for which changes in the system are significant enough, which alerts the human operator that the control behaviour must be adjusted. Here, the root mean square (rms) was calculated using:

$$\text{rms}(x(t)) = \sqrt{\frac{1}{T}\int_0^T (x(t))^2 \, dt}, \tag{6}$$

where T is the measurement window.

This is a simplified function compared to the one used in the original model. The original model required knowledge of the time at which the CE dynamics transition, such that the triggering function would not be activated before this time. This was deemed unnecessary, as false positives also occur in real-life, thereby making the model more realistic. Additionally, the original model used a small time value, such that transients in the initial part of simulation do not incorrectly trigger the mechanism. In the simulation of the modified model, a run-in time was used, making this small time value redundant.

If the adaptive logic is triggered ($K_{trigger}$ = 1), then new appropriate gains K_p and K_r are determined in the Adaptation step.

Inner Loop

As proposed by Hess [11], the adaptive change of the inner-loop gain K_r is determined initially. In [11] the following equation is used:

$$\Delta K_r = X_n(t) \cdot K_{\text{trigger}}\,(t) \tag{7}$$

Additionally, ΔK_r is filtered using a second-order low-pass filter. In the frequency domain, this is given by:

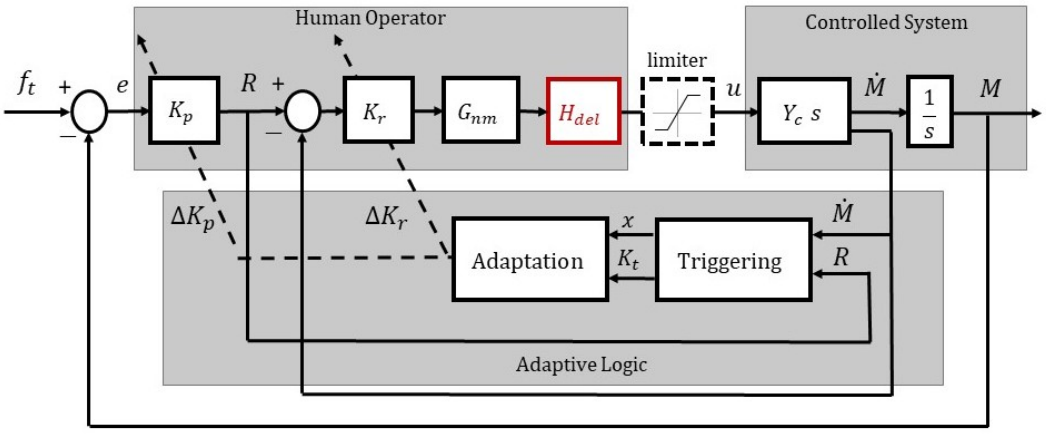

Fig. 1. The structure of Hess adaptive pilot model, with the three main parts; Human operator, Controlled Dynamics and Adaptive Logic. In the first step of the Adaptive Logic, Triggering, the signals $\dot{M}$ and R are used as inputs to obtain the x(t) signal as well as the output of the trigger function $K_{trigger}$. These are then used in the second step, Adaptation, to determine more appropriate gains depending on if $K_{trigger}$ is activated.

$$J(s) = \frac{\omega_{lp}^2}{s^2 + 2\zeta_{lp}\omega_{lp}s + \omega_{lp}^2} \tag{8}$$

Equation (7) is only activated for the duration of $K_{trigger}$ = 1, where the strength of adaptation is determined, see Figure 2. Here, the X_n variable is defined as follows:

$$X_n(t) = \frac{x(t)}{\text{rms}\left[R^2(t)\right]} \cdot \frac{1}{N} \tag{9}$$

Then, X_n is filtered using Equation (8). Note that Equation (7) and Equation (9) both use a second-order low-pass filter $J(s)$, where the ω_{lp} = 1 rad/s and ζ_{lp} = 1 [11].

In Equation (9) the x signal is normalized using rms(R^2) to ensure that adaptation is not dependent on the numerical magnitude of the signals (e.g., changing the forcing function f_t). The rms value of R^2 is chosen because it is used in the calculation of the x signal. rms(R^2) is used as a constant in the time-varying system, and is calculated from the steady-state system. The variable N represents the number of axes that are controlled by the human operator [11]. This variable results in a less aggressive control behaviour by the human operator when controlling multi-axis task relative to single-axis. In this paper, only a single-axis is considered, so N = 1.

In the modified model, these two equations were slightly adjusted to the following:

$$\Delta K_r = X_n(t) \cdot K_{a_r} \cdot K_{trigger}(t) \tag{10}$$

$$X_n(t) = \frac{x(t)}{\text{rms}\left[R^2(t)\right]} \tag{11}$$

The X_n signal is not filtered using $J(s)$, as this filter was superfluous since the x signal is already filtered using $H(s)$. Additionally, the filter $J(s)$ on ΔK_r influences how fast the adaptive gains transition. Therefore, a sensitivity analysis is carried out in Section V, to determine its effects on adaptation and whether the filter is necessary. Lastly, an adaptation constant, K_{a_r}, is introduced in the model which scales the strength of adaptation to prevent overreaction. This value is determined through a sensitivity analysis in Section V.

An example of how the adaptive mechanism works is shown in Figure 2 where X_n, $K_{trigger}$ and ΔK_r are displayed. When the gain adjustment is successful, the Triggering is no longer activated, and the gain is kept at that setting. The length of the $K_{trigger}$ determines the transient; where the length of the trigger is dependent on the time needed for the appropriate gain settings to be found.

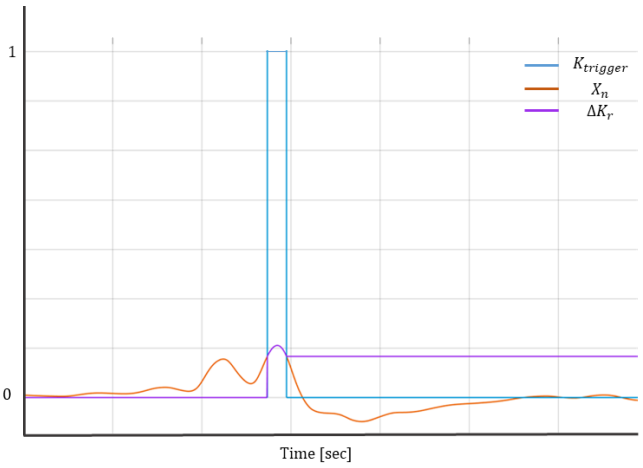

Fig. 2. An example of the adaptive mechanism showing how the gain Kr adapts when Triggering is activated ($K_{trigger}$ = 1)

Outer Loop

In the original model, the change of the outer-loop gain K_p is calculated using the following equation:

$$\Delta K_p = \begin{cases} 0.35 \cdot \Delta K_r & \text{if } \Delta K_r > 0 \\ 0 & \text{if } \Delta K_r \leq 0 \end{cases} \tag{12}$$

The first part of this equation indicates that ΔK_p must be proportional to ΔK_r following a ratio of 0.35. The second part of this equation indicates that ΔK_p does not change when

ΔK_r can decrease below its initial value. In Section IV it was found that these rules are contrary to the expected change of gains. Therefore, the rule for ΔK_p was also modified and is given by:

$$\Delta K_p = \Delta K_r \cdot K_{a_p} \tag{13}$$

Here ΔK_p is always proportional to ΔK_r as well as an adaptation constant K_{a_p} discussed in Section V.

In the original model, constraints are placed on the K_p and K_r gains. $K_{p_{initial}}$ and $K_{r_{initial}}$ represent the initial values of K_p and K_r which are chosen for the pre-transition system dynamics [11].

$$\begin{aligned} |K_p|_{\max} &= 2\,|K_{p_{initial}}| \\ |K_r|_{\max} &= 10\,|K_{r_{initial}}| \end{aligned} \tag{14}$$

In Section IV it is shown that these constraints are not applicable to the tracking task and data-sets used in this paper, thus not used. Additionally, the constants used in these constraints do not necessarily represent the physical limitations of the human operator, with the reasoning behind these specific values not reported in [11].

As proposed by Hess [11], the adapted gains are calculated as follows:

$$\begin{aligned} K_{r_{\text{final}}} &= K_{r_{\text{initial}}} + \Delta K_r \\ K_{p_{\text{final}}} &= K_{p_{\text{initial}}} + \Delta K_p \end{aligned} \tag{15}$$

where the initial gains ($K_{initial}$) are determined in the steady-state system through parameter estimation described in Section IV.

B. Replicated Hess Original Model

In order to get a better understanding of modeling the human adaptive behaviour and the applicability of Hess' model, the original Hess model was first replicated. This was done based on the description provided in [11]. A simulation was carried out for a single-axis pitch control task, for a total of 120 s, with a change in the CE dynamics occurring at 50 s. Initially, the CE dynamics represented a nominal system $Y_{c,1}(s)$; at 50 s a more challenging dynamics $Y_{c,2}(s)$ was introduced, representing a failed system, as shown in Equation (16).

$$Y_{c,1}(s) = \frac{1}{s(s+10)} \qquad Y_{c,2}(s) = \frac{e^{-0.2s}}{s(s+5)(s+10)} \tag{16}$$

Figure 3 shows the tracking performance from Hess' [11] (a) and the replicated (b) results. Figure 4 shows the human operator gains K_r and K_p adapting to the new CE dynamics for Hess' results (a) and the replicated model's (b). Comparison of the replicated model to the original model showed that the steady-state post-failure values of the adaptive gains (K_p and K_r) are slightly lower than the results published in [11]. The difference in gain adaptations is relatively small, where K_r differs by 1.2 and K_p by 0.7. However, this does affect the post-failure tracking accuracy, which can be observed from Figure 3. Another noticeable difference is the dip in the gain K_r response directly after failure, evident in Figure 4 (a), while in the replicated model K_r has a steady increase without the dip. These small differences in results could stem from several factors, such as differences in solvers and algorithms. Nonetheless, the results from the replicated model are overall very close to the published results and both models capture the essence of the adaptive human behaviour.

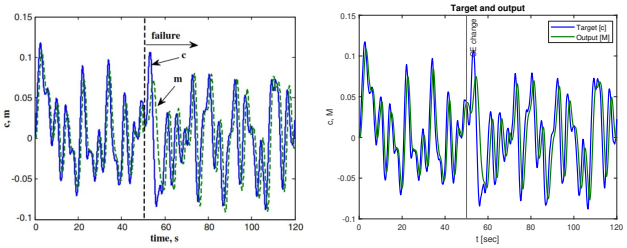

(a) Published (b) Replicated

Fig. 3. Pitch attitude tracking performance Hess' original model [11] (a) and replicated model (b)

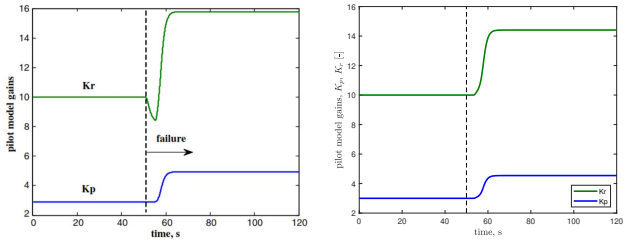

(a) Published (b) Replicated

Fig. 4. Pilot model gain adaptation Hess' original model [11] (a) and replicated model (b)

This section focused on the tracking task described by Hess in [11], however, the rest of the paper focuses on the tracking task and data-sets from [16]. This is described in the following section, Section III.

III. Method

A. Experiment Data

The independent variables and the results of the experimental data used in the model are obtained from a previous human-in-the-loop experiment, performed at the section of Control and Simulation at TU Delft [16]. A description of this previous experiment is included here.

1) Control Task: The control task considered in this paper is a pitch attitude pursuit task as shown in Figure 5. This human-in-the-loop experiment was similar to time-varying compensatory control tasks performed in earlier experimental research [17] [15].

2) Controlled Dynamics: The CE dynamics are given by the time-varying transfer function:

$$H_c(s,t) = \frac{k_c(t)}{s\,(s+\omega_b(t))}, \tag{17}$$

where k_c represents the time-varying gain, and ω_b the time-varying break frequency. These time-varying parameters are

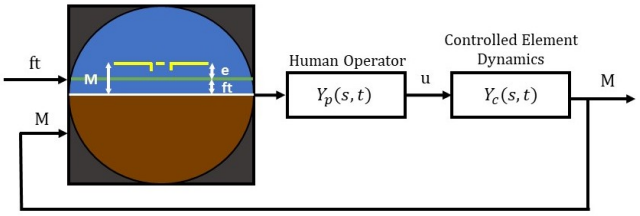

Fig. 5. Control Task Block Diagram

implemented using the following sigmoid function as a function of time t:

$$P(t) = P_1 + \frac{P_2 - P_1}{1 + e^{(-G(t-M))}} \tag{18}$$

In Equation (18), the transition from an initial parameter value to a final parameter value is described, where P_1 and P_2 represent the initial and final values of the parameters K_c or ω_b. The value of G controls the speed of adaptation, which is kept at a constant value of 100 s^{-1} simulating step-like (instantaneous) changes [15]. Lastly, the parameter M represents the moment of maximum rate of change. This value was set to $M = \frac{T_m}{3}$, where $T_m = 90s$ and represents the experiment's measurement time.

Four conditions were tested in the experiment; two of which were steady-state cases representing an approximate single integrator (DYN 1) or an approximate double integrator (DYN 2). The remaining two conditions represent time-varying simulations where the CE dynamics transitioned from the single integrator to the double integrator (DYN 12), and from the double integrator to the single integrator (DYN 21). For each condition, the CE parameters are shown in Table I.

In the experiment of [16], the time-varying tracking runs included two controlled element dynamic transitions, where $M_1 = \frac{T_m}{3}$ and $M_2 = \frac{2T_m}{3}$ which represented the times at which the CE dynamics transitioned. This means that the time-varying runs switched from a signal integrator to a double integrator and then again to a single integrator (DYN 121) and vice-versa (DYN 212). However, in this paper the second transition $M_2 = \frac{2T_m}{3}$ was disregarded.

TABLE I
TIME-VARYING CONTROLLED DYNAMICS

DYN	k_{c1} [-]	k_{c2} [-]	ω_{b1} [rad/s]	ω_{b2} [rad/s]	G [s^{-1}]	M [s]
1	90	90	6.0	6.0	-	-
2	30	30	0.2	0.2	-	-
12	90	30	6.0	0.2	100	M_1
21	30	90	0.2	6.0	100	M_1

3) Forcing Function: The forcing function f_t used in the experiment is defined by:

$$f_t(t) = \sum_{n=1}^{N_t} A_t[n] \sin\left(\omega_t[n]t + \phi_t[n]\right) \tag{19}$$

In this equation, $A_t[n]$, $\omega_t[n]$, and $\phi_t[n]$ represent the amplitude, frequency, and phase shift of the n_{th} sine wave. N_t is the number of sine waves, which in the experiment was ten. The frequencies, ω_t, are integer multiples n of the fundamental measurement frequency $\omega_m = \frac{2\pi}{T_m}$, this is done in order to avoid spectral leakage [18].

While the total measurement time in the experimental set-up is $T_m = 90$ s, the signal is chosen to be periodic with three phases, meaning that the period is equal to $P = \frac{T_m}{3}$, resulting in a forcing function period of 30 s. The advantage of having a periodic signal is that the time traces can be directly compared across the three periods, and periodicity preserves the task difficulty; meaning that the pilot is exposed to the same signal when transitioning from one set of dynamics to the other. Additionally, a large run-in time of 110 s was used. This was done in order to achieve steady-state values of the rms($\sqrt{|x|}$), a key parameter in the model's adaptive logic, as discussed in Section II.

The values for the forcing function's parameters used in the experimental set-up are listed in Table II [16]. Note that two forcing functions are shown here, which can be distinguished through the phase shifts ϕ_t. The first (Testing) forcing function, was used to estimate the human operator gains in the steady-state dynamics. The second (Validation) forcing function, was used for comparison of the modified Hess model to the experimental data results.

TABLE II
PARAMETER VALUES OF FORCING FUNCTIONS

			Testing	Validation
n [-]	ω_t [rad/s]	A_t [rad]	ϕ_t [rad]	ϕ_t [rad]
1	0.419	$2.905 \cdot 10^{-2}$	2.841	3.006
2	1.047	$1.961 \cdot 10^{-2}$	3.319	6.037
3	1.885	$1.020 \cdot 10^{-2}$	0.718	4.544
4	2.722	$6.032 \cdot 10^{-3}$	0.768	2.811
5	3.979	$3.356 \cdot 10^{-3}$	2.925	5.917
6	5.655	$1.983 \cdot 10^{-3}$	5.145	1.842
7	8.188	$1.230 \cdot 10^{-3}$	2.085	3.401
8	10.681	$9.331 \cdot 10^{-4}$	0.383	2.998
9	14.032	$7.541 \cdot 10^{-4}$	0.763	4.614
10	17.383	$6.674 \cdot 10^{-4}$	3.247	2.888

4) Participants and Procedures: Ten participants performed the experiment who did not have prior experience with tracking tasks. Each participant completed a training phase which allowed them to start the experiment phase. Details on how the participants were trained can be found in [16]. The data used in this research originates from the experiment phase, named testing runs. The data from the training phase was not used.

In the experiment phase, each participant completed three runs for the steady-state conditions (DYN 1 and DYN 2) called testing data-set. Then, for the time-varying conditions (DYN 12 and DYN 21), for each participant, five runs were collected for the testing data-set and three runs for the validation data-set. These tracking runs were averaged over for both steady-state (testing data-sets) and time-varying (testing and validating data-sets) conditions. Additionally, as previously mentioned, the experimental data for the time-varying runs consisted of two changes in CE dynamics (DYN 121 and DYN 212), while in this paper only one change in CE dynamics

occurred (DYN 12 and DYN 21). Therefore, only the data of the first 60 s was considered from the tracking runs.

Based on results from the experiment, some of the collected data-sets were found to be insufficiently consistent for fitting the model. This is attributed to the participants' inconsistent tracking. Therefore, data from participants S02, S05 and S07 for DYN 2 and DYN 21 was not used.

B. Data Analysis

This section provides an outline of the steps used to analyse the adaptive pilot model introduced in Section II, as visualized in Figure 6.

Step 1: Steady-State Modeling: The purpose of this step is to obtain a better understanding of the model in steady-state conditions, allowing for predictions to be made for time-varying conditions. This was accomplished by running the model for combinations of the K_p and K_r gains, while keeping the neuromuscular system and human time-delay constant. This resulted in insights on how changes in the gains lead to changes in tracking performance and control activity. This step is detailed in Section IV-A together with the results obtained. Note that in this step experimental data from the human-in-the-loop experiment was not used.

Step 2: Parameter Estimation: This step uses the mean steady-state data-sets. The purpose of this step is to parameterize the modified Hess model. This is accomplished by estimating the human operator gains (K_p and K_r), for each participant, through the use of a cost function which minimizes the difference between the model's controller output and the measured output of the human controller in the steady-state conditions. Additionally, once suitable gains are found, for each participant, the rms(R^2) value is calculated for both steady-state conditions. The description and results for this step can be found in Section IV-B.

Step 3: Sensitivity Analysis: Once the human operator gains were determined for each participant and for both steady-state conditions (Step 2), a single participant was selected for the full sensitivity analysis of the model. This analysis can be found in Section V.

The first part of this analysis is to understand the influence of the effective time delay τ_e in steady-state and time-varying conditions. Here, the mean steady-state data from the testing runs was used for DYN1. Additionally, for the time-varying conditions, the mean time-varying data from the testing runs for the DYN 12 condition was used.

The second part of this analysis is to tune the key model parameters in the adaptive logic. Here the testing data-sets of the mean time-varying runs were used; initially, for the DYN 12 condition, and then for the DYN 21 condition. The parameters in the adaptive logic included the break frequencies of the filter $H(s)$ on the x signal, the filter $J(s)$ on the adaptive gains, and the adaptation constants K_{a_r} and K_{a_p}, see Section II. These key model parameters were chosen based on the best quality-of-fit, by using the results from the experimental data. This was accomplished by calculating the Variance Accounted For (VAF) values of the control output (u) and model output (M), using the following equation:

$$\mathrm{VAF} = 1 - \frac{\mathrm{var}\,(u_\mathrm{h} - u_\mathrm{m})}{\mathrm{var}\,(u_\mathrm{h})} \tag{20}$$

VAF can vary between 0 (poor model fit) and 1 (perfect corresponding between the experiment data output u_h and model output u_m). Therefore, the key model parameters selected result in the highest VAF values in the region after the controlled dynamics transition, referred to as the post-transition region.

Step 4: Model Validation: the model was validated for all participants by quantifying the quality of the model using Equation (20).

To measure VAF, the output of the experiment output and the simulated output are both required. The experiment output used follows from the steady-state data used to calculate the quality-of-fit for both conditions (DYN 1 and DYN 2). Additionally, both the testing and validation data-sets were used to calculate the quality-of-fit for the time-varying runs for both conditions (DYN 12 and DYN 21).

Based on previous studies, in the steady-state condition, it is expected that the VAF is lower for control of the single integrator system (DYN 1) compared to the double integrator system (DYN 2) [16] [15]. Additionally, for the time-varying condition, it is expected that the VAF is higher for transitions from the single to double integrator case (DYN 12), compared to the transition from the double to single integrator case (DYN 21).

IV. Steady-State Analysis

A. Steady-State Modeling

The aim of this analysis is to investigate the steady-state system, which in turn allows for a better understanding of the time-varying system and the adaptive logic of the model. To achieve this, different combinations of the human operator gain values K_p and K_r were used to analyse the output of the model. For both the DYN 1 and DYN 2 conditions, K_p ranged between 0 and 15 with a step size of 0.01, while K_r ranged between 0 and 0.15 with a step size of 0.01.

When modeling the human operator, constant values were used for the neuromuscular system, as proposed in [11], ω_{nm} = 10 rad/s and ζ_{nm} = 0.707. This analysis was made for different time-delay τ_e constants varying from no delay to τ_e = 0.3 s. The results for the different τ_e can be found in Appendix A. In this section, the results are shown with τ_e = 0.2 s. This is based on the results in Section V, which showed a constant of 0.2 s should be used to represent the effective time-delay of the human operator.

The results of these gain combinations are shown using contour plots, where Figure 7 shows the results for DYN1 and Figure 8 shows the results for DYN 2. These figures show the values of the human operator gains (horizontal and vertical axes), which lead to different values of the root mean square of the error (rms(e)), in figures labelled (a) and root mean square values of the control activity u (rms(u)), in figures labelled (b). Additionally, for combinations of gain values which lead to an unstable open-loop system, no data is shown in the figures.

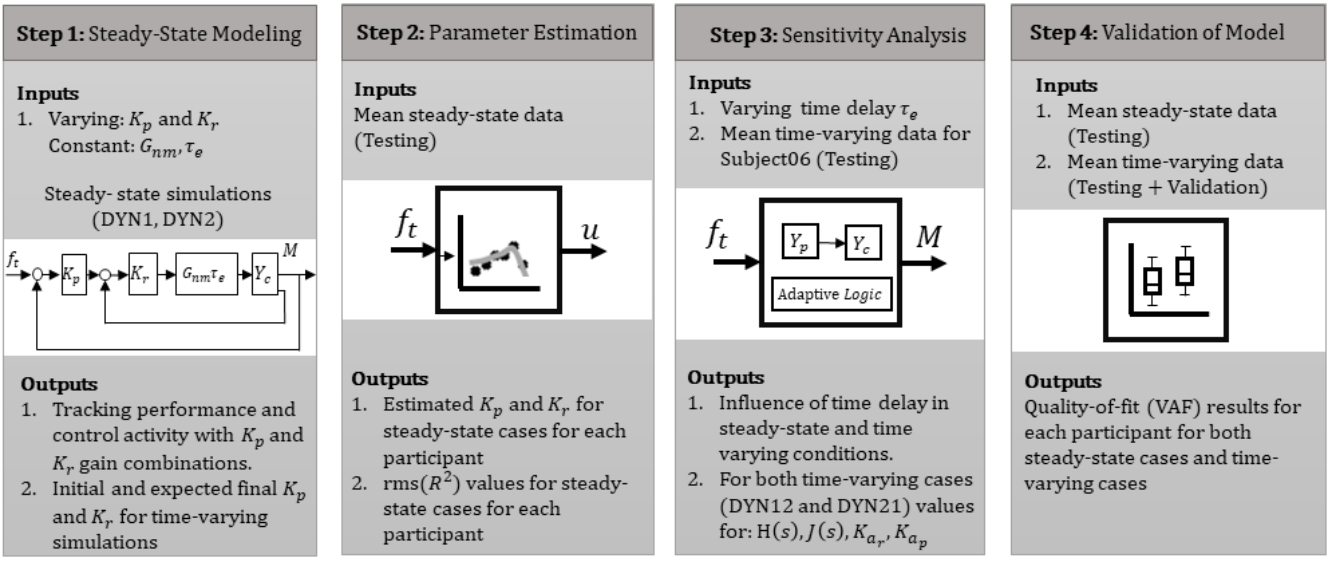

Fig. 6. Steps of analysis

For the DYN 1 condition the results of the K_p gain value range from 0 to 15, while K_r gain ranges from 0 to 0.1. The gain values which result in minimum rms(e) of 0.013 rad are K_p = 4.82 and K_r = 0.06. The open-loop stability characteristics with these gains result in a crossover frequency ω_c = 2.8 rad/s and a phase margin ϕ_m of 44 deg. For the DYN 2 condition, K_p ranges from 0 to 15, and K_r from 0 to 0.15. The gain values which result in minimum rms(e) of 0.016 rad are K_p = 1.52 and K_r = 0.11. The open-loop stability characteristics with these gains result in a crossover frequency ω_c = 3.5 rad/s and a phase margin ϕ_m of 5 deg. It can be observed from Figures 7 and 8 that in the case of DYN 12 condition, one would expect that when the CE dynamics transition, the gain K_p decreases to a lower value, while K_r would marginally increase. The opposite can be expected for the DYN 21 condition. It is also hypothesized that the crossover frequency ω_c and phase margin ϕ_m of the open-loop stability characteristics, increase and decrease respectively, for the DYN 12 condition. Additionally, these figures also show that higher gain values lead to better performance until the system becomes unstable, as expected. However, better performance requires more control activity from the human operator. Therefore, it can be expected that the human tries to achieve a trade-off between high tracking performance and limited control activity.

B. Parameter Estimation

The human operator gain values need to be tuned in order to approximate the human operator during a nominal steady-state run. These parameters are K_p and K_r.

The vector $\theta = \begin{bmatrix} K_r & K_p \end{bmatrix}$ is determined through an optimization problem using the following cost function:

$$\arg\min_{\theta} J(\theta) = \frac{1}{K}\left(\sum_{i=0}^{K-1}(u_h - u_m)^2\right) \qquad (21)$$

This was implemented by means of the nonlinear programming solver *fmincon*. Here, the difference between the model's controller output u_m and the measured output of the human controller from the experimental data u_h is minimized.

In order to avoid local minima, for each case the optimization was run ten times with different initial conditions. Overall, the results were consistent across the different optimization runs meaning that the results were for a real minimum.

Table III and Table IV show the estimated human operator gain values for both conditions (DYN 1 and DYN 2), respectively. Additionally, the tables also show the open-loop stability characteristics and the VAF values for the modeled control activity (u) and the output (M). These are the results from Step 2. For the DYN1 condition, the results for the VAF of the control activity u are highest for participant S06 being 24% higher than the average for all subjects. From the table it is also evident that this subject controls more aggressively compared to the rest of the participants, with a crossover frequency of ω_c = 1.58 rad/s. Meanwhile, the crossover frequencies for the remaining of the subjects are values between ω_c = 1.14 rad/s and lower. In [11], Hess selected the gain values for K_p and K_r such that the crossover frequency is ω_c = 1.50 rad/s. The similarity of the crossover frequency and the higher VAF values, is the reason Subject06 was chosen for the sensitivity analysis in Step 3.

The results from the estimated human operator gain values are consistent with the findings discussed in Section IV-A. For example, for DYN 12 condition, it is expected that Subject06's K_p gain decreases, while K_r slightly increases.

Lastly, it can be observed from Table IV that for Subject01 the estimated K_p and K_r gains result in very low VAF u and VAF M values. Therefore, the data from participant S01 was not used for the time-varying condition DYN 21.

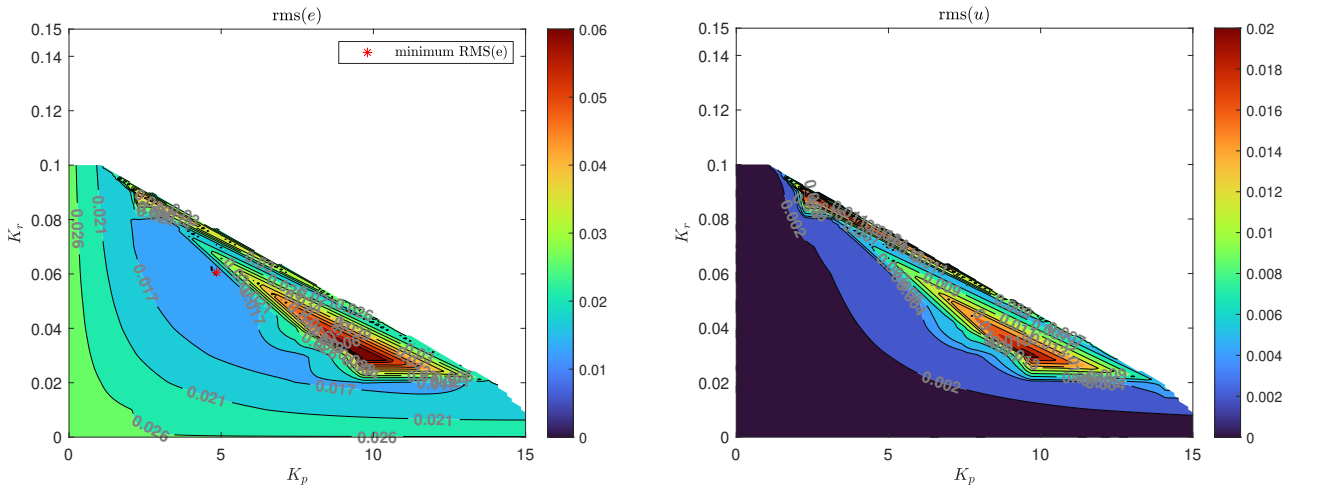

(a) (b)

Fig. 7. Contour plots for the DYN 1 condition showing how different combinations of K_p and K_r values lead to difference in (a) tracking performance - rms(e), (b) control activity - rms(u) (rms results in radians). The white region represents combinations of gain values which lead to an unstable open-loop system.

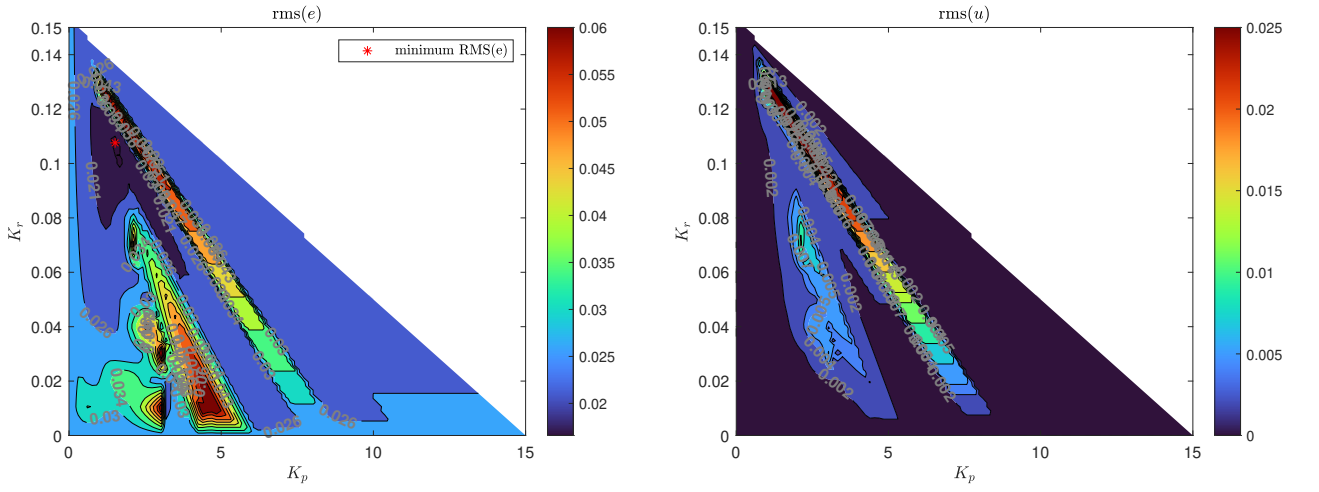

(a) (b)

Fig. 8. Contour plots for the DYN 2 condition showing how different combinations of K_p and K_r values lead to difference in (a) tracking performance - rms(e), (b) control activity - rms(u) (rms results in radians). The white region represents combinations of gain values which lead to an unstable open-loop system.

C. Adaptive Rules

Based on the results from Section IV-A and Section IV-B certain modifications to the adaptive logic described in Section II of original Hess model are required.

In the original Hess model, the rule for change of ΔK_p is given by Equation (12).

There are three disadvantages to this rule:

1) When $\Delta K_r > 0$, then ΔK_p also must increase
2) ΔK_p has to increase by the same constant (0.35) relative to ΔK_r
3) K_p does not change when $\Delta K_r < 0$

These rules are contrary to the expected change of gains for the experiment data used in this paper. From the steady-state analysis, it was shown that in the time-varying analysis K_p should change in the opposite sign of K_r. For example, in DYN 12 condition, K_r is expected to increase while K_p is expected to decrease. Additionally, in the DYN 21 condition, K_r is expected to decrease, and K_p to increase. Lastly, no reasoning is provided on why a constant of 0.35 was used and how it was determined, possibly heuristically developed. This constant does not match the expected change required for K_p with the experimental data used in this paper. Therefore, the rules for changing the gains are adjusted, as described in Section II.

Lastly, in the original model, constraints are imposed on how much the final gain values can change based on the initial

TABLE III
STEADY-STATE RESULTS FOR DYN 1

DYN 1						
Subject	K_p	K_r	ω_c [rad/s]	ϕ_m [deg]	VAF u [-]	VAF M [-]
00	2.38	0.06	1.14	72.08	0.68	0.86
01	1.27	0.09	0.75	80.92	0.38	0.70
02	1.80	0.06	0.84	76.68	0.64	0.87
03	1.33	0.09	0.75	80.34	0.57	0.91
04	1.77	0.08	0.96	76.80	0.67	0.96
05	1.77	0.07	0.91	76.77	0.61	0.84
06	3.18	0.06	1.58	65.14	0.75	0.91
07	1.52	0.08	0.83	78.79	0.48	0.90
08	1.64	0.09	0.97	78.02	0.66	0.84
09	1.64	0.09	0.97	78.02	0.59	0.89

TABLE IV
STEADY-STATE RESULTS FOR DYN 2

DYN 2						
Subject	K_p	K_r	ω_c [rad/s]	ϕ_m [deg]	VAF u [-]	VAF M [-]
00	1.45	0.08	1.80	38.04	0.74	0.79
01	0.47	0.14	1.30	62.84	0.25	0.43
03	0.85	0.10	1.38	61.59	0.25	0.79
04	1.09	0.09	1.95	35.64	0.50	0.85
06	1.10	0.07	1.33	51.55	0.75	0.92
08	0.98	0.08	1.99	43.00	0.51	0.54
09	1.55	0.09	1.93	44.97	0.25	0.80

gain values through Equation (14). This equation implies that the gain K_r has a wider range relative to K_p. For example, in the DYN 21 condition for Subject06 the initial K_p = 1.10 and when the system dynamics transition to a single integrator, the expected adjusted gain value would be K_p = 3.18. However, with the restriction imposed in the original model, the maximum value for K_p is 2.20. Furthermore, justification for the numerical restrictions on the gains is not provided. Therefore, in the modified model, these restrictions on gain values were removed.

V. SENSITIVITY ANALYSIS

A. Influence of time-delay

A sensitivity analysis was performed to analyse the effects of the effective time-delay τ_e on the adaptive model, for both the steady-state and time-varying conditions. For the steady-state case, only the simulated results for condition DYN1 are shown, while for the time-varying case the results for condition DYN 12 are presented. For both sets of results, the considered time-delay settings are τ_e = [0, 0.1, 0.2, 0.3] s. As discussed in Section II, the adaptive logic in the model is divided in two sequential steps; Triggering and Adaptation. The time-delay primarily influences the first step, Triggering, which then drives the Adaptation in the model. Therefore, for this analysis, the results show the influence of delay on the triggering mechanism.

The first part of the triggering mechanism is to calculate the x signal according to Equation (2) and filter the x signal as in Equation (3).

In this analysis, the filter settings were kept constant and equivalent to those used by Hess [11], where ω_{lp} = 1.5 rad/s and ζ = 1 [-].

The second part of the triggering mechanism is the trigger function, given in Equation (5). This function decides whether adaptation is required, by comparing whether:

$$\sqrt{|x|} > 3 \cdot \text{rms}\sqrt{|x|} \tag{22}$$

Here, the reason for incorporating $\text{rms}\sqrt{|x|}$ is to normalize the $\sqrt{|x|}$ signal. By normalizing the signal, the same magnitude of the signal is achieved, despite the different time-delays. Therefore, the normalized $\sqrt{|x|}$ is given by:

$$\frac{\sqrt{|x|}}{\text{rms}\sqrt{|x|}} \tag{23}$$

Where the model is triggered if the normalized $\sqrt{|x|} > 3$.

Additionally, note that varying the time-delay also has an effect on the human operator gains, which need to be adjusted depending on the time-delay. For example, a previous study has shown that increasing time-delay results in the human operator generating more lead [19]. However, in this analysis, the human operator gains were kept constant with the time-delay increases. While this is a limitation of the analysis, it is the best method to isolate the influence of the time-delay in the model.

1) Steady-state condition: In this analysis, as the CE dynamics do not change, Triggering is not expected to be activated. Figure 9 shows the influence of delay on the x signal. The top graph shows the x signal before it is filtered by $H(s)$ and the bottom graph shows the filtered x signal. Here, it can be observed that increasing the time-delay results in an increase of the magnitude in the x signal, as larger time-delay introduces larger tracking errors (Figure 10). Using linear regression, a relationship between the rms(x) and increase in time-delay was found in $\text{rms}(x) = 0.0018\tau_e + 0.0007$ with an R^2 value of 0.96. This in turn would affect the strength of adaptation, because the X_n signal is directly related to the x signal. Thus, a larger time-delay would mean that Adaptation would induce bigger changes in the gain values of K_r and K_p. Therefore, adaptation constants, K_{a_r} and K_{a_p}, were introduced in the model to account for this potential overreaction. These adaptation constants are discussed in Section V-C.

Furthermore, the left-most graphs in Figure 11 show the normalized $\sqrt{|x|}$ signal, while the right-most graphs of Figure 11 show the moment at which the trigger occurs. This is when $\frac{\sqrt{|x|}}{\text{rms}\sqrt{|x|}} > 3$. Additionally, the top graphs show the results when the x signal is not filtered, while the bottom graphs show the filtered x signal. From these, it can be observed that the effect of the time-delay τ_e on the triggering mechanism is very small. However, the filter on the x signal is of great importance, because this filter smooths out instantaneous peaks, which cause false positives. Several false positives can be seen for a delay of τ_e = 0.3 s, when the x signal is not filtered. Therefore, this filter is investigated in Section V-B.

2) Time-varying condition: In this investigation, triggering is expected to occur, as the CE dynamics transition from an effective single-integrator dynamics to an approximate double-integrator dynamics, at t = 30 s. The results of varying the time-delay on the triggering mechanism are shown in

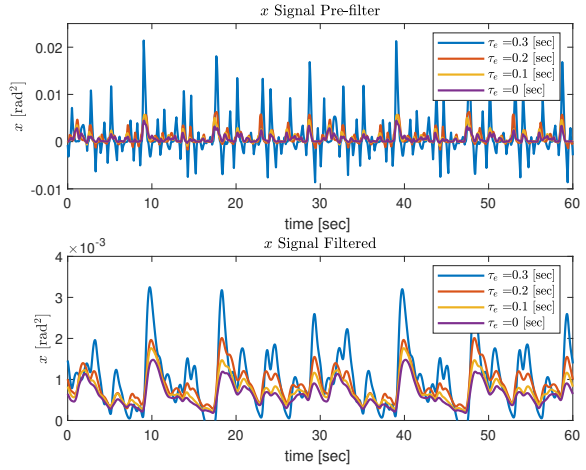

Fig. 9. The effect of increasing the time-delay τ_e on the x signal. The top graph shows the unfiltered x signal, while the bottom shows the filtered x signal

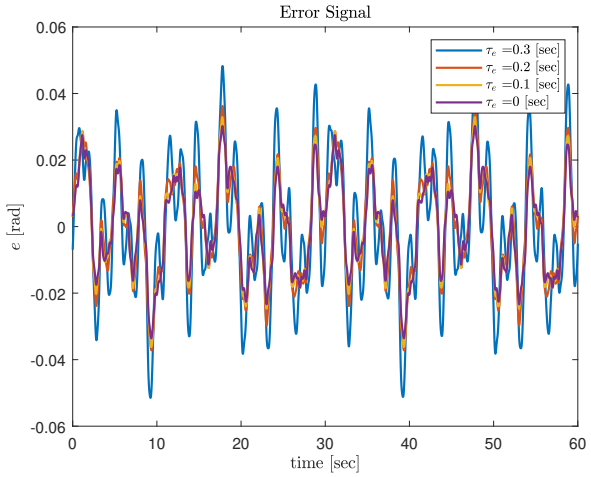

Fig. 10. The effect of increasing the time-delay τ_e on the error signal e in the model

Figure 12. From this figure, it can be observed that an increase in the time-delay results in an increase in the error in the model, as a higher spike in the Triggering mechanism can be seen. The magnitude of the spike directly influences the strength of adaptation as it is proportional to the X_n signal, see Equation (10) and Equation (11). Time-delays τ_e of 0, 0.1, 0.2, and 0.3 result in peaks of 8%, 16%, 22%, and 27% higher than the triggering limit, respectively. As discussed in Section V-A1, this results in a gain-adjustment overreaction in the model; therefore a corresponding correction to the Adaptation mechanism is discussed in Section V-C.

As discussed in Section II, a constant time-delay imposes a limitation as this time-delay depends on the human operator. A previous study estimated the corresponding time-delay for each participant for the equivalent data-sets considered in this paper, in both steady-state and time-varying conditions. Results showed that the time-delay is approximately 0.2 s for all participants and across different conditions [16]. Therefore, a time-delay τ_e of 0.2 s was implemented in the model.

B. Sensitivity on Triggering Logic

The investigation of time-delay showed that the filter $H(s)$ applied to the x signal smooths out instantaneous peaks (extreme values) which would otherwise cause false positives. Therefore, it can be concluded that a filter is required. Thus, an analysis is conducted to determine suitable values for the second-order low-pass filter. These are determined by varying the bandwidth of the filter $H(s)$, where the filter setting ω_{lp} = [1, 2, 3, 4] [rad/s].

The effects of varying the filter setting on the x signal is shown in Figure 13. Regardless of the bandwidth of the filter, the corresponding filtered signal has a smaller magnitude. However, a larger bandwidth filter allows the signal to have a larger magnitude (relative to a smaller bandwidth filter). This is also evident from Figure 13 which shows that the filtered signal with ω_{lp} = 1 [rad/s] has the smallest peak. If the bandwidth of the filter is too restrictive, the Triggering mechanism may not be activated. Furthermore, a less restrictive bandwidth results in higher peaks, thus inducing bigger changes to the gain values of K_r and K_p during Adaptation.

Additionally, the effects of varying the filter's setting ω_{lp} on the Triggering mechanism are shown in Figure 14. These results show that the bandwidth of the filter induces lag in the Triggering. A larger bandwidth allows for more of the peaks to pass through, thus causing the the triggering to take place earlier. Figure 14 (b) shows that Triggering is activated 3.8 s, 2.2 s, 2 s and 1.9 s from the time that the controlled dynamics transition, for ω_{lp} = 1, 2, 3, 4 [rad/s] respectively. As also explained by Hess [11], it should be noted that the human operator does not change his/her control strategy as soon as they notice a change in CE dynamics. Therefore, a larger filter bandwidth is likely to make the adaptive logic overreact. On the other hand, a filter with a very small bandwidth is not desired, as it significantly lowers the maximum amplitude of the signal. This in turn can result in the adaptive logic not being triggered, or triggered at a later point. However, this could be compensated by using a lower triggering limit.

The conclusion from this research is that the bandwidth of a filter influences how fast the logic is triggered. For this participant (S06), ω_{lp} = 1.5 [rad/s] would be a suitable value to use. This is the same value that was used in the original model by Hess [11]. Note that the human operator gains for this participant (S06), had a similar open-loop crossover frequency ω_c to the original Hess model. This means that while the triggering mechanism works for this particular subject, it could be expected that the triggering mechanism is not activated for the other participants, as they had lower values of crossover frequency.

C. Sensitivity on Adaptation Logic

1) Adaptation constants K_{a_r} and K_{a_p}: In Section V-A it was found that increasing the time-delay influences the strength of the adaptation. As a consequence, the adaptation constants K_{a_r} and K_{a_p} were introduced to the model as

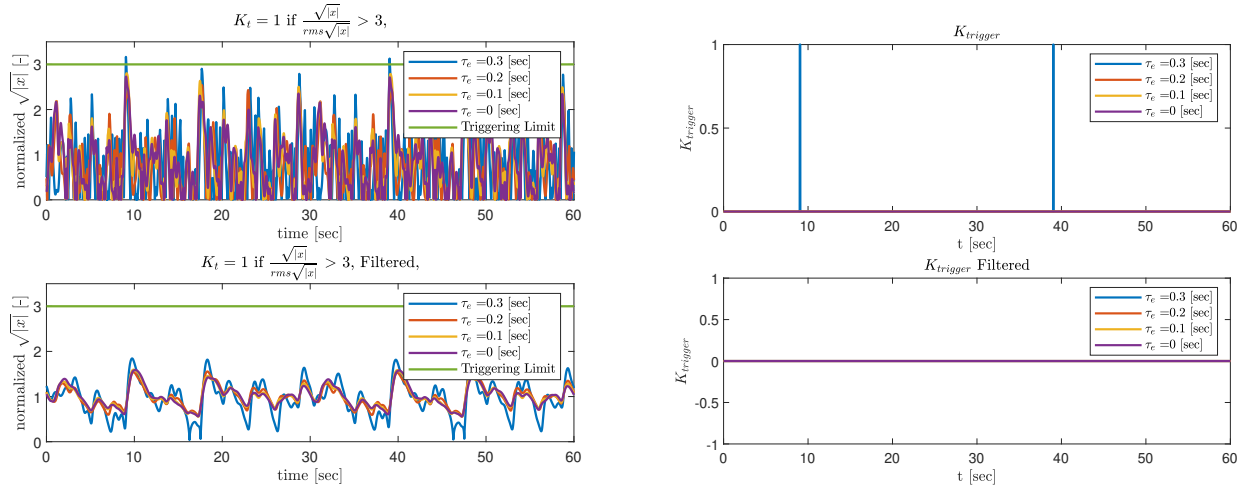

(a) (b)

Fig. 11. The effect of increasing the time-delay τ_e in a steady-state system (DYN 1) on (a) the Triggering Logic, and (b) the time during which the Trigger Logic is activated ($K_{trigger}$ = 1), for both the unfiltered (top), and filtered (bottom) x signals.

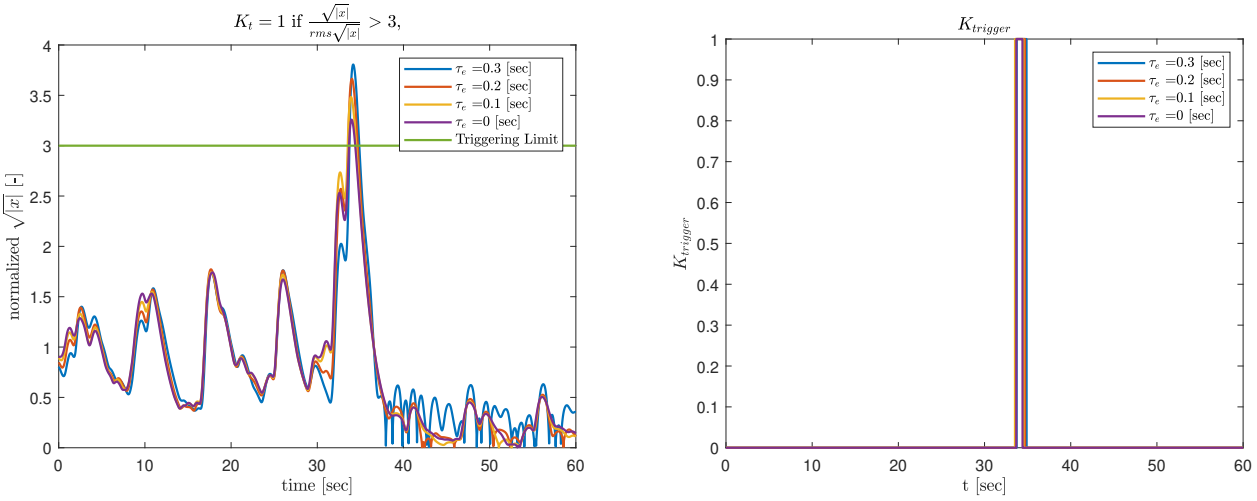

(a) (b)

Fig. 12. The effect of increasing the time-delay τ_e in a time-varying system (DYN 12) on (a) the Triggering Logic, and (b) the time during which the Trigger Logic is activated ($K_{trigger}$ = 1), for the filtered x signal.

scaling factors, to account for the increased magnitude of the x signal.

The adaptation constants, K_{a_r} and K_{a_p}, scale the change of K_r and K_p as described in Equation (10) and Equation (13), respectively. To determine the scaling factors that should be used, a sensitivity analysis was performed with varying adaptation constants. Table V shows the VAF values for the model output M and control output u. It can be seen that adaptation constants K_{a_r} = 0.0055 and K_{a_p} = - 150 lead to highest VAF values, thus these were chosen to be used in the adaptive model.

In order to show the influence of the adaptation constants on the Adaptation logic, two combinations of the K_{a_r} and K_{a_p} were selected from Table V. The cases are summarized in Table VI, and were selected as a sample of different adaptation constants. Figure 15 shows how the K_r (top graph) and K_p (bottom graph) gains adapted for the two cases. Both graphs show that there is a larger increase of ΔK_r and ΔK_p with larger values of the adaptation constants K_{a_r} and K_{a_p}, respectively. However, while the gain K_r increases to a larger value, the gain K_p decreases due to the negative sign on K_{a_p}. Lastly, in Figure 15, a spike and a dip can be observed during the transition of K_r and K_p gains respectively. This is due to the filter $J(s)$ applied to the change in gains, which is further discussed in Section V-C2.

2) Filter on gains: In the original model, Hess [11] used a second-order low-pass filter $J(s)$ on Equation (10), with ω_{lp} = 1 rad/s and ζ_{lp} = 1. The purpose of this filter is to introduce lag during gain transition. This aims to simulate human operator dynamics in time-varying systems, where gain

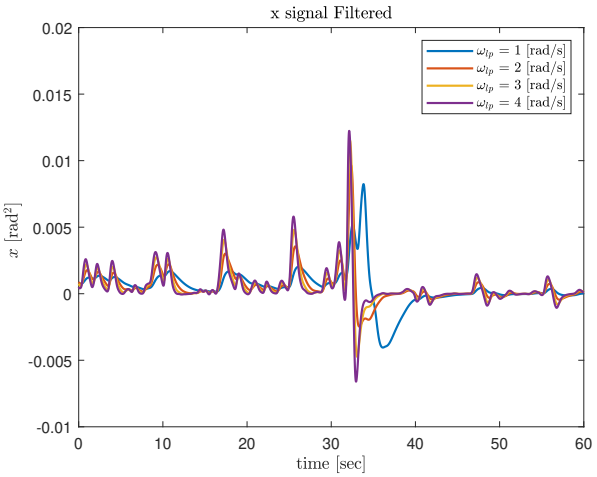

Fig. 13. The effect of varying the filter's $H(s)$ setting ω_{lp} in a time-varying system (DYN 12) on the x signal

TABLE V
VAF RESULTS FOR MODEL OUTPUT M AND CONTROL OUTPUT u WITH VARYING THE ADAPTATION CONSTANTS K_{a_r} AND K_{a_p}.

	VAF M	VAF u	VAF M	VAF u	VAF M	VAF u
K_{a_r}	K_{a_p} = -150		K_{a_p} = -200		K_{a_p} = -250	
0.0035	0.39	-3.25	0.87	0.64	0.85	0.67
0.0040	0.65	-1.02	0.90	0.79	0.73	0.46
0.0045	0.83	0.31	0.89	0.76	0.41	0.21
0.0050	0.89	0.73	0.72	0.47	0.12	0.09
0.0055	0.91	0.81	0.52	0.28	0.00	0.00
0.0060	0.89	0.78	0.19	0.11	0.00	0.00

TABLE VI
TWO CASES SELECTED TO SHOW THE INFLUENCE OF K_{a_r} AND K_{a_p} ON THE ADAPTATION

Cases	K_{a_r}	K_{a_p}
1	0.0055	-150
2	0.0045	-200

transitions are not expected to be instantaneous. Even when accounting for this, the settings in the filter used by Hess are conservative, causing a gain transition to take more that 5 s. Therefore, an analysis was conducted to investigate this filter and its effects on Adaptation. This was accomplished by varying the frequency of the filter ω_{lp}, from 1 to 10 rad/s, and in one scenario $\omega_{lp} = \infty$ rad/s. The influence of the filter on the adaptive gains starts from the moment when triggering occurs, as shown in Figure 16. Here, the shaded gray area i.e., transition region, represents the area where the filter affects the tracking performance. In the transition region, it can be seen that tracking output for a signal with smaller ω_{lp} oscillates for a longer time period compared to a signal with higher ω_{lp}.

The effect of the filter on the corresponding gain adaptation is visualized in Figure 17. Here, the gains for the filter with the smallest bandwidth (ω_{lp} = 1 rad/s), take more than 5 s to reach their final values, whereas for the case without a filter (NF) the change is instantaneous. This is also reflected on the

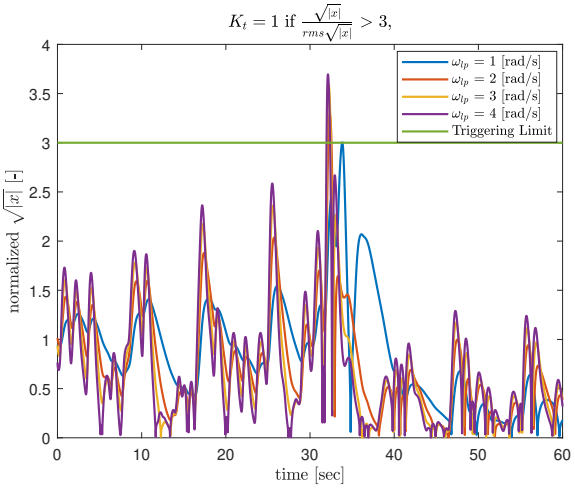

(a)

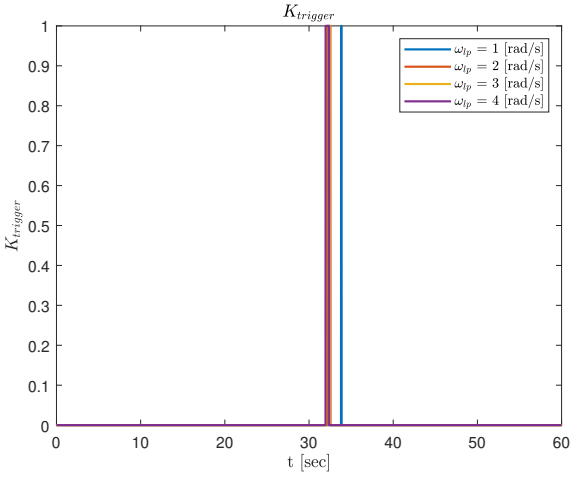

(b)

Fig. 14. The effect of varying the filter's $H(s)$ setting ω_{lp} [rad/s] in a time-varying system (DYN 12) on (a) the Triggering Logic, and (b) the time during which the Trigger Logic is activated ($K_{trigger}$)

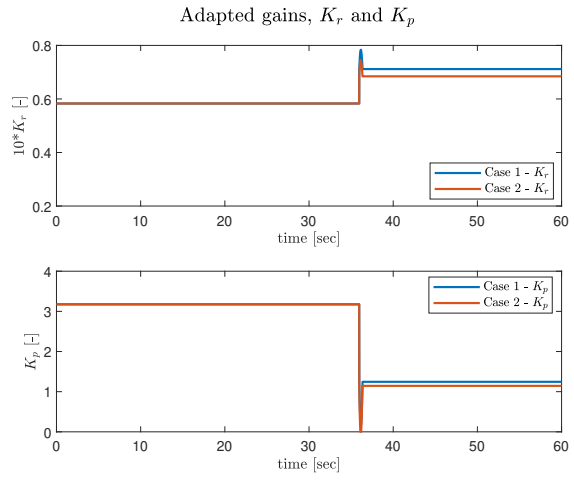

Fig. 15. Gain adaptations with varying adaptive constants K_{a_r}

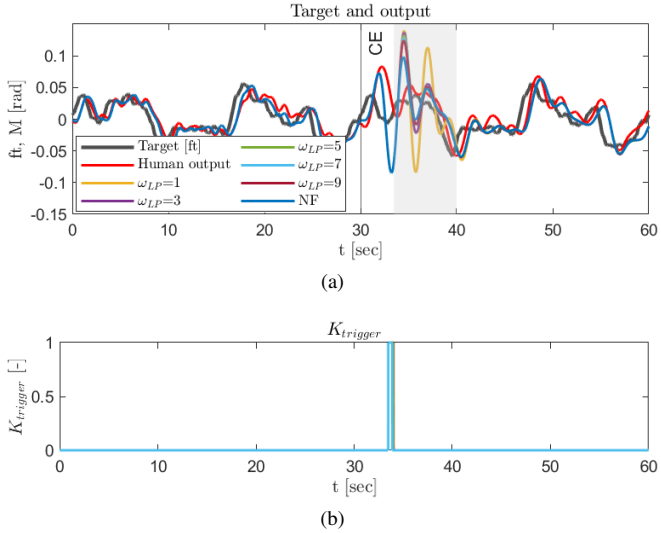

Fig. 16. Influence of filter on adaptive gains; (a) Tracking performance (b) Moment at which Triggering is activated

tracking performance in Figure 16, where the signal with the smallest bandwidth (ω_{lp} = 1 rad/s) oscillates for the longest time. Additionally, in Figure 17 a dip can be seen when the K_p gain transitions. This dip is only present for the cases where $\omega_{lp} > 5$ rad/s and for the case where $\omega_{lp} = \infty$ rad/s. The dip is due to the transient of the X_n signal during the time the Triggering is activated. For the cases where $\omega_{lp} < 5$ rad/s, this transient is filtered and therefore a smooth transition takes place.

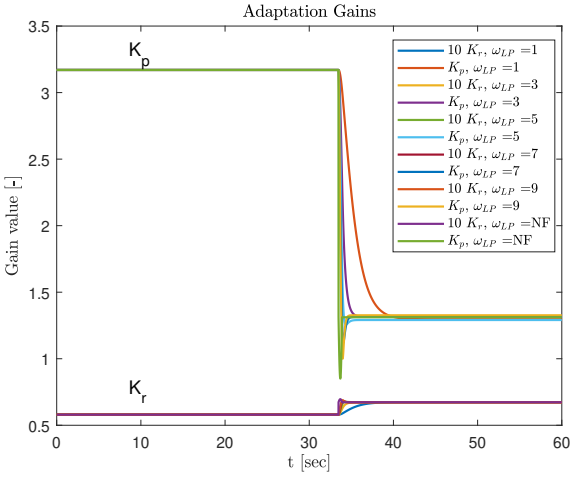

Fig. 17. Gain adaptations with varying the parameter ω_{lp} of the filter $J(s)$

An optimal value for ω_{lp} was selected based on the best quality-of-fit compared to the human data in the transition region. Here, the VAF values were calculated for the control output (u) and model output (M), as displayed in Table VII. While all VAF values indicate a bad fit, these results show that a filter should not be used on the adaptive gains as the VAF for both u and M is highest (least negative) for the case without a filter (NF). This implies a step-like transition in human operator gains.

TABLE VII
INFLUENCE OF FILTER $J(s)$ ON THE ADAPTIVE GAINS ON THE TRANSITION REGION SHOWN THROUGH VAF VALUES

ω_{LP} [rad/s]	VAF u	VAF M
1	-71.8089	-11.0072
2	-41.1341	-6.0413
3	-33.0899	-4.9315
4	-29.4432	-4.4665
5	-27.7575	-4.2260
6	-26.8538	-4.0512
7	-27.0408	-4.0592
8	-26.5183	-3.9094
9	-26.8465	-3.9274
10	-26.2914	-3.7786
NF	-21.21	-2.8

VI. Model Validation Results

In Section V the key parameters of the adaptive model were determined through a sensitivity analysis. This sensitivity analysis was performed on the data from one participant ($S06$). This section extends the results of the model validation for all participants for the time-varying conditions (DYN 12 and DYN 21). The results for the steady-state conditions can be found in Section IV.

A. Time-Varying Condition DYN 12

1) Results for DYN 12: In the DYN 12 time-varying condition, the CE dynamics transition from a single integrator to dynamics that approximate a double integrator system. The triggering mechanism was only activated for participant ($S06$), which can be seen from Appendix B. In order for the triggering mechanism to become activated for more of the participants, the bandwidth of the filter $H(s)$ on the x signal was increased from $\omega_{lp} = 1.5$ rad/s to $\omega_{lp} = 3$ rad/s, for all participants. Increasing the bandwidth of the filter results in a larger magnitude of the x signal, as shown in Figure 18. This figure shows the normalized $\sqrt{|x|}$ signal for participant (S00) who, with the original triggering mechanism $\omega_{lp} = 1.5$ rad/s, was not triggered. However, with $\omega_{lp} = 3$ rad/s the triggering is evident.

Consequently, as discussed in Section V, increasing ω_{lp} directly affects the strength of adaptation as the x signal is proportional to the X_n signal. Figure 19 shows the effect of increasing ω_{lp} on the X_n signal. In order to prevent the adaptive gains from overreacting (due to increasing magnitude of X_n), the adaptive constants K_{a_r} and K_{a_p} were recalculated for each participant.

Table VIII summarizes the model parameters for each participant. This table provides the initial K_p and K_r gain values of the pre-transition phase (determined in Section IV), and its corresponding open-loop stability characteristics. It also provides the values used for the key model parameters for all the participants. Table IX further shows the final adapted gains of the post-transition phase results for both the testing and validation data-sets. It is important to check the results for both the testing and validation data-sets to determine whether the model overfit to the testing data-sets. When no gains are listed, the triggering mechanism did not activate, thus

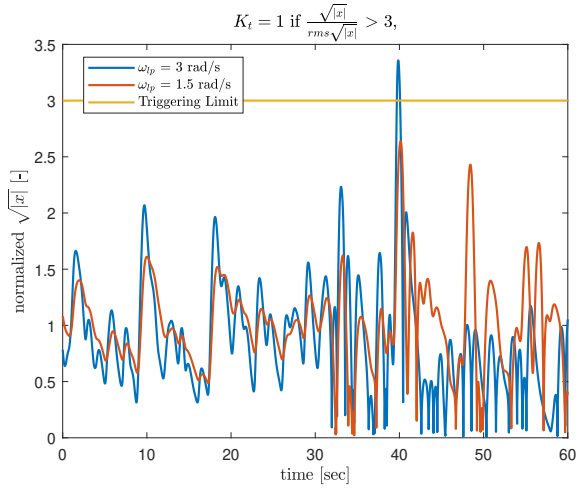

Fig. 18. Effect of increasing ω_{lp} of the filter $H(s)$ from 1.5 rad/s to 3 rad/s on the triggering mechanism for participant S00

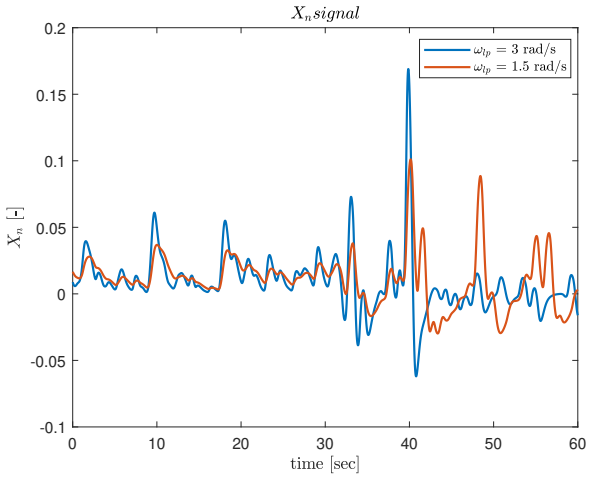

Fig. 19. Effect of increasing ω_{lp} of the filter $H(s)$ from 1.5 rad/s to 3 rad/s on X_n signal for participant S00

no change in the human operator's gains. Additionally, the open-loop stability characteristics are provided. Moreover, in Table VIII, the key model parameters for subjects S01 and S03 could not be determined, because the triggering mechanism did not activate for these participants in both the testing and validation data-sets. For subjects S04, S08, and S09, the triggering mechanism did not activate for the validation data-sets, while it did activate for the testing data-sets.

For subjects S00, S04, and S06, when the adaptation is triggered (see Table VIII and Table IX), the inner-loop gain K_r increases, meaning that the generation of lead in the feedback control increases. As expected, these results are in-line with the findings of Section IV and with previous studies of pursuit tracking tasks, where human operators generate lead for double integrator CE dynamics [16] [20]. However, this was not the case with subjects S08 and S09, where a slight decrease (ΔK_r is 0.003 for S08 and 0.002 for S09) in the K_r gain is evident. A possible explanation for this is that subjects S08 and S09 already had a high K_r gain in the pre-transition phase (0.016 points above average). Therefore, their control strategy was already suitable for DYN 2.

2) Further investigation in the DYN 1 condition: When inspecting the initial gain values for each participant (steady-state condition DYN 1), a large discrepancy can be observed between participant S06 and the rest of the participants. S06 has a significantly more aggressive control behaviour (ω_c = 1.6 rad/s) relative to the other participants. An analysis was conducted to compare the control behaviour for each participant, and the results are shown in Figure 20. In this figure, the y-axis shows the rms(x), the x-axis shows the rms(R^2), and a color map is used to show the error signal (rms(e)), for each participant. Participant S06 exhibits the best control strategy relative to the other participants (ω_c between 0.75 and 1.1 rad/s), with the lowest error value of rms(e) = 0.0154 rad. For S06, the outer-loop gain K_p is significantly larger than the rest of the participants, yielding higher rms(R^2) and thus rms(x) values. Participants S08 and $S09$ have large inner-loop gain K_r values, as well as above average K_p gains. This results in more aggressive control strategy relative to the rest of the participants. However, they are not necessarily more accurate, resulting in large error values rms(e) = 0.0180 rad for both participants.

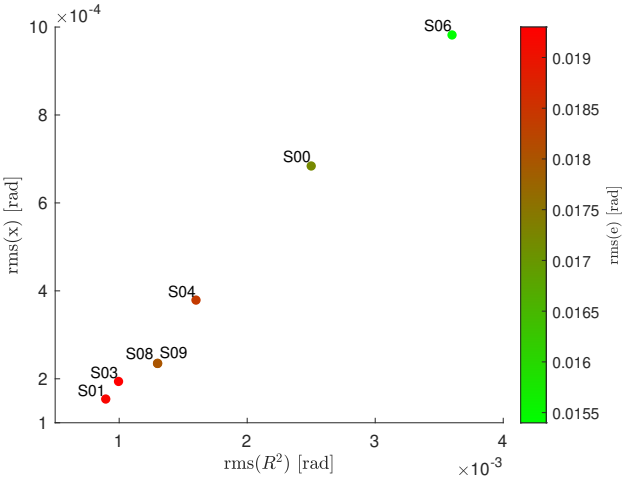

Fig. 20. Analysis of control strategy per subject for condition DYN 1 ($S08$ and $S09$ overlapping)

Participants S01 and S03 show the most low-gain control strategy, reflected in the lowest K_p values and highest tracking error, rms(e) = 0.0192 rad and 0.0193 respectively. The crossover frequency ω_c for these participants is 0.75 rad/s, which is much lower relative to the other participants. Hess originally designed the model for human operators with initial gain values yielding a ω_c of 1.5 rad/s [11]. Therefore, it can be concluded that the model can accurately capture the transient control behaviour of participants with higher control activity, and who accurately follow the target signal. However, the model is not triggered for participants with less steady-state tracking performance i.e., when ω_c is lower than 0.9 rad/s.

Figure 20 also shows that the magnitude of the x signal varies per participant where rms(x) is around six times smaller

TABLE VIII
MODEL SETTINGS FOR TIME-VARYING CONDITION DYN 12

Subject	DYN 1 Initial gain values		DYN 1 Open-loop characteristics		Key Model Parameters			
	K_p [-]	K_r [-]	ω_c [rad/s]	Φ_m [deg]	$H(s)$ ω_{lp} [rad/s]	$J(s)$ ω_{lp} [rad/s]	K_{a_p} [-]	K_{a_r} [-]
00	2.379	0.058	1.138	72.076	3	∞	-40	0.17
01	1.266	0.095	0.753	80.921	-	-	-	-
03	1.325	0.085	0.753	80.338	-	-	-	-
04	1.773	0.067	0.906	76.768	3	∞	-150	0.038
06	3.175	0.058	1.577	65.137	3	∞	-150	0.0055
08	1.642	0.091	0.972	78.024	3	∞	-10	0.05
09	1.642	0.091	0.972	78.024	3	∞	-5	0.03

TABLE IX
ADAPTIVE GAIN RESULTS FOR TIME-VARYING CONDITION DYN 12, FOR BOTH TESTING AND VALIDATION DATA-SETS

Subject	Testing data-sets				Validation data-sets			
	DYN 2 Adapted gain values		DYN 2 Open-loop characteristics		DYN 2 Adapted gain values		DYN 2 Open-loop characteristics	
	Kp [-]	Kr [-]	ω_c [rad/s]	Φ_m [deg]	Kp [-]	Kr [-]	ω_c [rad/s]	Φ_m [deg]
00	1.465	0.080	1.529	51.949	1.472	0.080	1.537	51.585
01	-	-	1.300	62.839	-	-	1.300	62.840
03	-	-	1.358	58.380	-	-	1.358	58.380
04	1.263	0.070	1.235	55.794	-	-	1.840	34.086
06	1.244	0.071	1.218	56.796	1.275	0.071	1.252	55.681
08	1.660	0.088	1.881	45.558	-	-	1.991	43.000
09	1.653	0.089	1.877	46.392	-	-	1.933	44.974

for S01 than for S06. Consequently, the X_n signal also differs in magnitude per subject. Therefore, model tuning, where the adaptive constants K_{a_r} and K_{a_p} are determined, needs to be participant based.

3) Comparison between results for the testing and validation data-sets: The results for participants S04, S08 and S09 show that, while the adaptive logic was triggered for the testing data-sets, this did not happen for the validation data-sets. Therefore, a Monte Carlo analysis was conducted to investigate whether the forcing function influences the triggering logic of the model. Note that the only difference between the testing and validation data-sets is the forcing function. In this analysis the time at which the system dynamics transitioned, M_1, was varied for both the testing and validation forcing functions, from 10 to 50 seconds, for a total of 1,000 different M_1. The results for a single participant (S09) are discussed below for conciseness, as no significant differences were found between participants. The results for the remaining participants can be found in Appendix C. Figure 21 shows the histograms of the response time for both the testing and validation data-sets. The response time T_r, is the time from when the CE dynamics transition M_1 until the triggering mechanism in the model is activated. When the triggering mechanism is activated, the response time T_r is similar (between 0 to 12 s) to experimental values reported in previous studies of time-varying systems [17] [21]. This implies that the model is effective at replicating the reaction time of the human operator for this time-varying condition.

It is important to note that for the testing and validation data-sets, the triggering mechanism was activated for 53 % and 74 % of the total M_1 transitions, respectively. In order to investigate whether possible time variations in the forcing function affect the triggering mechanism, the trigger time is plotted relative to the forcing function. Figure 22 (a) shows the results for the forcing function used for the testing data-sets, while Figure 22 (b) shows the results for the validation. Results show that triggers tend to occur when the gradient of the forcing function is larger relative to other sections where there is a small gradient. This is particularly evident for the validation data-sets in Figure 22 (b).

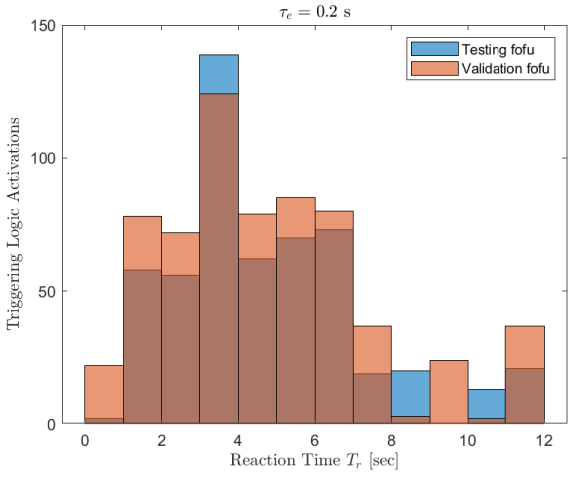

Fig. 21. Monte Carlo analysis showing the reaction time T_r for subject S09

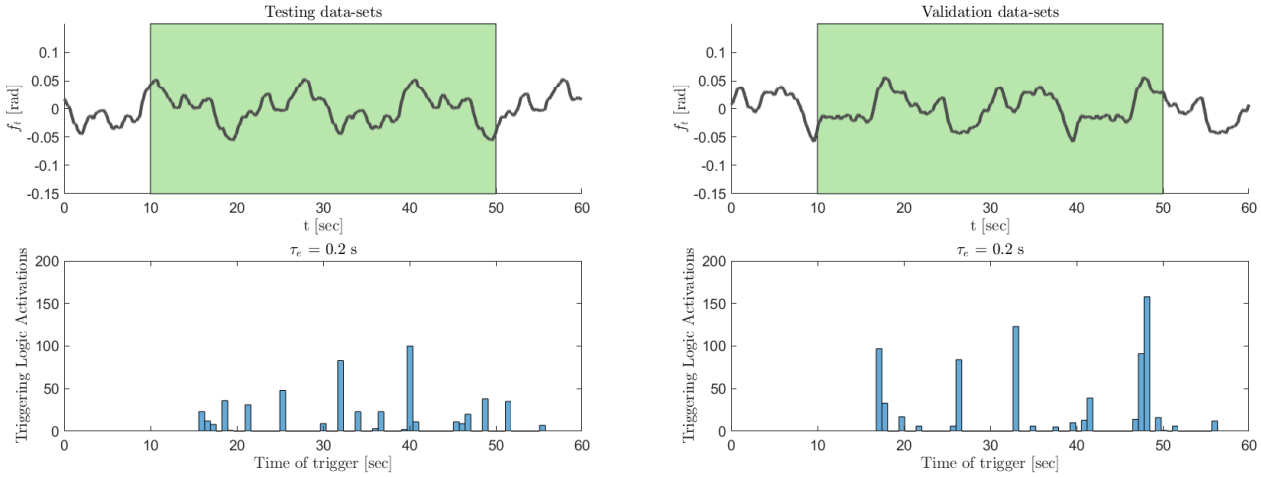

(a) Testing data-sets

(b) Validation data-sets

Fig. 22. (a) Time of trigger for testing forcing function, (b) Time of trigger for validation forcing function

Figure 22 is useful for investigating the cases where Triggering is activated. However, it is equally important to investigate those cases with no activation. When the system dynamics transition at the region with only minor variations in the forcing function, the tracking error increases, but not enough to activate a trigger. Then, one would expect that the trigger is activated as soon as there are larger variations in the forcing function. However, in this model, the Triggering is activated based on the Trigger limit (3rms($\sqrt{|x|}$)), the value of which also increases after transition. An example of such a case is shown in Figure 23, where Figure 23 (a) shows the tracking performance of the model output M, and Figure 23 (b) shows the Triggering logic where both $\sqrt{|x|}$ and the Trigger limit (3rms$\sqrt{|x|}$) are plotted. In this example, the CE dynamics transitioned at 30 s, however, as seen from Figure 23 (b), $\sqrt{|x|}$ does not exceed the Trigger limit. Then, at around 50 s, another large spike is evident in $\sqrt{|x|}$, but since the Trigger limit has increased, the trigger is not activated.

Nevertheless, further investigation is required to determine the relationship between the trigger mechanism and the forcing function. It would also be important to consider participants which have a low tracking error in the pre-transition phase.

4) Quality-of-fit results for condition DYN 12: Table X shows the VAF values of the testing and validation data-sets. The table shows the VAF values of the control output (u) and model output (M) in the pre-transition and the post-transition phases, accounting for the 0-30 and 40-60 s intervals in the simulation, respectively. It also provide the mean VAF values for the cases when Triggering is activated, when Triggering is not activated, and the mean values for all cases.

The total mean VAF values for the testing data-sets and validation data-sets are similar (within a maximum of 0.05 points), meaning that there is no overfitting of the model. Additionally, the total mean VAF values for the control output u (between 0.44 and 0.65) are lower compared to those reported in literature (between 0.6 and 0.8) [22]. However, for the cases when the Triggering is activated, the mean VAF results for the control activity u are 0.71 and 0.63 for the pre-transition and post-transition phases, respectively. These results are comparable to literature, where mean VAF results of 0.6 and 0.75 are reported for the pre-transition and post-transition phases respectively [16].

Moreover, for all cases, the VAF values for both control output u and model output M are lower in the post-transition phase, relative to the pre-transition phase. This was also observed in the steady-state cases where the mean VAF values for the control activity u were found to be 0.63 and 0.5, for DYN 1 and DYN 2 respectively. This implies that the model is less accurate in fitting the experimental data for DYN 2. Note that VAF is a measure of quality-of-fit between the experimental data and the model output, which does not imply low-error in the tracking task. Lastly, the mean VAF values in the pre-transition phase are 30 % lower for both control output u and model output M for the cases when the Triggering was not activated, compared to the cases where it was activated. Lower VAF values in the pre-transition phase could be a reason for the Triggering not being activated. This requires further research.

B. Time-Varying Condition DYN 21

In this time-varying condition, where the CE dynamics transition from an approximate double integrator to a single integrator, the adaptive logic is not triggered for any of the participants. The results for this condition are provided in Appendix D. This means that while the CE dynamics change, the human operator gains do not need to adapt to maintain performance. Therefore, the initial gain values used for this condition, provided in Table IV, remain the same when the controlled system transitions to DYN 1. This results is not unexpected, as the human operator is transitioning to more easily controlled dynamics. Therefore, there is no large error build-up after transition. This can be seen in Figure 24 where the triggering mechanism is shown for a single participant,

TABLE X
VAF RESULTS FOR CONDITION DYN 12 OF THE TESTING AND VALIDATION DATA-SETS

	Testing data-sets					Validation data-sets				
		Control activity u		Model output M			Control activity u		Model output M	
Cases:	n	Pre-transition	Post-transition	Pre-transition	Post-transition	n	Pre-transition	Post-transition	Pre-transition	Post-transition
Triggering Activated	5	0.68	0.56	0.91	0.79	2	0.78	0.71	0.92	0.89
Triggering Not Activated	2	0.44	0.15	0.85	0.76	5	0.59	0.33	0.89	0.76
Total Mean	7	0.60	0.44	0.89	0.78	7	0.65	0.45	0.90	0.81

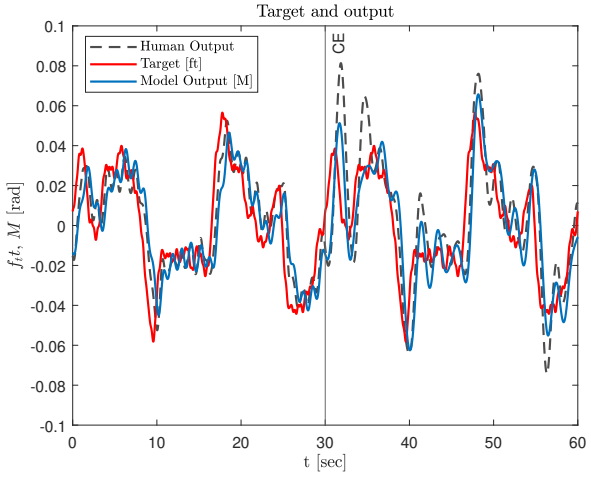

(a) Tracking performance

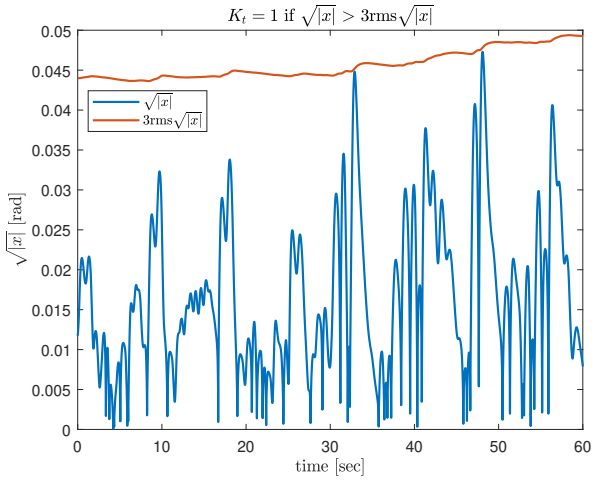

(b) Triggering logic

Fig. 23. A case where the model is not triggered for DYN 12 where the CE dynamics transition at 30 s (a) Tracking performance showing the forcing function f_t, output of the model M, and output of the human from the experiment data (b) Triggering logic showing $\sqrt{|x|}$ and the Triggering limit ($3\text{rms}\sqrt{|x|}$)

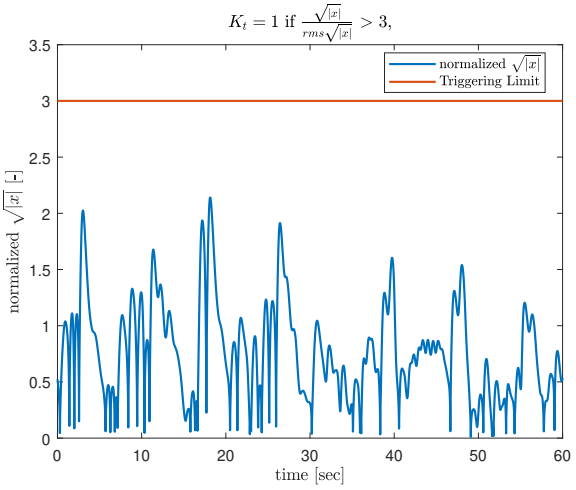

Fig. 24. An example of a case where the model is not triggered for DYN 21 where the CE dynamics transition at 30 s. This was the case for all participants in this time-varying condition. The figure shows the normalized $\sqrt{|x|}$ signal and the Trigger limit

as there are no differences between participants. Here the controlled dynamics transition at 30 s to the single integrator. The magnitude of the normalized $\sqrt{|x|}$ signal is large for the pre-transition phase, decreasing when the system dynamics transition to the single integrator.

Hess designed this model to investigate incidents with transitions from CE dynamics that are easier to control, to more challenging CE dynamics. Therefore, in order for the model to also be triggered in this condition, major changes to the logic would be required.

Figure 25 shows a box plot of the VAF of the (a) control output (u) and (b) model output (M) which shows the quality-of-fit in transition DYN 21. The figure only shows the pre-transition results and the post-transition phase, accounting for the 0-30 and 40-60 s intervals in the simulation. Additionally, the results for the mean values of VAF u and VAF M are given in Table XI. The results for this non-adaptive model, where the gains remain the same, indicate that the quality-of-fit for the control activity u slightly decreases (by 0.04 points) in the post-transition range. This suggests that the subjects who participated in the experiment adjusted their strategy once the controlled dynamics transitioned. However, the model was not able to capture this human adaptive behaviour. On the other hand, the mean VAF values for the model output M are higher in the post-transition phase compared to the pre-transition phase. This indicates that the single integrator (DYN 1) is modeled better, which is consistent with the steady-state cases, where DYN 1 had higher VAF values compared to DYN2 (see Section IV). One method to improve the quality-of-fit results would be to incorporate time-varying rather than constant parameters of the human operator limitations, i.e., effective time-delay τ_e and neuromuscular dynamics. This is discussed further in Section VII.

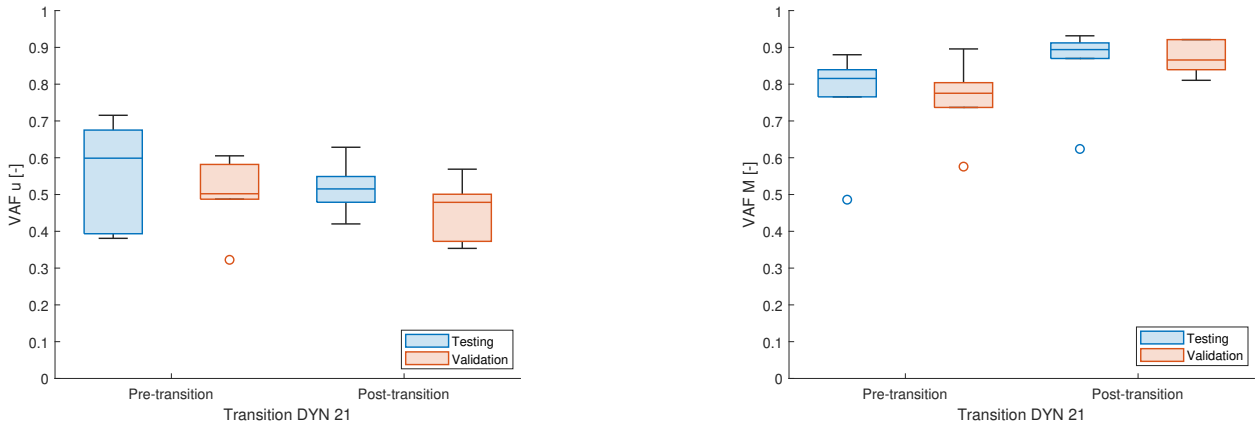

(a) (b)

Fig. 25. VAF results for condition DYN 21 for (a) Control activity u, (b) model output M

TABLE XI
MEAN VALUES FOR VAF IN DYN 21 CONDITION

Dataset	Control Activity (u)		Model Output (M)	
	Pre-transition	Post-transition	Pre-transition	Post-transition
Testing (n = 6)	0.56	0.52	0.77	0.85
Validation (n = 6)	0.50	0.46	0.76	0.87

VII. DISCUSSION

This research focuses on obtaining a better understanding of the adaptive human control through the use of a model that predicts *how* the human operator adapts to changes in the CE dynamics in a pursuit tracking task. This model is the one developed by Hess [13] [14] [11]. However, this model has several limitations. Therefore, the aim of this research was to extend the framework underlying Hess' model and validate it using experimental data.

Initially, to obtain a better understanding of the applicability of the model, it was successfully replicated as shown in Section II-B. The remaining work, necessary to accomplish the aim of this research, was broken down into four steps as described in Section III.

In the first step, Steady-State Modeling, the sensitivity analysis allowed for hypotheses to be made for the time-varying conditions: for condition DYN 12 it was expected that, after transition, K_p would decrease and K_r would increase, with the opposite outcome for DYN 21. The second step, Parameter Estimation, allowed for the human operator gains to be tuned to approximate human adaptation from the experimental data. Results from the estimated human operator gain values were consistent with the findings of the first step.

The second step resulted in the steady-state quality-of-fit results expressed through the VAF. The median VAF values for the control activity u were found to be 0.63 and 0.5 for conditions DYN 1 and DYN 2, respectively. A previous study which used the same experiment data reported median VAF values to be 0.64 and 0.75 for conditions DYN 1 and DYN 2, respectively [16]. While the VAF results for condition DYN 1 are almost identical, the VAF results for condition DYN 2 are significantly lower for this model. This contradicts previous research where lower VAF values are reported for DYN 1 compared to DYN 2 [15]. These differences in results may stem from the fact that, in this model, the human operator's limitations, i.e., effective time-delay τ_e and the neuromuscular dynamics, remained constant over time. These parameters affect the open-loop stability characteristics. Previous research found that these parameters may be considered constants when controlling dynamics equivalent to those used in this paper (DYN 1 and DYN 2) [15] [22]. Nevertheless, an investigation should be performed to find out to what extent this would improve the quality-of-fit of the model. Therefore, in addition to the human operator gains K_p and K_r, the parameters τ_e, ω_{nm} and ζ_{nm} also need to be determined in the parameter estimation step. This would result in a more accurate and complete estimation of the human operator, which could improve the results of both the steady-state and time-varying conditions.

One of the most significant limitations of the original Hess' model is that it does not incorporate the human time-delay. Therefore, in the third step, Sensitivity Analysis, an analysis was conducted to investigate the effects of time-delay on the adaptive model, for both steady-state and time-varying conditions. This research allowed for the implementation of a constant time-delay in the model. Additionally, it was demonstrated that introducing time-delay in the model affects the strength of adaptation. Consequently, adaptation constants were introduced to account for overreaction in the model. These constants were selected based on the results of the experiment for each participant. A more sophisticated approach would be for the model to determine these values while the simulations take place, based on the tracking performance and open-loop stability of the human operator.

Moreover, the results from the sensitivity analysis of the filter $J(s)$ showed that the rate of change of the human operator gains is step-like when the system dynamics transition in the DYN 12 condition. However, this result is only based

on one participant. While previous studies showed that the transition in the human operator gains is indeed instantaneous, further research is required to model the rate of change more accurately [15].

The fourth step, Model Validation, presented the results of the time-varying conditions. In the condition DYN 12, for the participants where the Triggering was activated, the hypothesis from the steady-state analysis was proven to be correct. The human operators generate more lead (K_r increases) for double integrator controlled dynamics, and to maintain open-loop stability decrease K_p. This implies that the model is able to capture this adaptive human behaviour. Furthermore, analysis of the control strategy of each participant showed that Triggering activation depends on the tracking performance in the pre-transition phase. Control strategy of subjects with low-gain and high tracking error resulted in the Triggering mechanism not being activated. This suggest that this model is sensitive to the tracking performance in the pre-transition phase, requiring low tracking error and higher crossover frequencies ($\omega_c > 0.9$ rad/s).

Lastly, results for the DYN 21 time-varying condition showed that the model is not able to capture this change in human behaviour. This was anticipated, as other models have also shown to have difficulties capturing this transition [16]. In addition, this model was not originally designed to capture transitions which result in more easily controllable dynamics [13]. The mean VAF values of the control activity u show that the quality-of-fit accuracy decreases by 8% for the post-transition range relative to the pre-transition range and for both testing and validation data-sets. This implies that the participants change their control strategy once the system dynamics change, and the model is unable to capture this. Further analysis is needed to determine to what extent the participants still generate lead once the CE dynamics change.

VIII. Conclusion

This paper presents the analysis, modification and validation of a previously proposed model of the human adaptive behaviour for time-varying dynamics in a pursuit tracking task.

Experimental data was used to parameterize the model, where the human operator gains were estimated for each participant. Based on the results from the steady-state system, the adaptive rules of the original model were modified and several simplifications were made. This allowed the adaptive logic of the model to work for the time-varying conditions. A sensitivity analysis was performed to obtain a better understanding and tune the parameters of the adaptive logic, which allowed for the inherent time-delay of the human operator to be implemented in the model.

The results from the condition where the controlled dynamics varied from a single to a double integrator showed that when Triggering was activated, the model accurately predicts the transient control behaviour of the participants. Whenever Triggering was not activated, VAF results for the pre-transition phase were 30 % lower than when Triggering was activated. The control strategy of each participant influences whether Triggering will activate, with activations occurring for participants with crossover frequency larger than 0.9 rad/s in the pre-transition phase. The model was not able to capture the change in control behaviour for transitions from double to single integrator dynamics, where the adaptive logic of the model was not triggered.

Overall, this research resulted in a more representative model of the human adaptive behaviour, implemented with the inherent human time-delay and, for the first time, this model was validated using experimental data.

References

[1] IATA, "Loss of control in-flight (loc-i)." [Online]. Available: https://www.iata.org/en/programs/safety/loss-of-control-inflight/

[2] Tohidi, S.S. and Yildiz, Y., "Adaptive human pilot model for uncertain systems," in *2019 18th European Control Conference (ECC)*. IEEE, 2019, pp. 2938–2943, doi:10.23919/ECC.2019.8795847.

[3] Stern, E., "Individual differences in the learning potential of human beings," *npj Science of Learning*, vol. 2, no. 1, pp. 1–7, 2017.

[4] Young, L.R., "On adaptive manual control," *Ergonomics*, vol. 12, no. 4, pp. 635–674, 1969.

[5] Mulder, M., Pool, D.M., Abbink, D.A., Erwin R.B., Zaal, P.M.T., Frank M.D., van der El, K., and van Paassen, M.M., "Manual control cybernetics: State-of-the-art and current trends," *IEEE Transactions on Human-Machine Systems*, vol. 48, no. 5, pp. 468–485, 2018, doi:10.1109/THMS.2017.2761342.

[6] McRuer, D.T. and Jex, H.R., "A review of quasi-linear pilot models," *IEEE Transactions on Human Factors in Electronics*, no. 3, pp. 231–249, 1967, doi:10.2514/6.2010-8092.

[7] Mulder, M., Pool, D.M., Van der El, K., Drop, F.M., and Van Paassen, M.M., "Manual control with pursuit displays: New insights, new models, new issues," *IFAC-PapersOnLine*, vol. 52, no. 19, pp. 139–144, 2019, doi:10.1016/j.ifacol.2019.12.125.

[8] Stark, L. and Young, L.R., "Biological control system-a critical review and evaluation, developments in manual control," 1965.

[9] Miller, D.C. and Elkind, J.I., "The adaptive response of the human controller to sudden changes in controlled process dynamics," *IEEE Transactions on Human Factors in Electronics*, vol. HFE-8, no. 3, pp. 218–223, 1967, doi:10.1109/THFE.1967.233971.

[10] Phatak, A.V. and Bekey, G.A., "Model of the adaptive behavior of the human operator in response to a sudden change in the control situation," *IEEE Transactions on Man-Machine Systems*, vol. 10, no. 3, pp. 72–80, 1969, doi:10.1109/TMMS.1969.299886.

[11] Hess, R.A., "Modeling human pilot adaptation to flight control anomalies and changing task demands," *Journal of Guidance, Control, and Dynamics*, vol. 39, no. 3, pp. 655–666, 2016, doi:10.2514/1.G001303.

[12] Young, L.R., Green, D.M., Elkind, J.I., and Kelly, J.A., "Adaptive dynamic response characteristics of the human operator in simple manual control," *IEEE Transactions on Human Factors in Electronics*, vol. HFE-5, no. 1, pp. 6–13, 1964, doi:10.1109/THFE.1964.231648.

[13] Hess, R.A., "Modeling pilot control behavior with sudden changes in vehicle dynamics," *Journal of Aircraft*, vol. 46, no. 5, pp. 1584–1592, 2009, doi:10.2514/1.41215.

[14] Hess, R.A., "A model for pilot control behavior in analyzing potential loss-of-control events," *Proceedings of the Institution of Mechanical Engineers, Part G: Journal of Aerospace Engineering*, vol. 228, no. 10, pp. 1845–1856, 2014, doi:10.1177/0954410014531218.

[15] Zaal, P.M.T., "Manual control adaptation to changing vehicle dynamics in roll-pitch control tasks," *Journal of Guidance, Control, and Dynamics*, vol. 39, no. 5, pp. 1046–1058, 2016, doi:10.2514/1.G001592.

[16] Terenzi, L., Zaal. P., Pool D.M., and Mulder M., "Adaptive manual control: a predictive coding approach," in *AIAA SCITECH 2022 Forum*, 2022, p. 2448, doi:10.2514/6.2022-2448.

[17] van Ham, J., "Predicting adaptive human control behavior to changing controlled element dynamics based on statistical variations in error and error rate," *MSc Thesis*, 2021.

[18] van der El, K., "How humans use preview information in manual control," *PhD Thesis*, 2018.

[19] Hess, R.A., "Effects of time delays on systems subject to manual control," *Journal of Guidance, Control, and Dynamics*, vol. 7, no. 4, pp. 416–421, 1984, doi:10.2514/3.56380.

[20] van der El, K., Pool, D.M., Damveld, H.J., van Paassen, M.M., and Mulder, M., "An empirical human controller model for preview tracking tasks," *IEEE Transactions on Cybernetics*, vol. 46, no. 11, pp. 2609–2621, 2015, doi:10.1109/TCYB.2015.2482984.

[21] Plaetinck W., Pool D.M., van Paassen M.M., Mulder M., "Online identification of pilot adaptation to sudden degradations in vehicle stability," *IFAC-PapersOnLine*, vol. 51, no. 34, pp. 347–352, 2019, 2nd IFAC Conference on Cyber-Physical and Human Systems CPHS 2018. [Online]. Available: https://www.sciencedirect.com/science/article/pii/S2405896319300229

[22] Zolner, H., Daan P.M., Damveld H., van Paassen, M.M., Mulder, M., "The effects of controlled element break frequency on pilot dynamics during compensatory target-following," in *AIAA Modeling and Simulation Technologies Conference*, 2010, p. 8092, doi: 10.2514/6.2010-8092.

Part II

Preliminary Thesis Report

N.B.: This part has been graded under AE4020 Literature Study

1

Introduction

Transportation has played a critical role in the development of civilizations and improving the welfare of societies. The importance of transportation is vital to economic, political, social and environmental aspects, with humans being responsible for controlling these vehicles. Understanding *how* humans control vehicles allows for safer and improved vehicle design [1]. Therefore, throughout the years research has been conducted in the field of manual control. This enables us to understand and describe how humans control vehicles through the use of mathematical models [2]. Examples of such models include the crossover model, developed by McRuer and Jex; which describes how the human operator adapts to the dynamics of the system under control [3]. This model serves as the basis for understanding pilot control behavior.

In aviation, Loss of control (LOC) incidents are a notorious problem and are one of the most significant contributors to fatal accidents [4]. In order to investigate these events, it is important to understand the pilot's control behaviour in response to sudden changes in the vehicle dynamics. Nevertheless, humans have unique adaptive behavior abilities which allows them to lessen the effect of these incidents; thereby becoming essential elements of many control systems [5]. Understanding how pilots adapt their control strategy to maintain stability has several advantages. Technologies such as autopilots and automatic landing systems rely on the pilot's adaptive capabilities to quickly adjust their control strategies when detecting failures. Therefore, modeling human's adaptive behaviour does not only improve automation, but may improve training procedures and in turn increase safety in aviation.

While several researchers have investigated the human's adaptive behavior, theoretical framework on what *triggers* human adaptation is lacking. In other words: When does the pilot perceive that the dynamics of the system are changing, triggering the pilot to adapt? Therefore, the main research question of this thesis is:

What triggers humans to adapt to changes in controlled element dynamics, and how can the behaviour of an adaptive human pilot be modelled, for a pursuit tracking task?

In order to answer this question, research will be carried out into the current state-of-the-art models which represent the human adaptive behaviour. Here, the main goal is to focus on the phases of adaptation: detection, identification and modification [6]. While the goal is to obtain a model which captures these phases, special attention will be given to the detection phase, with the aim to gain insight into which factors influence human adaptation. Consequently, the next phase of the preliminary thesis will be recreating an existing model based on the literature review; performing simulation-based analysis

of the human adaptive behaviour. This will be done in order to later validate the model through the use of experimental data, which will allow for improvements and modifications to the model. Ultimately, the goal of this thesis is to create a more complete model of the time-varying human adaptive behaviour in the field of manual control.

This report is structured as follows: Chapter 2 serves as an introduction to understanding human pilot adaptation and control behaviour through an overview of theory in manual control. Chapter 3 summarizes the current state-of-the-art models representing the human adaptive behaviour. Then, Chapter 4 describes how one of the models from Chapter 3 is replicated, in order to attain a better understanding of the human adaptive behaviour; it also provides a comparison between the original results of the model and the results obtained through the replicated model. Following that, Chapter 5 provides a sensitivity analysis of the model. In addition, Chapter 6 outlines the future developments of this research. Lastly, the conclusion of this preliminary research can be found in Chapter 7.

2

Manual Control Behaviour

In 1940, Koppen concluded that to design an aircraft effectively, the designer must have knowledge of how the human pilot interacts with the aircraft [7]. Research in the human control activity of vehicles is essential, as it contributes to understanding how pilots control aircraft. Having a model which represents the control behaviour of the human pilot enables designers to analyze certain characteristics of the Pilot-vehicle system (PVS), which is vital to understanding Aircraft-pilot coupling (APC) events. One of the most common APC events is Pilot-induced oscillations (PIO), which originates from anomalous interactions between the aircraft and pilot. Therefore, in manual control, human pilot models are essential for flight safety.

This chapter serves as an introduction towards understanding adaptation and the control behaviour of the human pilot. Additionally, the current approaches to modeling pilot behaviour are reviewed. The final section of this chapter focuses on the different display modes in manual control models which are responsible for how the human pilot interprets information during a tracking task.

2.1. Phases of Adaptation

Human's have an exceptional ability to adapt and react to the environment they are exposed to, through learning and associations between the stimuli and their responses [8]. In fact, pilot capabilities to detect failures and their ability to rapidly adapt are the primary reasons that vehicles are not fully autonomous [9]. One of the first reported experiments on the adaptive human behaviour was performed by Young *et al.* in 1964 [6]. In this experiment, the adaptive human behaviour was investigated following sudden changes in the Controlled Element (CE) dynamics for a compensatory tracking task. One of the most important conclusions that was drawn from this experiment was that the adaptation process should be considered in three phases, namely: detection, identification, and adjustment. The adjustment phase is also referred to as the modification phase.

The first phase, detection, is defined as the recognition that a change has occurred in the system. In the experiment performed by by Young *et al.*, in this phase the human controller detects the change in CE. Once the change is detected, the next phase is identification, where the human controller has to identify the nature of the change in order to determine a new strategy to control the change. In this phase, the human controller identifies the new CE dynamics. Lastly, the third phase, adjustment, is where the human controller adjusts their control strategy to the new CE dynamics. This phase also involves reducing errors which may have evolved in the process of adaptation [6].

2.2. Human Pilot Control Behavior

Rasmussen proposed a framework, visualized in Figure 2.1, that captures the nature of the pilot control behavior. Here, three levels of processing are distinguished, reflecting the cognitive levels of human behaviour [10]. The lowest level, *skill-based behaviour*, represents the sensory-motor performance, where tasks by the human are performed without conscious control. The second level is the *rule-based behaviour* which represents human behaviour that is based on rules or procedures which may have been derived from previous experience or instructions. Lastly, *knowledge-based behaviour* occurs during unfamiliar situations when the human cannot rely on rules. Thus, in this level the human uses high-level cognitive problem-solving skills, where the human devises a plan either physically (through trial and error), or conceptually (by predicting the outcome of his/her actions).

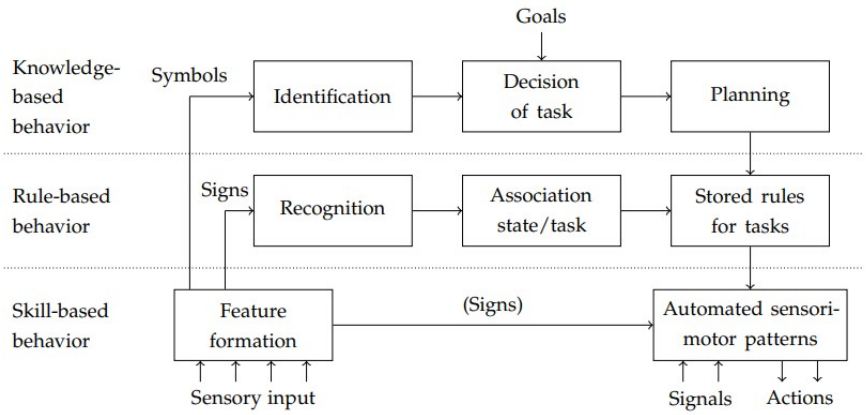

Figure 2.1: Levels of human pilot control behavior [10]

As Rasmussen states, there is no distinct boundary between skill-based and rule-based performance as it is dependent on the level of training of the pilot. However, skill-based performance is when the person is unable to describe on what information he/she bases his/her control strategy. In this level, the human pilot perceives sensory information as signals through different senses (input), with the motor performing an action through the limbs (output). This is termed as sensorimotor processing, which is the process by which sensory information (inputs) are coupled with the motor response (output) in the Central Nervous System (CNS) [11]. The three levels of behaviour are all relevant for the phases of adaptation during system failure tasks where detection is skill-based, identification is rule-based, and adjustment is knowledge-based [12]. Adaptation of the pilot due to a change in the vehicle dynamics occurs in the detection phase of adaptation, as skill-based behaviour where sensorimotor control takes part. This is because stimuli provoke the human pilot to adapt his/her control behaviour, where the adaptation is mostly unconscious. The human pilot can perceive sensory input through various senses such as: visual, auditory, tactile, vestibular and proprioceptive. As the human controls the vehicle, he/she can also sense the inputs the pilot exerts on the vehicle as *feedback*. Moreover, the human pilot has an *internal model* of the task which is constructed through experience from training and knowledge of the vehicle. The CNS develops this model as an internal representation which consists of the following elements [13]:

- General knowledge of the vehicle behaviour such as structure and parameter values
- Knowledge of how disturbances influence the vehicle
- Knowledge of the task being performed, which includes goals to be achieved, task instructions, signals displayed, etc.

Having a clear understanding of the vehicle dynamics and thus a precise internal model would allow for more efficient interactions with the vehicle and the external world.

2.3. Pilot-Vehicle System Modeling

Tustin [14] and Elkind [15] were one of the pioneer researchers into manual control behavior for tracking tasks. Their research led to more elaborate analysis and models of the manual control behavior for *compensatory* tracking tasks. Later, in the 1960's, one of the most famous model of the human manual control was established by McRuer *et al.* [16], known as the *crossover model*. This model is termed the classical approach to defining mathematical models, employing the frequency-domain synthesis where variables that are described in the time domain are transformed into the frequency domain [17].

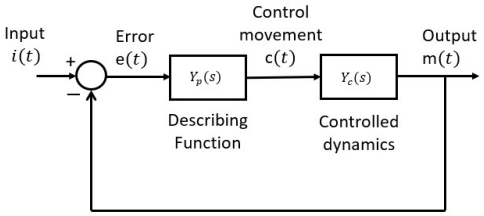

Figure 2.2: Control diagram of a tracking task

Figure 2.2 shows a typical control diagram for compensatory tracking task. In this figure, $Y_p(s)$ and $Y_c(s)$ represent the transfer functions of the pilot control dynamics and of the system to be controlled, respectively. The key element established from this model is that the human controller can *adapt* his/her own control behavior to the dynamics of the systems which is being controlled. Equation (2.1) describes the essence of the model where the dynamic characteristics of the open-loop response of the system near the crossover frequency ω_c (i.e., where $|Y_{OL}(j\omega)|_{\omega=\omega_c} = 1$) are described by:

$$Y_{OL} = Y_p(j\omega)Y_c(j\omega) = \frac{\omega_c}{j\omega}e^{-j\omega\tau_e} \tag{2.1}$$

McRuer proposed several formulations for the pilot control dynamics $Y_p(s)$. The simplest of which, the simplified precision model, is given by:

$$Y_p(s) = K_p\frac{1+T_Ls}{1+T_Is}e^{-j\omega\tau_e} \tag{2.2}$$

In this equation, T_L and T_I represent the lead and lag equalization parameters, respectively, which are adjusted by the pilot to achieve a single integrator open-loop frequency response, while the gain K_p is adjusted in order to place the crossover frequency ω_c where necessary. Lastly, the parameter τ_e represents the effective time delay due to lags in processing information. Note that for simplicity this model only focuses on the linear portion of the pilot control dynamics $Y_p(s)$. The non-linear and time-varying behaviour of the pilot was not captured, however, this is typically modeled through a remnant which is an approach called quasi-linear modeling [3].

A different approach to modeling the pilot behaviour was proposed by Kleinman *et al.* called the Optimal Control Model (OCM), which was developed the 1970s [18]. The model is based on estimation theory and assumes that the human can be modelled as a motivated, goal oriented controller who behaves in an optimal manner by minimizing a defined cost function. The general structure of the model is shown in Figure 2.3 where the limitations of the human are also evident through the time delay and the neuromuscular dynamics. The Kalman filter is used to estimate the human's deduction of system states from the information displayed, while the Kalman predictor models the human's compensation for the human's inherent time delay. Then optimal control $u_c(t)$ is achieved through an optimal feedback law.

Both types of modeling approaches can achieve equivalent results [20]. However, as Mulder *et al.*

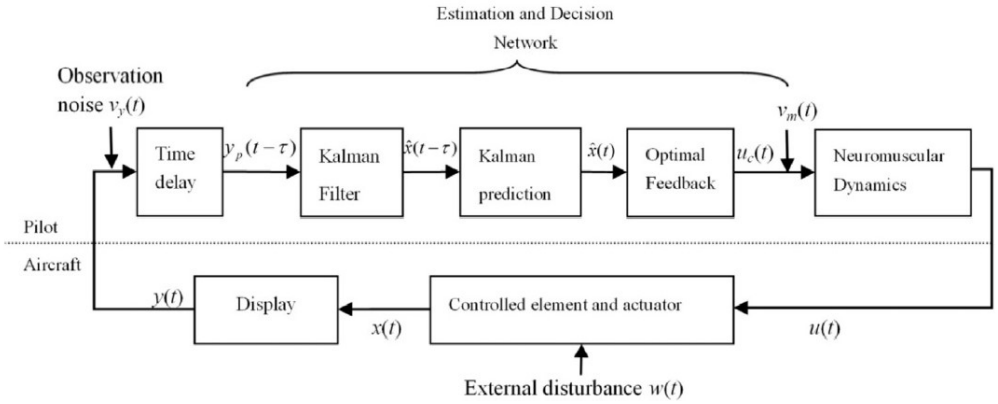

Figure 2.3: Model of optimal human behaviour [19]

stated the classical approach is preferred over the optimal control models. Optimal control models are more complex and over-parameterized [2].

2.4. Display Types

Display refers to the (visual) representation of any available source of information. The human controller (HC) can infer information differently, depending on the nature of how it is presented. In manual control a tracking task can be commonly visualized through a compensatory, pursuit or a preview display. A preview display is outside the scope of this project and will not be discussed.

In a compensatory tracking display, illustrated in Figure 2.4(a), only the current error $e(t)$ is presented to the HC. As shown in the control diagram for compensatory tracking in Figure 2.5(a), the error $e(t)$ is the difference between the systems response $x(t)$ and the target $f_t(t)$. During this tracking task, the HC *compensates* for the error by moving the control stick in the direction such that the error is nullified.

In a pursuit tracking display, illustrated in Figure 2.4(b), the target $f_t(t)$, the error $e(t)$, and the CE output $x(t)$ are visually represented. This yields three describing functions in the model as shown in Figure 2.5(b). In this control task, the HC *pursues* the target by moving the control stick such that it coincides with the target.

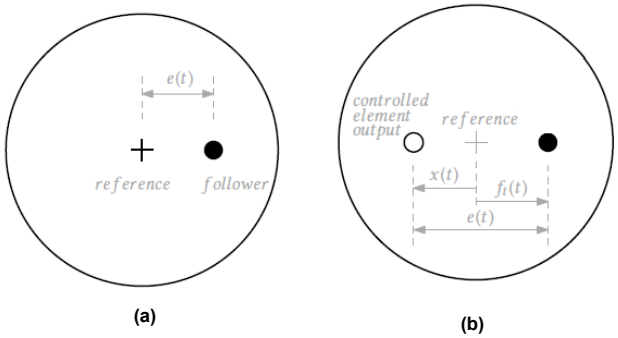

Figure 2.4: Compensatory display (a) and pursuit display (b) [21]

In cybernetic theory, the compensatory tracking task is predominantly used, as it is simpler to model and is more restrictive, forcing the HC to react on statistical characteristics of the error [2]. Additionally, this is the only display where we know what the human is looking at, i.e., the error. On the other hand, in a pursuit task, the HC has a greater opportunity to recognize characteristics from the target $f_t(t)$ and observe his/her own response through the output x and even its first derivative $\dot{x}$. However, it is important to mention that while the HC has three variables visually presented, this does not imply

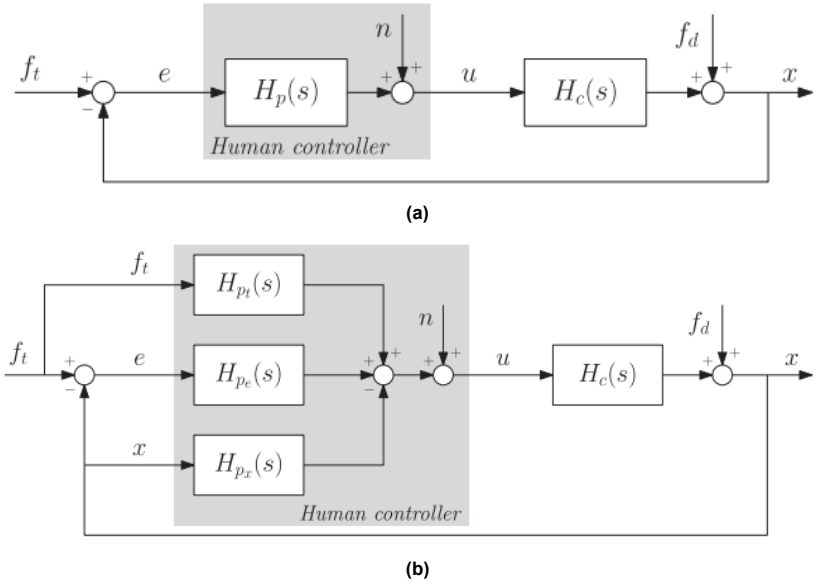

Figure 2.5: Control diagrams for compensatory tracking (a) and for pursuit tracking (b) [2]

that he/she will make use of all the variables during a tracking task. Moreover, previous studies have shown that when tracking a single integrator, both compensatory and pursuit displays yielded equivalent performance results. However, when tracking a double integrator, pursuit displays are superior as they yield lower error scores [22] [23] [24]. In addition, pursuit displays are preferred by pilots as explicit information permits them to establish stable performance more efficiently [25]. However, a consensus on a mathematical model which captures human behaviour in a pursuit tracking task has not been reached. Nevertheless, as described in [26] the model developed by Van der El *et al.* [21], also shown in Figure 2.5(b), shows promising results as a generic crossover-model-like alternative for a pursuit tracking task.

2.5. Conclusions

The aim of this chapter was to introduce research in the field of manual control which shows that humans have an extraordinary capabilities to detect failure and adapt to rapidly changing vehicle dynamics. This chapter showed that the adaptive human behaviour can be considered in three phases, namely: detection, identification, and modification. Therefore, a human adaptive model should capture these phases. Additionally, according to the framework proposed by Rasmussen, the three levels of behaviour are all relevant for the phases of adaptation, where detection is skill-based, identification is rule-based, and modification is knowledge-based behaviour. When designing a model of the human adaptive behaviour, the detection phase should give an insight on what *triggers* the HC to adapt. During this phase it is proposed that the CNS of the HC has an internal model, constructed through experience from training and knowledge of the vehicle, of the task which is being performed, enabling the HC to adapt when required. Furthermore, theory from the crossover model should be used to validate the designed model, through checking whether the open-loop (Y_pY_c) for pre- and post-transition parameters are integrator like in the region of the crossover frequency. Verification should be conducted on whether the crossover frequency and phase margin data are comparable to results of available literature. Lastly, research into different display models showed that the HC infers information differently depending on the nature of how it is presented. Since in a pursuit display the HC can recognize characteristics from the target signal and observe his/her own response, it is superior to the compensatory display if the HC makes use of all the variables displayed. In order learn how to implement this theory into a model the next chapter investigates the current literature available on state-of-the-art models that predict HC adaptation.

3

Models of Human Adaptive Behaviour

The human controller has to control the aircraft while the dynamics of the vehicle may vary with time. As described by Hess, this variation can occur naturally through changes in the aircraft flight condition. However, it can also be deliberately induced by changes in the controlled system itself. For example, due to control system or structural aircraft damage, that affect the system's stability. The study of how the human pilot is able to accommodate these changes is the study of the *adaptive human pilot* [27].

As discussed in previous chapters, there are different factors that trigger the human controller to adapt. Consequently, Young [9] defined four adaptive functions which are responsible for human adaptation in manual control, these are visualized in Figure 3.1. The first adaptive function is *Input Adaptation and Prediction* which pertains to the capabilities of the humans to recognize patterns in the input signal, such as periodicity. Additionally, Elkind found that the control strategy of the human controller is also dependent on the bandwidth of the input signal, thus influencing adaptation [15].

The second adaptive function, *Controlled Element Adaptation*, refers to the ability of the human controller to adapt to changes in the system dynamics. Rapid changes in the CE dynamics are associated with sudden failures in the system, while slowly varying dynamics can be associated with variations in aircraft handling qualities, for example with changes in altitude.

The third adaptive function, *Task Adaptation*, refers to optimization of the control loop based on an objective. For instance, if the objective of the task is to minimize error, then the human controller has a different control strategy when compared to an objective to minimize the control effort. Lastly, the fourth adaptive function, *Programmed Adaptation*, is based on the fact that the human controller can employ a certain control strategy based on knowledge of the environment. For example, from knowledge and experience the human controller adopts a different control strategy on a slippery road compared to a dry road.

In order to narrow down the scope of the project, the main focus of the thesis will be on adaptation due to sudden changes in the CE dynamics. This is because failure in the system can be replicated through this adaptive function and previous research has focused on this type of adaptation in the field of manual control, in particular in the section of Control and Simulation at TU Delft. The advantage on focusing on a well established field of research is that experimental data and theoretical models already exist, which allows for comparison, evaluation, and validation of the results.

3.1. Review of Past Research

In the past, some research has been carried out focusing on creating qualitative and quantitative mathematical models, which predict how the human pilot would adapt to changes in the vehicle dynamics.

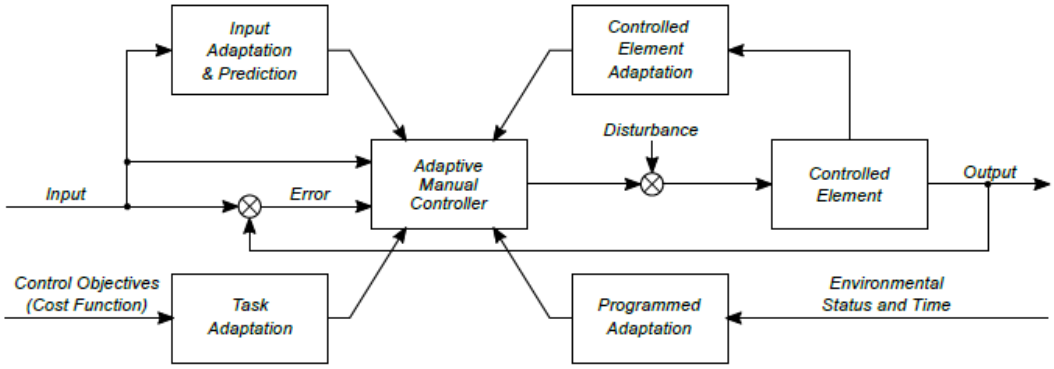

Figure 3.1: Adaptive Functions in Manual Control [9]

These are outlined below.

3.1.1. Young and Stark Model

In 1965, Young and Stark developed a model reference approach, visualized in Figure 3.2 to describe how humans adapt during a tracking task [28]. This model is based on characteristics present in biological systems: an internal model. The solid lines in the model represent a conventional closed loop control diagram for a compensatory tracking task, while the dotted lines correspond to the hypothetical paths of the adaptive process. The internal model is based on the idea that the human controller has a reference model of the system being controlled, and uses this reference model to make predictions about the dynamics of the system. This reference model is represented by the ”Model of the Controlled Element” block, which Young *et al.* call the *heart* of the scheme.

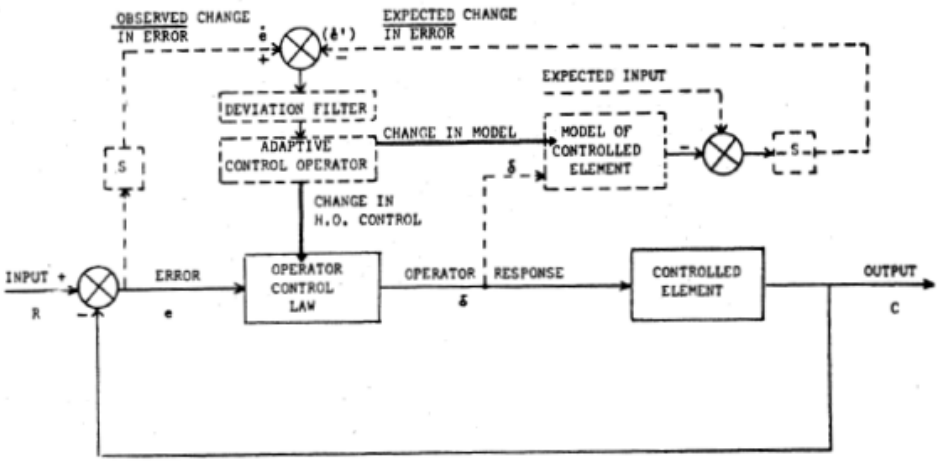

Figure 3.2: The model representing manual adaptive control for compensatory tracking [28]

Adaptation is triggered when the error between the expected (from the internal model) and the actual change in error significantly differ. This is done through the use of a ”deviation filter” which rejects insignificant deviations and passes significant deviations. If significant deviations are filtered, then the ”adaptive control operator” changes the control strategy in order to compensate for assumed changes in the CE dynamics.

The disadvantage of this model is that it is conceptual, and only represents a schematic of the adaptive process. Therefore, a method to implement the internal model is not defined and no definition on what significant differences in deviation filter is specified. In 1977, Veldhuyzen *et al.*, developed a similar

model where the structure of the internal model as well as the decision making element (deviation filter) is described [13]. However, the focus of the concept is modeling human control of large ships.

Furthermore, Young and Stark conducted an experiment with a compensatory tracking task, where the participants were asked to control and indicate (through pressing a button) when they detect a change of CE dynamics. The participants were divided into three groups, namely: active controller, inactive controller and passive monitor as visualized in Figure 3.3.

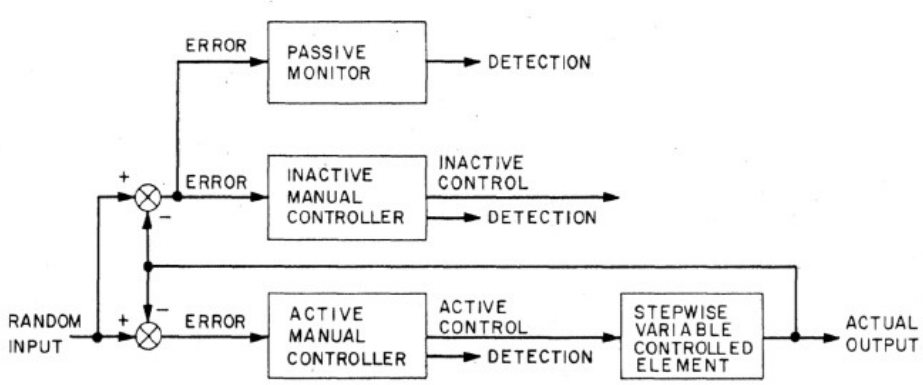

Figure 3.3: Scheme of experimental conditions [9]

The first group, active controller, actively controlled the system. The second group, inactive controller, initially controlled the system. However, after a certain time, without being informed, their output was disconnected and were shown the error generated from the active controller. Where as the third group, passive monitor, only observed the error.

Table 3.1 shows the results of the experiment where the time of detection (in seconds) of change in CE dynamics is presented for the participates. The results show the transitions in CE dynamics from a single integrator (SI) to a double integrator (DI), and vice-versa. From the results it can be observed that detection for the passive monitor is significantly slower compared to the two other participant groups. The passive monitor group only observed the error and did not actively engage in controlling the system. These results imply the passive monitor has a significant delay in detection due to lack of knowledge of the system which alludes to the absence of the internal model of the dynamics of the controlled system. Therefore, the importance of this experiment is that it highlights the role of internal models in motor control tasks.

Table 3.1: Results of experiment, showing time for the detection of change in CE dynamics

	Transition in CE dynamics	
Participant Group	**SI to DI [sec]**	**DI to SI [sec]**
Active Controller	1.36	1.23
Inactive Controller	1.56	1.45
Passive Monitor	5	2.48

3.1.2. Miller and Elkind Model

In 1967, Miller and Elkind, developed a model of the adaptive response of the human controller for the compensatory tracking task as evident from Figure 3.4 [29]. This model is based on a statistical analysis of when the human controller detects a change. Similarly to the model of Young *et al.*, Miller *et al.* use the idea that human controller has an internal model of the controlled process which they call a mental model. Thus, detection of change in the CE dynamics occurs when there is a large difference between the error rate that the human *expects* (from the mental model) and the error rate that the human controller *observes* (from the display).

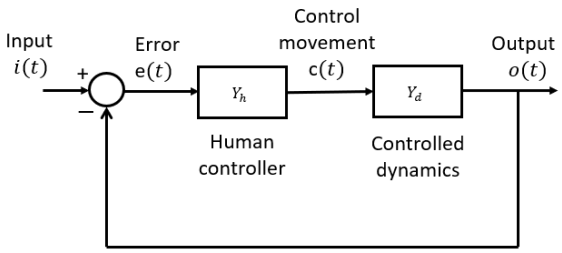

Figure 3.4: Block Diagram of the system [29]

For this model, Miller *et al.* considered a controlled element with transfer function which is a single integrator i.e., $Y_d = \frac{K_d}{s}$. Then the following manner is used to calculated the observed error rate. From the control diagram shown in Figure 3.4, Equation (3.1) and Equation (3.2) can be inferred.

$$e(t) = i(t) - o(t) \tag{3.1}$$

$$\frac{do(t)}{dt} = K_d c(t) \tag{3.2}$$

These two equations can be combined to formulate the observed change in error rate as shown below, given that the control dynamics are time-invariant over an interval of time.

$$\Delta\frac{de}{dt} = \Delta\frac{di}{dt} - K_d\Delta c \tag{3.3}$$

Then Miller *et al.* define the expected error rate as:

$$\widehat{\Delta\frac{de}{dt}} = -K_m\Delta c \tag{3.4}$$

In this equation, K_m represents the gain of the controller's mental model of the controlled process. Note that $\Delta\frac{di}{dt}$ is not part of this equation as in Equation (3.2), because the target is unpredictable. Additionally, the difference between the two error rates is called the discrepancy: $\Delta\epsilon$

As mentioned above, according to Miller *et al.* detection occurs when the difference between the observed change in error rate $\Delta\frac{de}{dt}$ and the expected change in error rate $\widehat{\Delta\frac{de}{dt}}$ is large relative to its time invariant standard deviation $\sigma_{\Delta\epsilon}$. This large difference is defined by Miller *et al.* through an acceptability limit. Therefore, detection occurs when the acceptability limit (C) is exceeded. In mathematical terms this is formulated as:

$$C = \frac{\Delta\epsilon}{\sigma_{\Delta\epsilon}} = \frac{[-K_m\Delta c] - [\Delta(di/dt) - K_d\Delta c]}{\sqrt{(\Delta c)^2\sigma^2_{(K_m - K_d)} + \sigma^2_{\Delta(di/dt)}}} \tag{3.5}$$

The disadvantage of this model is that it cannot be applied to higher than first order CE dynamics.

3.1.3. Phatak and Bekey

In 1969 Phatak and Bekey proposed a model for compensatory tracking which captures the human adaptive process called the 'Supervisory Control Model' illustrated in Figure 3.5 [30], [31], [32]. Phatak

et. al based the model on knowledge that the human operator detects failure based on large differential change of the error and error-rate. Through an internal mode, the human operator has knowledge of the nominal error values for the pre-failure system dynamics; once these values exceed a certain limit, defined through decision limits, the human operator is triggered to adapt the control strategy [31]. This process is repeated over a series of decision limits with boolean conditions, where if the condition is met the human operator dynamics are adapted, and re-evaluated for the next decision limit. This is done continuously to adapt to the current CE dynamics until suitable operator dynamics are reached.

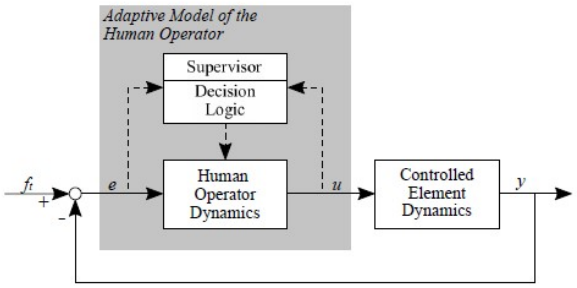

Figure 3.5: Structure of the human-operator adaptive model [33] [30]

A recent study performed by Van Ham *et. al.* at the Control and Simulation department of TU Delft [33], investigated whether the limits of the first decision region proposed in the *supervisory control algorithm* are also applicable to CE dynamics different to the ones used in the original research [30]. The results of this study showed that the original limits proposed for the algorithm, do not apply to different CE dynamics, thus new detection limits were required. Therefore, while this is a promising framework for modeling the human adaptive process, it is lacking standardized limits which do not need to be adjusted based on the CE dynamics used.

3.1.4. Hess Model

Lastly, the most recent model on the human adaptive behaviour was developed by Hess where the model uses a pursuit display [34], [35], [36]. The pilot model used is pursuit as it is assumed that the human controller can sense the output-rate, as opposed to compensatory models where the error-rate is distinctive. Hess' preliminary research into modeling detection indicated that the human controller has an internal model of the vehicle that is being controlled [27]. According to Hess, the internal model is described by the proprioceptive feedback signal and the pilot's direct inputs to the control stick. The proprioceptive signal, originating in the pilot's central nervous system (CNS), enables pilots to have senses of position and movement of their limbs [37]. Hess argues that this proprioceptive signal is proportional to the output rate of the system during a tracking task, where the output rate is observed by the pilot through the system's output. However, when the nominal CE dynamics changes, the relationship between the proprioceptive signal and the output rate is lost, which triggers the pilot to detect that the vehicle dynamics have changed, thus a new control strategy is necessary. This preliminary research motivated Hess to develop a model which captures the adaptation of the human pilot.

Figure 3.6 captures the structure of the adaptive model, which can be used for a single-axis tracking or could be modified to represent a multi-axis control task. As evident from the figure, the model is composed of two-loops, where the outer loop is a proportional controller (gain K_p) representing the position loop. In the inner loop the pitch and/or roll attitude are controlled, representing the rate loop (gain K_r) [38]. Hence, K_p influences how large the human control output is, while K_r influences the magnitude of its rate of change. The G_{nm} element represents the pilot's neuromuscular system which is a simplified model of the pilot's limb which creates the control inputs and is given by Equation (3.6). Additionally, the "limiter" element represents the physical limits in the actuator of the control stick. Hess argues that including the limiter makes the model more realistic. Moreover, the adaptation of the human pilot is represented through the "adaptive logic" element, where the output rate $\dot{M}$ and the R signals are fed into the adaptive logic. The underlying principle of the adaptive model is that adaptation of the

human pilot to changes in the CE occurs through modification of the inner loop gain K_r, while changes in the outer loop gain K_p provides improved tracking performance.

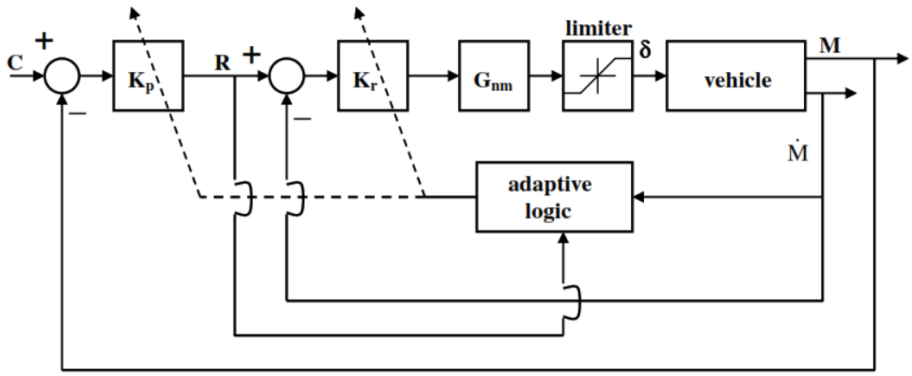

Figure 3.6: Adaptive model of the human pilot [34]

Detection of a change in CE dynamics is based on the sign and magnitude of the error signal in the inner loop, which is defined through a criterion signal x as shown in Equation (3.7). This equation denotes that x is proportional to the square of the error signal of the rate loop. The low-pass filter in this equation introduces smoothing and lags into the human adaptation process [36].

$$G_{nm} = \frac{10^2}{s^2 + 2(0.707)10s + 10^2} \tag{3.6}$$

$$x = \text{sgn}\{|R| - |\dot{M}|\} \cdot [|R| - |\dot{M}|]^2 \cdot \frac{1.5^2}{s^2 + 2(1.5)s + 1.5^2} \tag{3.7}$$

Note that due to an inconsistency in Hess's paper [36], the damping of the low-pass filter in Equation (3.7) slightly differs from the one repoted in Hess' paper. This was concluded after obtaining the actual model from Ronald Hess, as well as through comparison with his previous papers [34] [35].

Hess then defines a trigger function which determines whether adaptation is necessary which is described through Equation (3.8).

$$K_{\text{trigger}} = \begin{cases} 0 \text{ if the instantaneous value of } \sqrt{|x|} < 3 \cdot \text{rms}[\sqrt{|x|}] \text{ or } t < t_c \\ 1 \text{ if the instantaneous value of } \sqrt{|x|} \geq 3 \cdot \text{rms}[\sqrt{|x|}] \text{ or } t \geq t_s \end{cases} \tag{3.8}$$

In this equation, the square root of x, ($\sqrt{|x|}$), is used because the square of the error signal is used to obtain x as evident from Equation (3.7). Moreover, the expression $3 \cdot \text{rms}[\sqrt{|x|}]$ represents the acceptability limit, where the factor of 3 defines the lower limit of a trigger which alerts the human pilot that changes in the system are significant. Additionally, t_c represents the time in the simulation when the CE dynamics are changed and t_s represents a small time value such that transients in the initial simulation do not incorrectly trigger the adaptive logic.

The adaptive change of the inner loop gain K_r is given by Equation (3.9). Where the variable x_n is defined in Equation (3.10). In both of these equations, Hess uses a second order low-pass filter which, as mentioned above, introduces smoothing and lags into the adaptation process. In addition, N represents the number of response variables begin controlled by the pilot which is based on the principle that the pilot is less aggressive in multi-axis than in single-axis tasks. The variable, $rms(R^2)$, is obtained during nominal situation, where no system changes are present.

$$\Delta K_r = x_n K_{\text{trigger}} \cdot \frac{1}{(s^2 + 2s + 1)} \tag{3.9}$$

$$x_n = \frac{x}{\text{rms}\,[R^2]} \cdot \frac{1}{(s^2 + 2s + 1)} \cdot \frac{1}{N} \tag{3.10}$$

The last part of the adaptive logic is Equation (3.11) which is used to change the outer loop gain K_p. While ΔK_r can be decrease below its initial value, this equation denotes that ΔK_p cannot. Hess bases this relation under the reasoning that a reduction in K_r results in reduction in the outer loop, thus no change in K_p is required. However, when K_r is increased, a larger K_p is needed to compensate for a possibly lower phase margin [36].

$$\Delta K_p = \begin{cases} 0.35 \cdot \Delta K_r & \text{if } \Delta K_r > 0 \\ 0 & \text{if } \Delta K_r \leq 0 \end{cases} \tag{3.11}$$

The final modification of the adaptive logic is shown in Equation (3.12) where limits are placed on the K_p and K_r gains. K_{p-nom} and K_{r-nom} represent the initial values of K_p and K_r which are chosen for the nominal CE dynamics. These limits are included to make the model more realistic and are based on findings from a previous study [39].

$$\begin{aligned} |K_p|_{\text{max}} &= 2\,|K_{p-nom}| \\ |K_r|_{\text{max}} &= 10\,|K_{r-nom}| \end{aligned} \tag{3.12}$$

In addition, Hess showed the capabilities of the model through the use of computer simulations. For instance, Hess showed that the model is capable of handling tasks in which the controlled element resembles a pure integrator, a single integrator and a double integrator [34]. These controlled elements require the human operator equalization that ranges from a pure gain, to lead, and to lag.

Moreover, Hess performed a desktop human-in-the-loop tracking experiment in order to compare the results with the computer simulated pilot model. The experiment had one well-trained participant and was conducted for a single-axis control task with a compensatory display. This is different to the simulated pilot model which is based on a pursuit display. To quantify the quality of the simulated pilot model, the Variance Accounted For (VAF) was used, as shown in Equation (3.13).

$$\text{VAF} = 1 - \frac{\text{var}\left(\delta\,(t_i)_{\text{human}} - \delta\,(t_i)_{\text{model}}\right)}{\text{var}\left(\delta\,(t_i)_{\text{human}}\right)} \tag{3.13}$$

With $\delta(t)_{human}$ and $\delta(t)_{model}$ representing the control output of the human in the experiment and that of the simulated model, respectively. VAF can vary between 0 (poor model fit) and 1 (perfect corresponding between $\delta(t)_{human}$ and $\delta(t)_{model}$). Hess calculated the VAF value to be 0.73 which is considered to be high [36].

While the rule-based model is simple it has several disadvantages. The adaptive logic is developed empirically and is ad-hoc in nature, thus lacking theoretical justification. However, the selection of the equations for the adaptive logic are based on guidelines defined by Hess. These are defined in [34], where the most important guideline is that the pre- and post-transition pilot model parameters must follow the crossover model. This guideline is used to validate the model through checking whether the open-loop (Y_pY_c) for pre- and post-transition parameters are integrator-like in the region of the crossover frequency. Here, the open-loop transfer function refers to $\frac{M}{E}$, with the $\dot{M}$ (inner loop) closed. Moreover, the model requires knowledge about the time at which the CE dynamics have changed (t_c) and the human model is missing a inherent time-delay term. Nevertheless, the delay term could have been deliberately omitted as the model already has delay which is evident from the three second order

low-pass filters used throughout the adaptive logic. Lastly, the capabilities of Hess' model are only demonstrated using computer simulations with limited experimental research. This leads to limited verification of the model's results. Comparison of the model's results to experimental data would not only lead to validation of the model, but also improvements and modifications to the proposed adaptive logic.

3.2. Conclusions

The main conclusion drawn from the existing state-of-the-art human adaptive behaviour models is that humans are capable of adapting their control behaviour when a change in the system dynamics occurs. Current mathematical models of the adaptive human behaviour are based on the idea that the humans have a reference model of the controlled system, known as an internal model. This enables humans to detect when a change in the system has occurred from off-nominal tracking errors and error rates for a compensatory tracking task, and output rates for a pursuit tracking task. Detection triggers the human operator to adjust his/her control strategy to the appropriate settings for the new CE dynamics.

Moreover, the models discussed in this chapter predict how humans would adapt to a failed system, represented through a change in CE dynamics. This is contrary to other models which are used for identifying human time-varying dynamics from measured data. The superiority of these predictive models is that they can be re-created. Therefore, one of the models discussed in this chapter will be replicated in order to further investigate the human adaptive process. As evident from the review of past research in Section 3.1, most models that predict human adaptation are for a compensatory tracking task. Only a single model, Hess' model, uses pursuit tracking which is the relevant tracking task for this research. Thus, this model is selected to be replicated. Further discussion of the selection of the model and its implementation is detailed in Chapter 4.

4

Replication of the Hess Model for Adaptive Human Behaviour

While Chapter 3 provides a review of the literature available on the human adaptive behaviour, this chapter aims to analyse one of the models available that predict human adaptive behaviour. This allows for better understanding of the applicability of the model and the modeling of human adaptive behaviour. One way of accomplishing this is through replication of one of the models through the use of the computer simulations.

The first part of this chapter discusses the reasoning behind the selection of the model, with the following section describing how the model was implemented in MATLAB and Simulink. The second part of this chapter discusses the results obtained from implementing the model by comparing these results to the results reported from the original model.

4.1. Selection of Model

The model selected for replication is the adaptive human pilot model developed by Ronald Hess [34], [35], [36]. There are several advantages of this model relative to the other models. The main advantage of using this model is that it was developed for a pursuit tracking task which, as discussed in Chapter 2, is preferred over a compensatory tracking task. Additionally, this is one of the latest models developed in the field of manual control and Hess provides detailed explanations of the model [36]. Moreover, the model is more versatile, relative to the other models, as it can be implemented for multi-axis tracking. Lastly, it incorporates all the phases of adaption (detection, identification, and modification). Furthermore, as discussed in Section 3.1.4, there are several drawbacks to Hess' model. The model lacks theoretical justification as it is empirically developed. Additionally, the reasoning behind certain design decisions of the model is not present, such as the absence of the inherent time-delay term. Moreover, the model lacks verification using experimental research, with the capabilities of the model shown through computer simulations. Note that in this chapter, Hess' model is referred to as the original model, whereas the model created based on Hess' publications, described in Section 3.1.4, is referred to as the replicated model.

4.2. Implementation of Replicated Model

The computer simulation for single-axis pitch control task, was simulated for 120 seconds; with a system failure occurring at a time t_c of 50 seconds. A schematic of Hess' model is depicted in Figure 4.1, while the Simulink block diagram of the computer simulation can be found in Appendix A, which visualizes

how the adaptation logic, discussed in Section 3.1.4, was implemented.

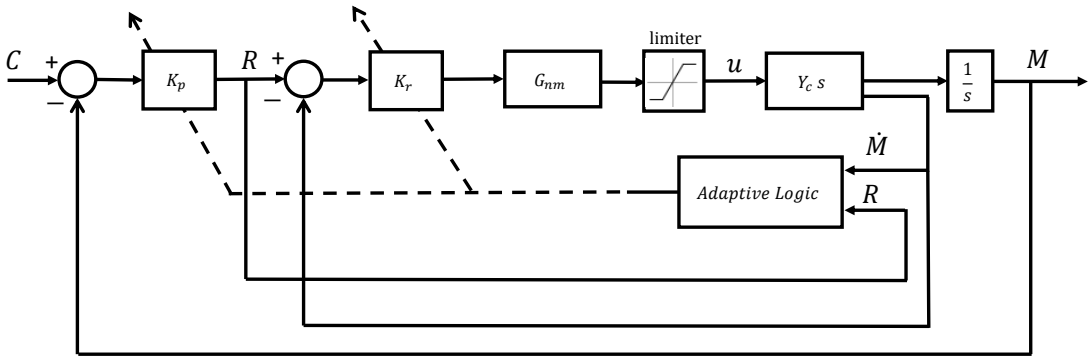

Figure 4.1: Hess' adaptive pilot model

In this simulation, failure of the system is introduced through a change in controlled element dynamics from relatively simple $Y_{c,1}$ to more challenging $Y_{c,2}$ dynamics, where the transfer functions are given as:

$$Y_{c,1}(s) = \frac{1}{s(s+10)} \qquad Y_{c,2}(s) = \frac{e^{-0.2s}}{s(s+5)(s+10)} \tag{4.1}$$

The Bode plots, showing the frequency response of these two transfer functions are visualized in Figure 4.2 where $Y_{c,1}$ represents the *nominal system* CE, and $Y_{c,2}$ represents the *failed system* CE. In this figure, the significant decrease in the gain as well as a time delay (due to $e^{-0.2s}$) evident in the phase diagram, can be observed.

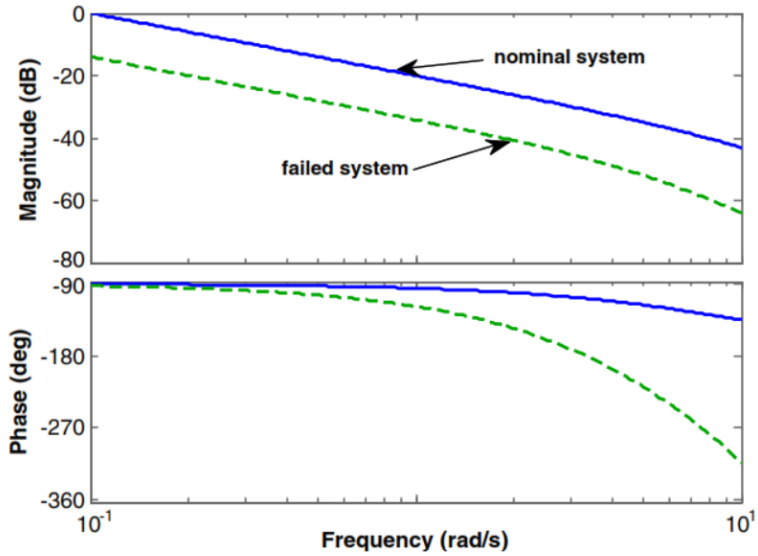

Figure 4.2: Frequency response of the *nominal* and *failed* CE dynamics in the original publication by Hess [36]

The transition from $Y_{c,1}$ to $Y_{c,2}$ was implemented in the simulation by creating both transfer functions, and passing them through weighting functions shown in Figure 4.3. In Simulink, the weighting functions were implemented using a ramp function. Hess states that the interval over which the vehicle dynamics change is instantaneous, hence the rapid change of weighting functions as visualized in Figure 4.3. Furthermore, the model requires information from the output rate $\dot{M}$ as well as the output M. Therefore,

in order not to differentiate in time to obtain $\dot{M}$, which could be destabilizing, the controlled elements $Y_{c,1}$ and $Y_{c,2}$ were defined as $\frac{s}{s(s+10)}$ and $\frac{e^{-0.2s}s}{s(s+5)(s+10)}$, respectively, which outputs the output rate $\dot{M}$. Then, in order to obtain the output M, an integrator was used.

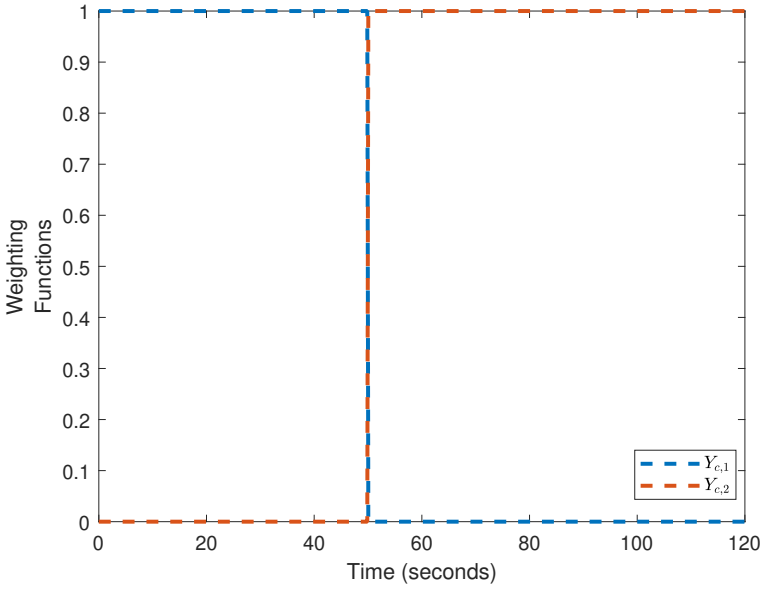

Figure 4.3: Weighting function for implementing time-varying CE dynamics

Additionally, a pilot model with only the simple $Y_{c,1}$ vehicle dynamics and without the adaptive logic was created, termed the nominal situation model. This was done in order to determine the constant $RMS(R^2)$ from Equation (3.10). In the nominal situation model, the CE dynamics representing the failed system $Y_{c,2}$ was not introduced. The Root Mean Square (RMS) of the R^2 signal in time, was calculated using Equation (4.2).

$$RMS(x(t)) = \sqrt{\frac{1}{T}\int_0^T (x(t))^2\, dt} \tag{4.2}$$

Where T is the total simulation time, which in this case is 120 seconds.

The command input signal C, also named as the forcing function, was simulated with a random-appearing sum of eleven sine waves. Figure 4.4 illustrates how Hess created the forcing function, where the signal is passed through multiple gains as well as a low-pass filer. Additionally, an overview of the properties of the eleven sine waves is given in Table 4.1. In this table, it is evident that Hess multiplies the amplitude of each sine wave to its corresponding frequency; a procedure not typically followed at the section of Control and Simulation at TU Delft when creating a forcing function. The reasoning behind doing this is unknown. From this table, it can also be observed that the measurement time T_m is 240 sec, resulting in a base frequency of $\omega_m = \frac{2\pi}{T_m} = 0.026$ [rad/s]. Moreover, the first gain used to create the forcing function is used to scale the signal, however, the reasoning behind the exact values used is also unknown. The signal then passes through a second order low-pass filer ($H_{LP} = \frac{1}{s^2+2s+1}$). Lastly, another gain is used which converts the signal to radians. Figure 4.5 shows the forcing function immediately after the summation of the sine waves, as well as the final outcome of the forcing function after scaling and passing the signal through the filter.

Since the signal is filtered, the corrected amplitudes and phases were calculated in order to obtain the parameters of the final outcome of the forcing function. Figure 4.6 shows the unfiltered signal $x(t)$ and the filtered signal $y(t)$ as well as their corresponding amplitudes and phases. Note that the unfiltered signal $x(t)$ and the filtered signal $y(t)$ shown in Figure 4.6, correspond to the same signals which are

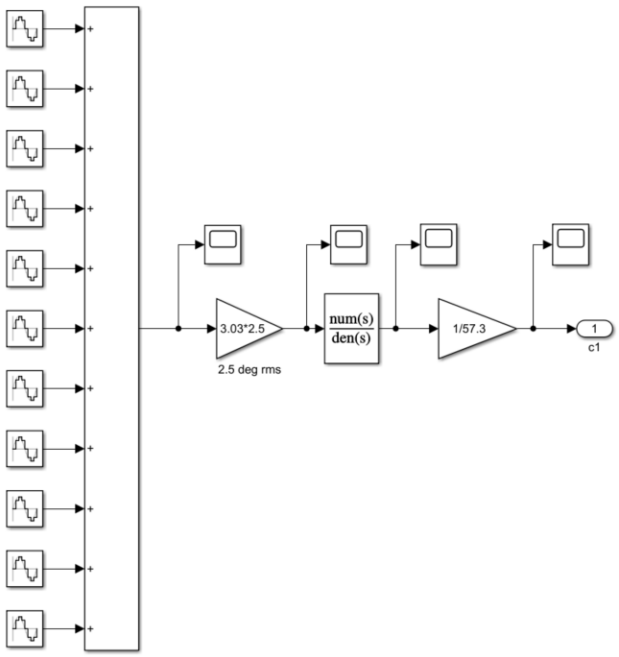

Figure 4.4: Forcing Function

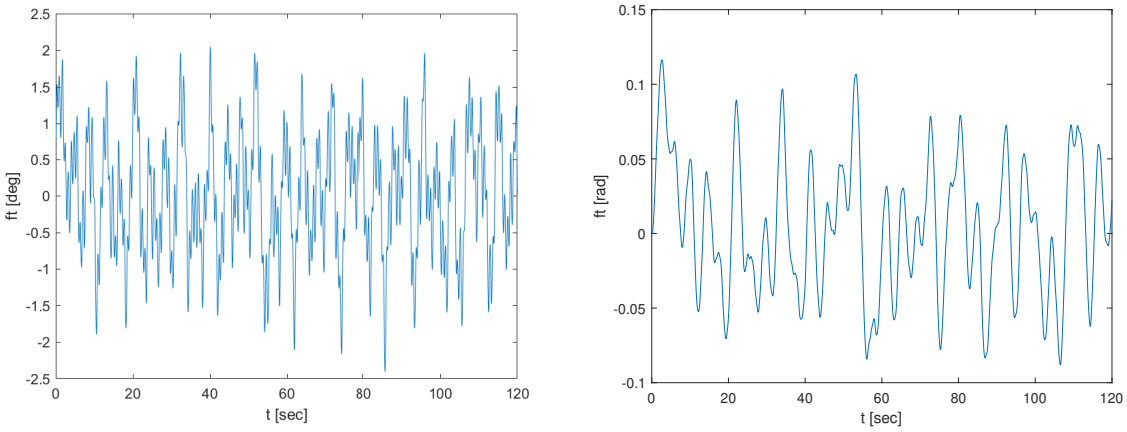

Figure 4.5: Signal right after summing the sine waves (a) and final outcome of signal after low-pass filtering (b)

shown in Figure 4.5. Lastly, an overview of the properties of the (filtered and scaled) forcing function is given in Table 4.2.

Table 4.1: Parameter values of sine waves: in mathematical representation (a) and corresponding numerical values (b)

(a)

Forcing Function (Pre-Filter)			
N	A	ω rad/s	ϕ rad
1	0.5 ω_1	$2\pi\cdot$ (7/240)	-2.88/57.3
2	0.5 ω_2	$2\pi\cdot$ (11/240)	2.1/57.3
3	0.5 ω_3	$2\pi\cdot$ (16/240)	0.41/57.3
4	0.5 ω_4	$2\pi\cdot$ (25/240)	-1.96/57.3
5	0.5 ω_5	$2\pi\cdot$ (38/240)	1.57/57.3
6	0.5 ω_6	$2\pi\cdot$ (61/240)	-0.93/57.3
7	0.05 ω_7	$2\pi\cdot$ (103/240)	-2.31/57.3
8	0.05 ω_8	$2\pi\cdot$ (131/240)	2.83/57.3
9	0.05 ω_9	$2\pi\cdot$ (151/240)	0.53/57.3
10	0.05 ω_{10}	$2\pi\cdot$ (181/240)	1.93/57.3
11	0.05 ω_{11}	$2\pi\cdot$ (313/240)	0.77/57.3

(b)

Forcing Function (Pre-Filter)			
N	A	ω rad/s	ϕ rad
1	0.092	0.183	-0.050
2	0.144	0.287	0.037
3	0.209	0.419	0.007
4	0.327	0.654	-0.034
5	0.497	0.995	0.027
6	0.799	1.597	-0.016
7	0.135	2.697	-0.040
8	0.172	3.429	0.049
9	0.198	3.953	0.009
10	0.237	4.739	0.034
11	0.410	8.194	0.013

Table 4.2: Parameter values of forcing function

Forcing Function (Filtered)			
N	A cm	ω rad/s	ϕ rad
1	0.012	0.183	-0.413
2	0.018	0.287	-0.524
3	0.024	0.419	-0.786
4	0.030	0.654	-1.193
5	0.033	0.995	-1.538
6	0.030	1.597	-2.039
7	0.002	2.697	-2.472
8	0.002	3.429	-2.525
9	0.002	3.953	-2.637
10	0.001	4.739	-2.692
11	0.001	8.194	-2.885

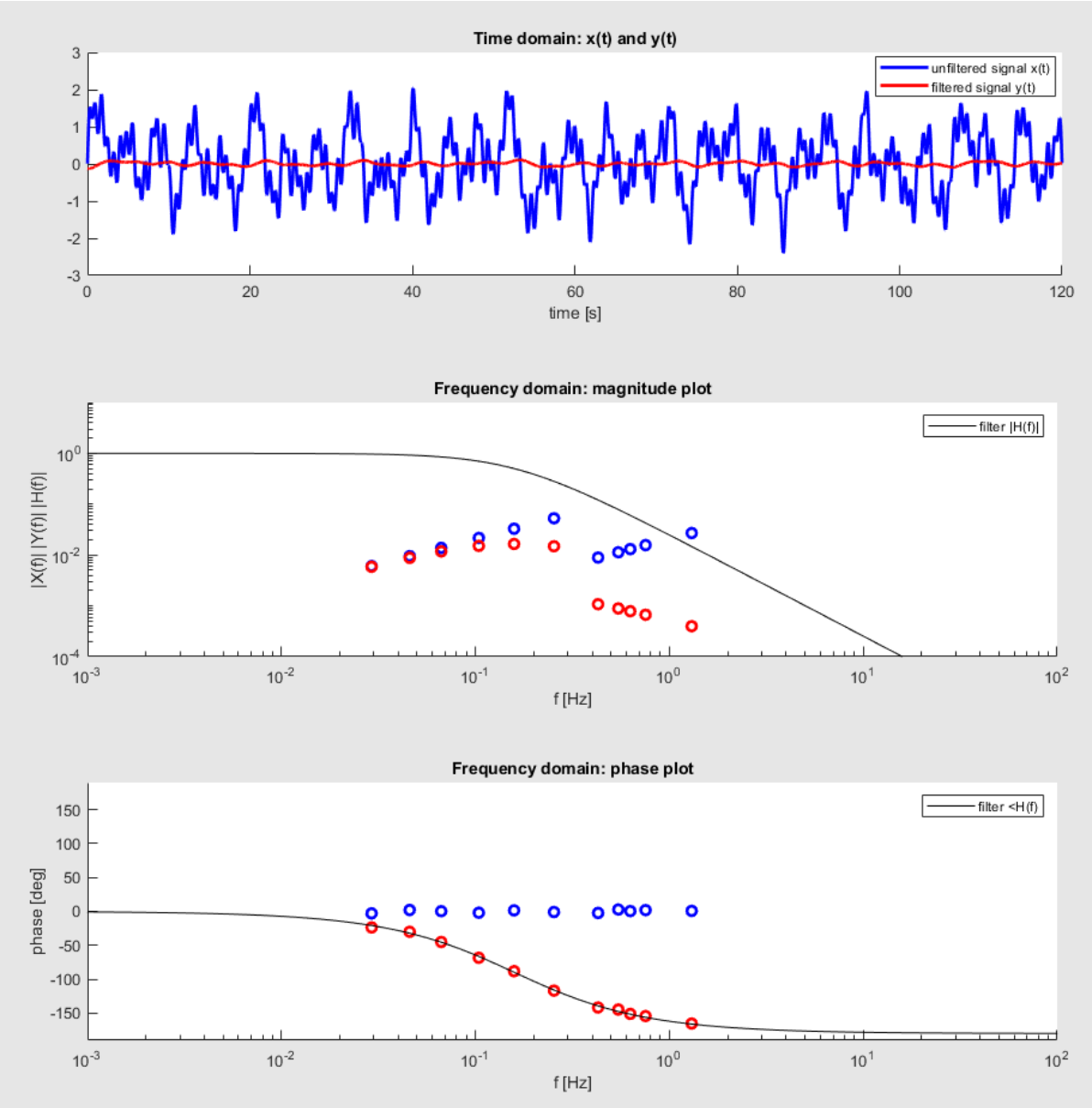

Figure 4.6: Filtering the forcing function

4.3. Results

In this section, the results from Hess' original model, which can be found in [36], are compared to the results from the replicated model. Figure 4.7 shows the tracking performance results from Hess' model (a) and the replicated model (b). Figure 4.8 shows the gains K_r and K_p adapting to the failed system dynamics using the adaptive logic, for Hess' results (a) and the replicated model's (b). As expected, the pre-failure tracking results are identical. However, the steady-state post-failure values for the K_r and K_p gains in the replicated model are slightly lower than the results from Hess' model paper. The replicated model gain K_r = 14.4 compared to Hess' model which is $K_r \approx 15.8$. Since, the K_r gain is lower for the replicated model, then K_p is also lower compared to Hess' model due to the relation between the gains described through Equation (3.11). While the difference in gain adaptations is relatively small, it does affect the post-failure tracking accuracy, which is visible from Figure 4.7. Here, it is evident that steady-state post-failure tracking differs for both models: the output M of the implemented model undershoots the target function c, unlike Hess' model where the output M overshoots the target function c. Furthermore, another noticeable difference is the dip in the K_r response directly after failure, evident in Figure 4.8 (a), while in the replicated model K_r has a monotonous increase without the dip. The reasoning for these small differences in results is unknown. However, after a discussion with Ronald Hess regarding the results it was concluded that these differences could possibly stem from the fact that Hess used an different (older) adaptation logic algorithm for his simulations. Additionally, Hess used an older Simulink version (Matlab 2011a), with perhaps a different solver compared to the one used to replicated the model (Matlab 2021a), which could induce a different transient behaviour.

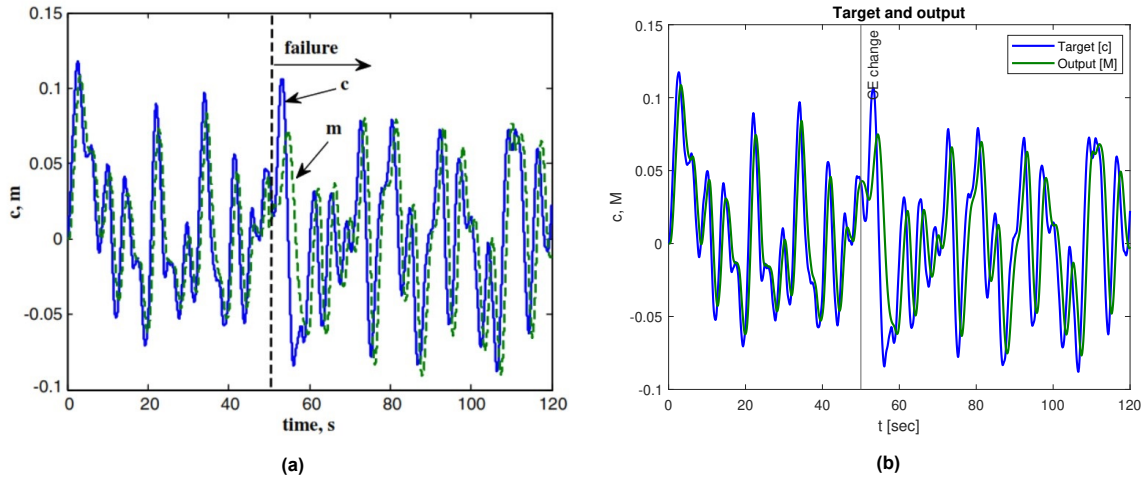

Figure 4.7: Pitch attitude tracking performance Hess' original model [36] (a) and replicated model (b)

Moreover, as discussed in Section 3.1.4, the validity of the adaptive model can be verified through checking whether the human pilot after adaptation follows the crossover model theory, i.e., Equation (2.1). Since Hess' model is multi-loop, the following equations were used to calculate the dynamic characteristics of the open-loop response of the system ($Y_{OL}^{outer} = Y_p Y_c$):

$$Y_{OL}^{inner} = K_r G_{nm} Y_c s \tag{4.3}$$

Yields an inner loop crossover frequency ω_c^{inner} and an inner loop phase margin ϕ_m^{inner}

$$Y_{CL}^{inner} = \frac{Y_{OL}^{inner}}{1 + Y_{OL}^{inner}} \tag{4.4}$$

$$Y_{OL}^{outer} = K_p Y_{CL}^{inner} \frac{1}{s} \tag{4.5}$$

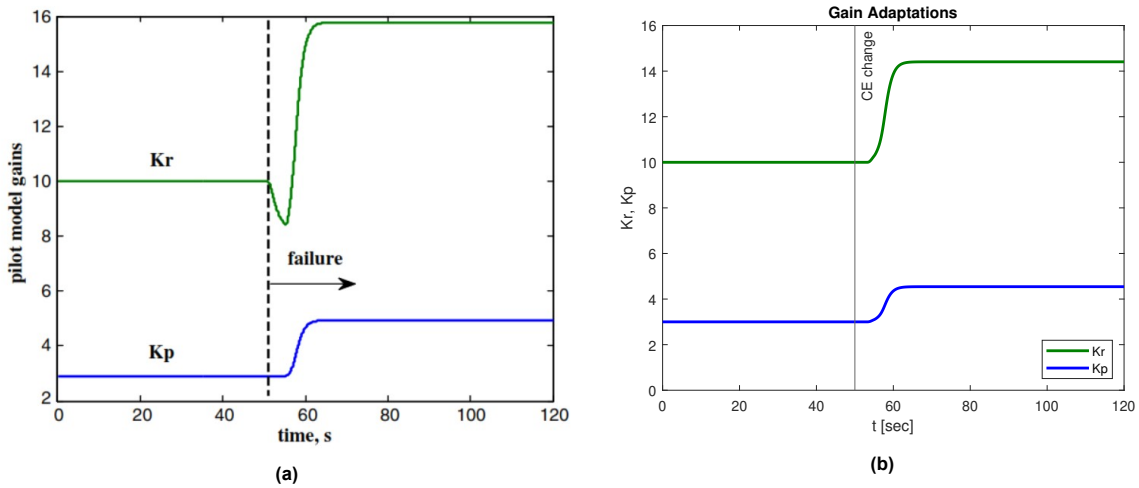

Figure 4.8: Pilot model gain adaptation Hess' model [36] (a) and replicated model (b)

Yields an outer loop crossover frequency ω_c^{outer} and an outer loop phase margin ϕ_m^{outer}. Note that OL refers to open loop, while CL refers to closed loop.

Figure 4.9 shows Hess' reported open-loop bode plot for both pre- and post-transition of CE dynamics. In the pre-transition case the crossover frequency ω_c^{outer} = 1.5 [rad/s], while for post-transition ω_c^{outer} = 1.6 [rad/s], the phase margin ϕ_m^{outer} for both cases is not reported. It is evident from this figure that near pre-transition performance is achieved with the adaptive logic, and that the adapted pilot model follows the open-loop response characteristics of the crossover model.

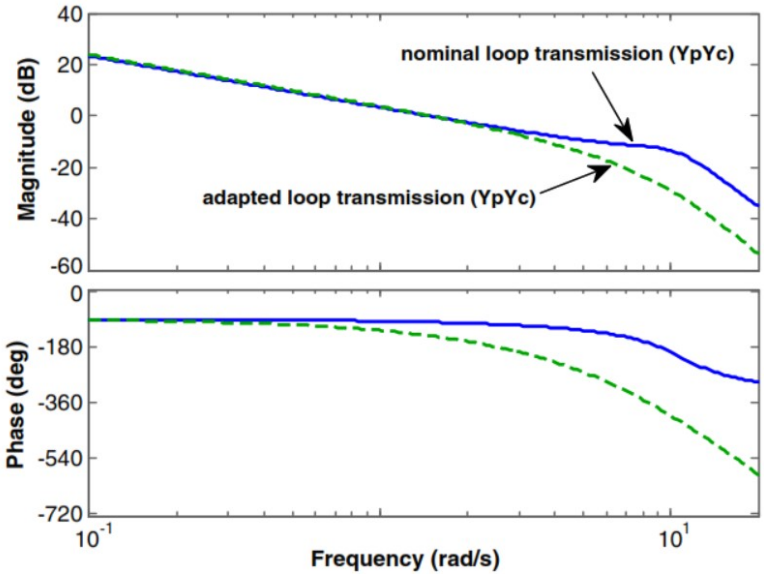

Figure 4.9: Comparison of nominal and adapted Y_pY_c open-loop bode diagram [36]

Figure 4.10 shows several different open-loop Y_pY_c bode diagrams, the first bode plot is the pre-failure (nominal), this is identical to the "nominal loop transmission (YpYc)" shown in Figure 4.9, represented by the blue line. The second bode plot shows post-failure adaptation with gain values K_r and K_p from the original model, which can be seen from Figure 4.8(a), where $K_r \approx 15.8$ and $K_p \approx 5$. The third bode plot shows post-failure adaptation with the replicated model; the gain values can be seen from Figure 4.8(b), where $K_r = 14.4$ and $K_p = 4.5$. Lastly, the fourth bode plot shows the open-loop Y_pY_c response in post-failure if the gains K_r and K_p had not adapted. The open-loop stability characteristics

for all of the bode plots are summarized in Table 5.2.

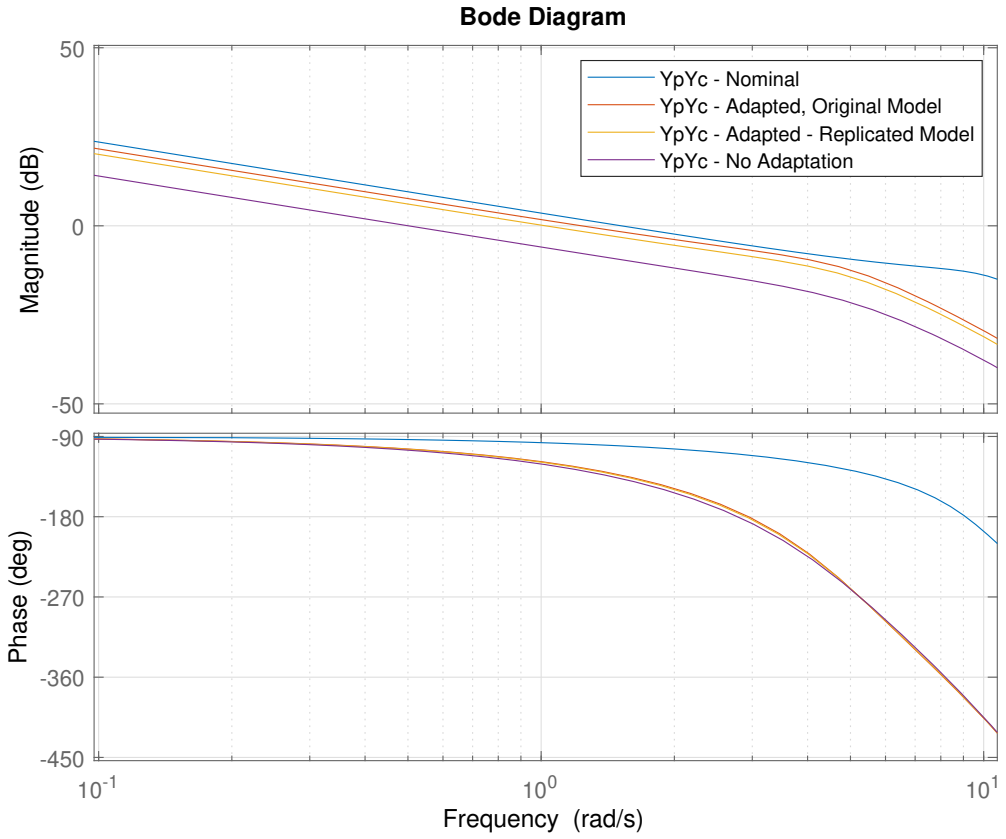

Figure 4.10: Open-loop bode plots comparing different scenarios

Table 4.3: Summary of open-loop stability characteristics

	K_r, K_p	**Phase margin** ϕ_m **[deg]**	**Crossover frequency** ω_c [rad/s]
$Y_pY_{c,1}$ – **nominal**	$K_r = 10$, $K_p = 3$	80	1.5
$Y_pY_{c,2}$ – **original model**	$K_r \approx 15.8$, $K_p \approx 5$	55	1.2
$Y_pY_{c,2}$ – **replicated model**	$K_r = 14.4$, $K_p = 4.4$	61	1
$Y_pY_{c,2}$ – **No adaptive logic**	$K_r = 10$, $K_p = 3$	75	0.5

When inspecting the open-loop characteristics for the adapted (post-failure) case from Table 5.2 it can be observed that the crossover frequency ω_c = 1.2 [rad/s] calculated using the K_r and K_p gains values reported in Figure 4.8(a) is different compared to the crossover frequency ω_c = 1.6 reported by Hess which can also be computed from Figure 4.9. Hess' reported crossover frequency ω_c = 1.6 [rad/s] is therefore possibly a mistake.

Lastly, in order to obtain a better understanding of the adaptive pilot model, a more in-depth analysis of each of the model's signals is carried out. However, since Hess does not provide the results of his signals from the original model, a comparison cannot be made. According to Hess, detection of a change in the vehicle dynamics is based on the sign and magnitude of the error signal of the inner loop, defined as the x signal through Equation (3.7). In this equation, the R signal and output rate $\dot{M}$ are visualized in Figure 4.11. Whereas, the pre-filtered x signal is visualized in Figure 4.12 (a), and the final outcome of the x signal is shown in Figure 4.12 (b).

Furthermore, as described through Equation (3.8), the human pilot is triggered to adapt when the value of $\sqrt{|x|}$ is bigger than, or equal to, the *acceptability limit* defined as 3 rms($\sqrt{|x|}$). This is visualized

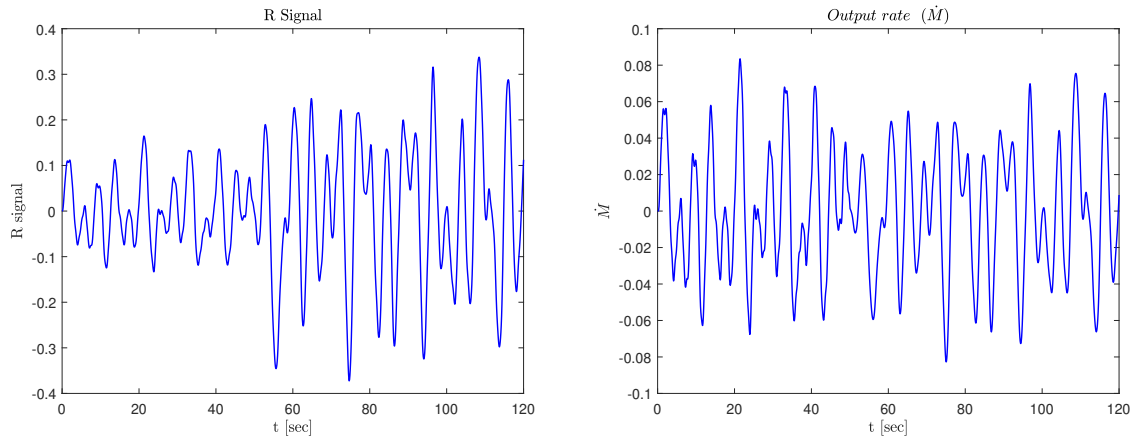

(a) (b)

Figure 4.11: R signal (a) and output rate $\dot{M}$ signal (b) of the replicated model

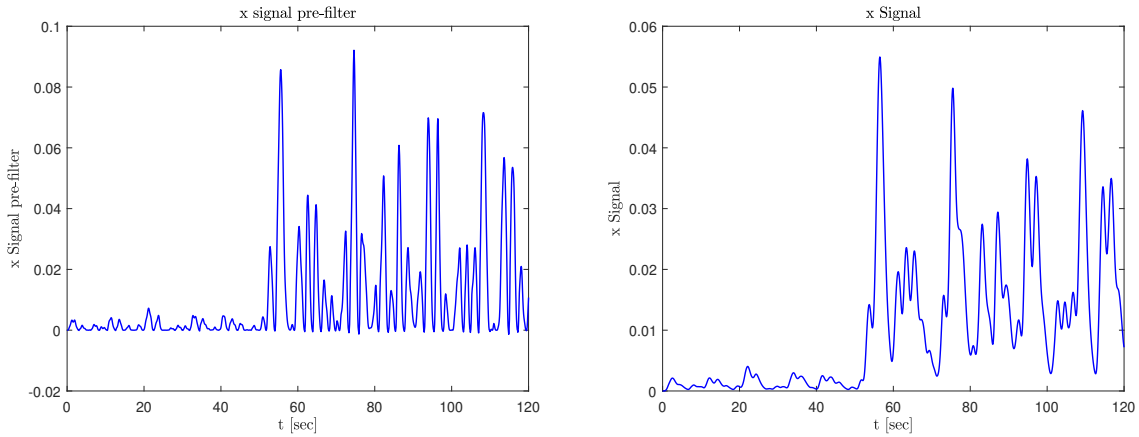

(a) (b)

Figure 4.12: Pre-filtered x signal (a) final outcome of x signal (b)

through Figure 4.13(a), where every time the acceptability limit is exceeded, a trigger can be observed in Figure 4.13(b). Here, two triggers of different durations can be seen. At each trigger, the pilot model uses K_r and K_p gain variations to adapt to the rapid change in CE dynamics. The change of the inner loop gain, ΔK_r, is dependent on the strength of the X_n signal as well as the duration of the trigger, as described through Equation (3.9) and Equation (3.10). On the other hand the change of the outer loop gain ΔK_p is solely dependent on ΔK_r, through the relations described in Equation (3.11). Therefore, even though the adaptive model is triggered twice, the first trigger does have a significant impact on the gain variations, as can be observed from Figure 4.15. This is because the first trigger happens over a very short period of time, and at that time the X_n signal is very small, which can be seen from Figure 4.14. Moreover, Figure 4.12 and Figure 4.14 show the pre-filtered and filtered signals of x and X_n respectively. From these figures the effect of these filters can be seen; they are effectively smoothing the signals and introducing lag.

Finally, Figure 4.16 shows the error and control activity of the tracking task. A large error peak can be observed when failure occurs, however, this error decreases once the adaptive logic is triggered and adaptation occurs. Additionally, the control activity increases when failure is introduced, which is expected since the CE dynamics are much more challenging compared to the nominal CE dynamics.

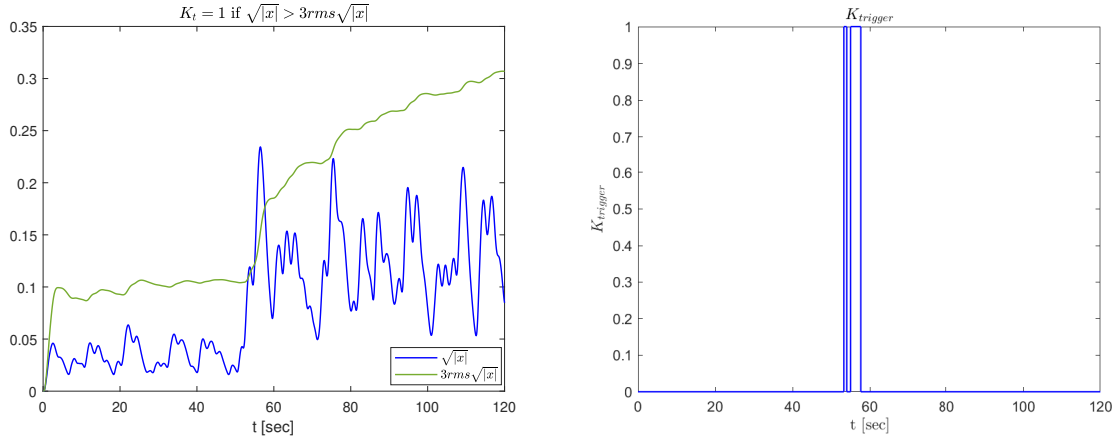

(a) (b)

Figure 4.13: Triggering Function

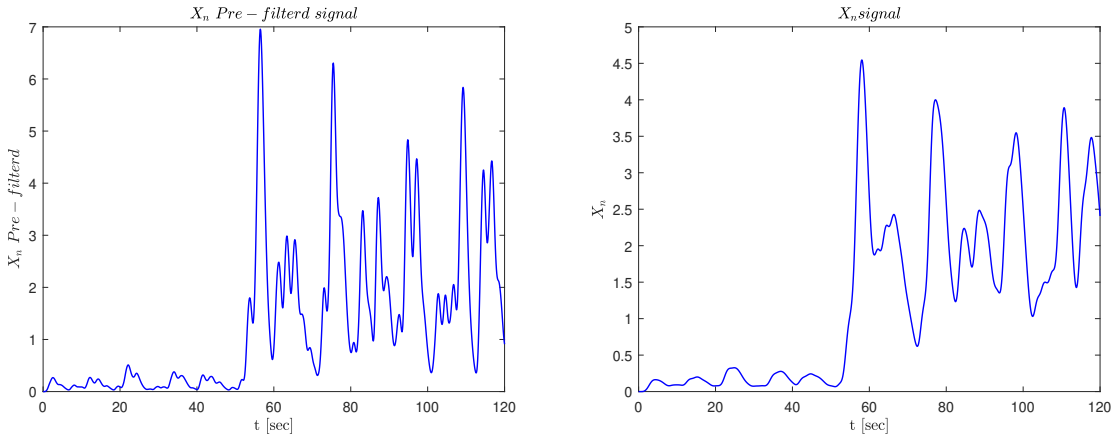

(a) (b)

Figure 4.14: X_n signal pre-filtered (a), filtered (b)

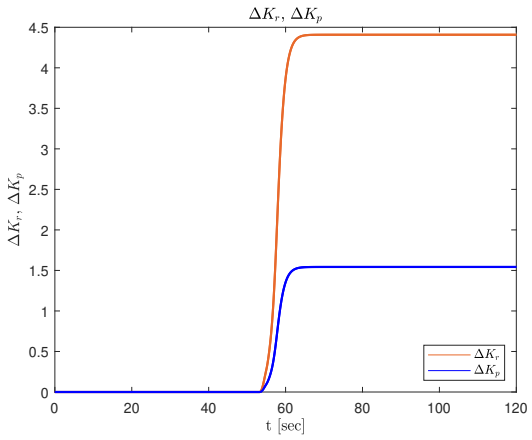

Figure 4.15: Change of K_r and K_p gain adaptations

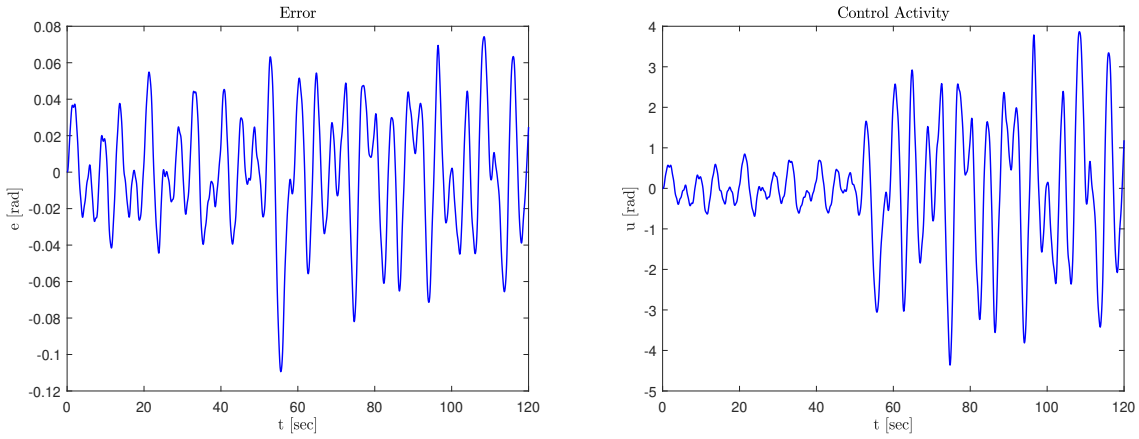

(a) **(b)**

Figure 4.16: Error (a), Control activity (b)

4.4. Additional Investigation into Hess' Model

This section aims to understand how different parameters of Hess' model, in particular the gains K_r and K_p, are tuned for specific CE vehicle dynamics Y_c. The values of both K_r and K_p are dependent on a defined set of CE vehicle dynamics, Y_c. Therefore, in order to be able to use this model for different vehicle dynamics, it is important to tune these gains accordingly. While this section only provides a summary of the investigation, a detailed description is provided in Appendix B. The investigation was carried out to check whether the gains K_r and K_p can be selected based on theory, such as the Crossover model, rather than the current method, proposed by Hess, which is heuristic. In order to accomplish this, Hess' model was re-structured into a single loop model, by combining the inner and outer loops of the original model. When comparing the re-structured model to Hess' original model it was shown that the models are not equivalent, therefore Hess' original model cannot be re-written using the structure of McRuer's model. Thus, it was decided that the gain values K_r and K_p for a defined set of controlled element dynamics will be determined based on time-domain parameter estimation techniques. This will be accomplished using existing results from experimental data conducted at the Control and Simulation department at TU Delft [40], which is further discussed in Chapter 6.

4.5. Conclusions

This chapter attempted to replicate Hess' adaptive pilot model, which portrays one way that the human pilot adaptation might take place during a single-axis, pursuit tracking task. While there are slight differences in the published results of the original model and the replicated model, both models capture the essence of the adaptive human behaviour. That is that, during a pursuit tracking task, the pilot uses information from a signal which is proportional to the inner-loop error, to decide whether adaptation is required based on the pilot's internal model through a trigger function. Once the trigger function is activated, the pilot is triggered and thus uses gain value variations in order to adapt to the rapidly changing vehicle dynamics. Now that Hess' model has been replicated, the next chapter provides a further investigation into the model through a sensitivity analysis.

5

Sensitivity Analysis

The aim of this chapter is to analyse the replicated model, discussed in Chapter 4, through a sensitivity analysis of specific parameters of the model. The first part of this chapter investigates the effect on adaptation due to (small) changes in the time t_c when the CE dynamics change (failure occurs). Then, a second investigation is conducted, where the time period over which the CE dynamics change is varied. The purpose of this analysis is also to examine its effect on adaptation.

5.1. Varying the time at which CE dynamics change

The purpose of this analysis is to check whether small changes in the failure time t_c, influence adaptation. While significant differences in the results are not expected, this analysis is still necessary in order to verify this. Figure 5.1 shows how the CE dynamics change from $Y_{c,1}$ to $Y_{c,2}$ for different t_c values.

Figure 5.2, Figure 5.3, and Figure 5.4 show the results for three different t_c times, namely t_c = 48.5 [sec], t_c = 50 [sec], and t_c = 51 [sec], respectively. The results for all the t_c values can be found in Appendix C. Table 5.1 summarizes the open-loop stability characteristics based on the results. From these results it can be concluded that there are no significant changes in the pilot-model adaptation for small changes in the time t_c.

Table 5.1: Summary of open-loop stability characteristics

t_c **[sec]**	K_r, K_p	**Phase margin** ϕ_m **[deg]**	**Crossover frequency** ω_c **[rad/s]**
48.5	$K_r = 14.394$, $K_p = 4.537$	60.19	1.03
49	$K_r = 14.405$, $K_p = 4.542$	60.14	1.03
49.5	$K_r = 14.407$, $K_p = 4.543$	60.13	1.03
50	$K_r = 14.408$, $K_p = 4.543$	60.13	1.03
50.5	$K_r = 14.396$, $K_p = 4.543$	60.14	1.03
51	$K_r = 14.407$, $K_p = 4.543$	60.13	1.03

However, through this analysis, one of the limitations of the model can be seen: gains K_r and K_p have no ”memory”. This can be explained with the help of Figure 5.5, which shows the model's results when failure is introduced at time t_c = 54.6 [sec]. These results show that the model is triggered twice, and that the gains K_r and K_p increase with the first trigger and then decrease with the second trigger. ΔK_r is dependent both on the length of the trigger and the size of the X_n signal as shown through equation Equation (5.1). Therefore, from the results it can be noticed that the second ΔK_r value is smaller than the first. However, the way in which the new gains are calculated currently is: $K_r\ (new)$ = $K_r\ (nominal)$ + ΔK_r. This means that the current trigger is not taken into account when calculating the following value of K_r. Therefore, an improvement to the model is required which has ”memory” of the

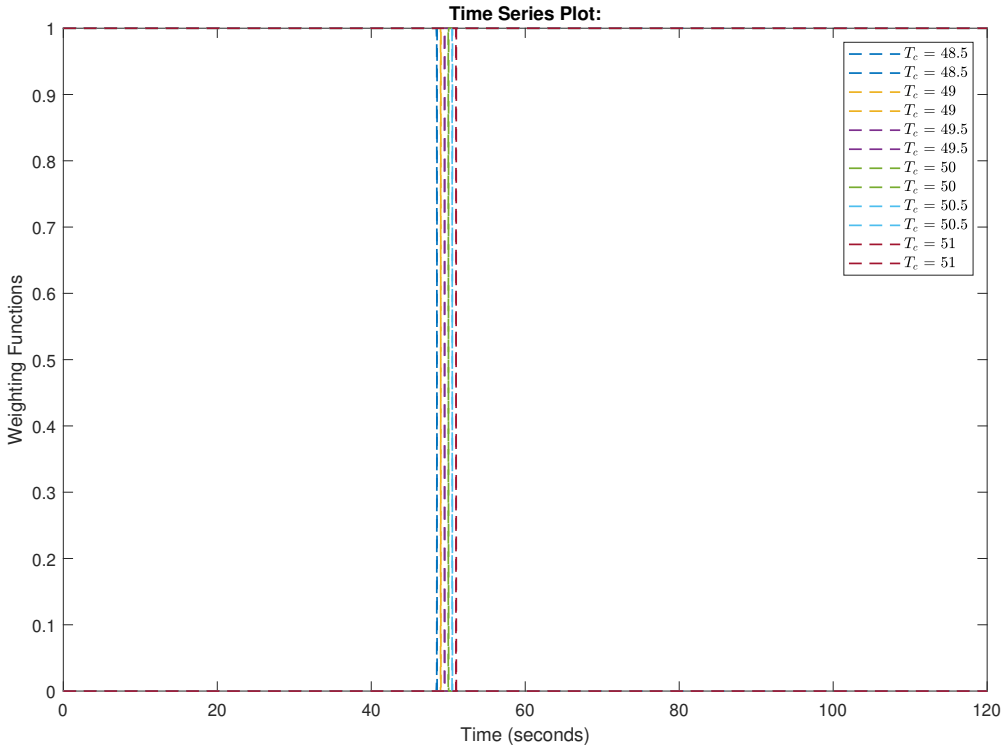

Figure 5.1: Varying the time t_c at which the CE dynamics change

gains, thus taking into account the previous triggers with corresponding ΔK_r (if any previous triggers are present), when calculating the final adapted gains. In Figure 5.5 this would result in a stronger adaptation, where the adapted gains are further increased with the second trigger.

$$\Delta K_r = x_n K_{\text{trigger}} \cdot \frac{1}{(s^2 + 2s + 1)} \tag{5.1}$$

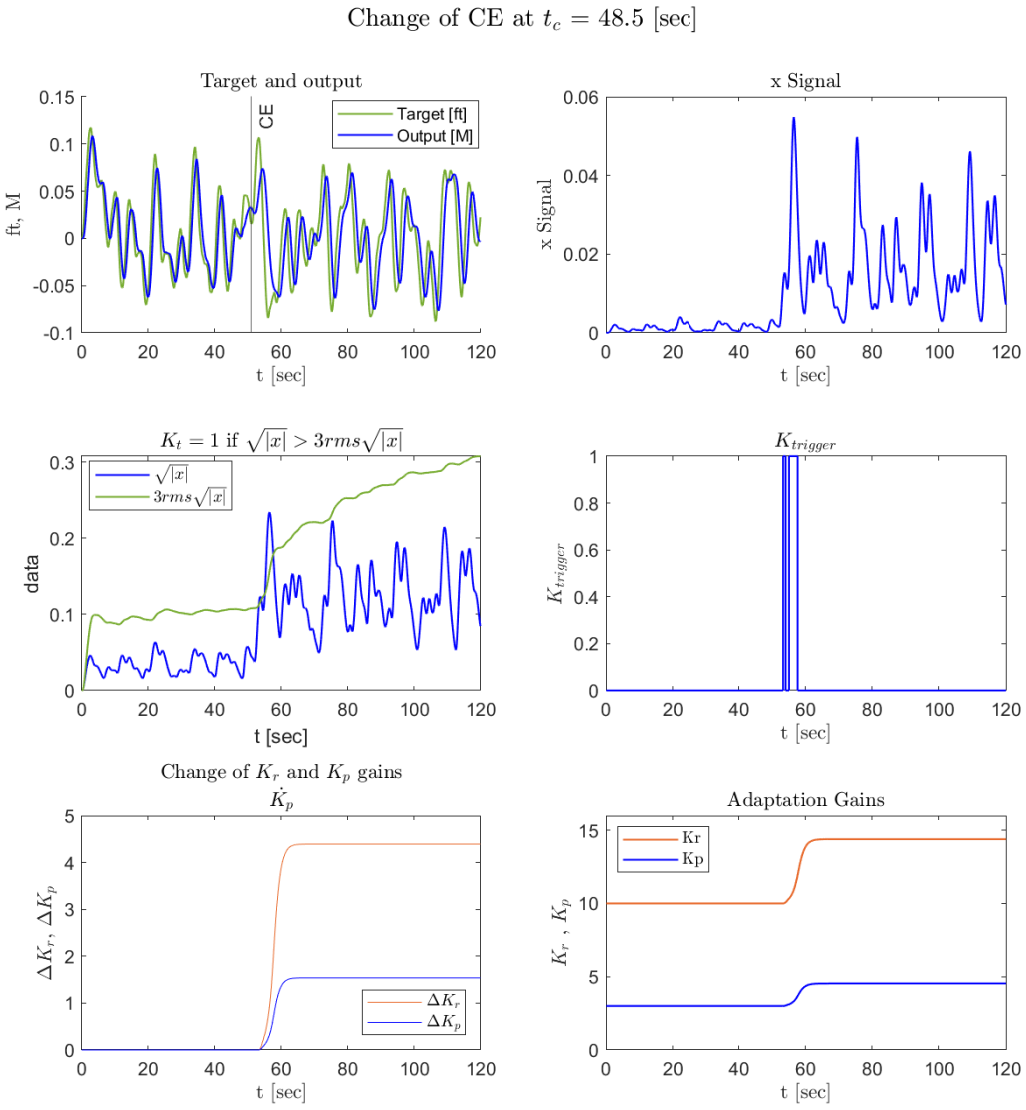

Figure 5.2: Change of CE dynamics at T_c = 48.5 sec

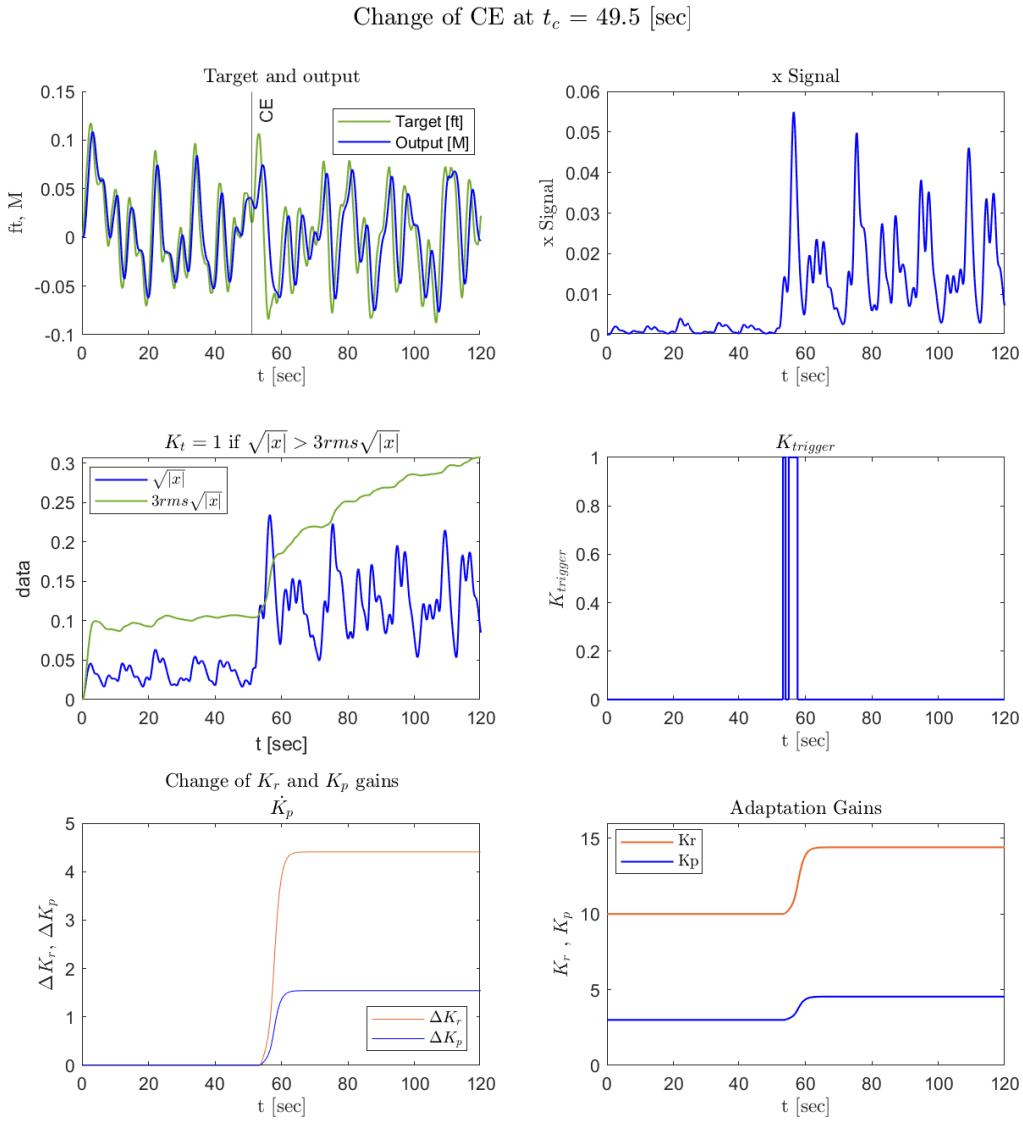

Figure 5.3: Change of CE dynamics at T_c = 49.5 sec

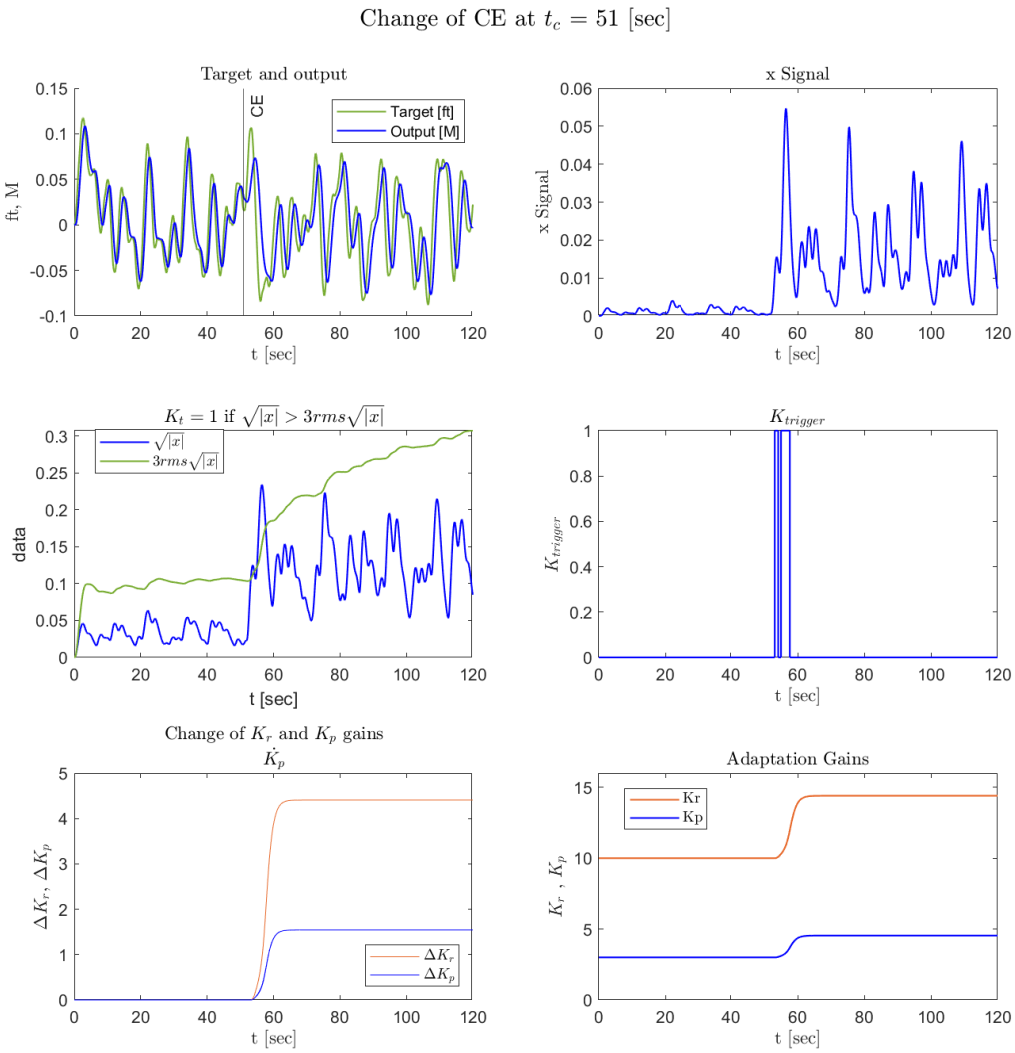

Figure 5.4: Change of CE dynamics at T_c = 51 sec

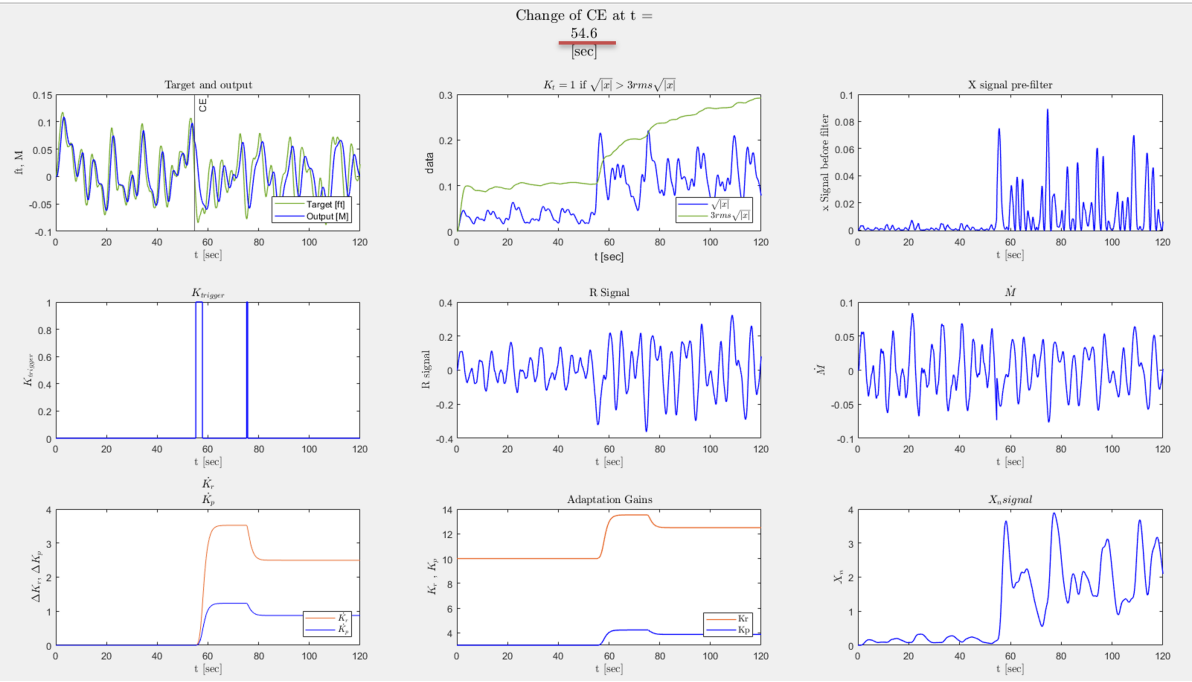

Figure 5.5: Change of CE dynamics at T_c = 54.6 sec

5.2. Varying the interval over which CE dynamics change

In this section the time period, referred to as DELT, over which the CE dynamics change from $Y_{c,1}$ to $Y_{c,2}$ is varied. The purpose of this analysis is to understand whether there are significant differences in the adaptation of the model with varying time interval lengths. The hypothesis is that humans have a faster and stronger reaction to instantaneous (fast/big) changes in CE dynamics when compared to small/slow changes. Figure 5.6 shows the weighting functions of varying the time period DELT from instantaneous change (0.05 sec) to slow changes (15 sec) in the CE dynamics. The implementation of the weighting functions is discussed in Chapter 4 where an instantaneous change is described. Furthermore, Hess implemented the change in the CE dynamics with a specific time of change referred to as t_c which is 50 sec as discussed in Chapter 4. Therefore, the interval at which the change in CE dynamics occurs is: [t_c, t_c+DELT], as evident from Figure 5.6. Another method of implementing the change in CE dynamics would be instead having the half-time of each interval coincide for all weighting functions. Nevertheless, neither implementation is superior over the other.

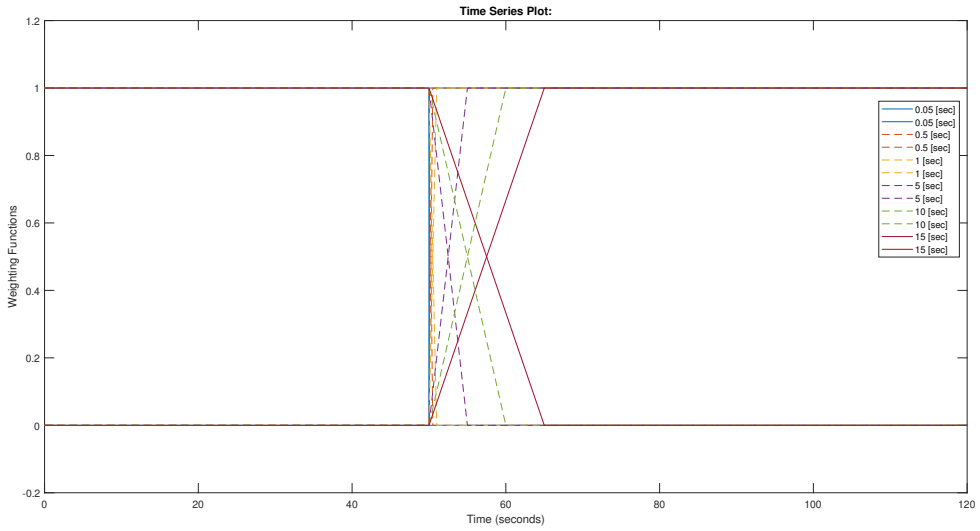

Figure 5.6: Varying the time period over which CE dynamics change

Figure 5.7, Figure 5.8 and Figure 5.9 show the results for three different time period, namely DELT = 0.05 [sec], 5 [sec] and 10 [sec], respectively. The results for all the time periods can be found in Appendix D, with Table 5.2 summarizing the open-loop stability characteristics based on the results of each time period, DELT. From Figure 5.7 and Figure 5.8 it can be observed that the shorter time interval(0.05 [sec]) is triggered twice compared to the larger interval (5 [sec]), due to the slight difference in the x signal, hence, the gain values K_r and K_p are slightly bigger for the the shorter time interval. The difference in x signal stems from the fact for the smaller time interval, the inner-loop error (difference between $\dot{M}$ and R) is bigger when the change of CE dynamics occurs more suddenly. This alludes to the fact that the human pilot gets more startled when the change of CE dynamics occurs in a shorter time period. In Figure 5.9, for the slowest change in CE dynamics, the human pilot is triggered at a later time relative to the faster-occurring changes in CE dynamics. This is to be expected due to the implementation of the change of CE dynamics, as the failed system dynamics $Y_{c,2}$ are introduced at a later time. Additionally, the values of the adapted gains K_r and K_p are significantly smaller due to two factors. Firstly, the change in CE dynamics occurs at a different time of the forcing function, where the target signal has smaller peaks, resulting in different results. Additionally, the time interval is larger thus adaptation is slower.

The conclusion of this analysis is that adaptation is stronger for instantaneous change in CE dynamics compared to slow changes. The difference in adaptation is not significant for DELT values between 0.05 [sec] and 5 [sec], compared to DELT values of 10 [sec] and 15 [sec] as evident from Table 5.2. One factor to consider is that the latter DELT values (10 sec and 15 sec) are in a different region of the

forcing function because their time period is much bigger which also influences adaptation.

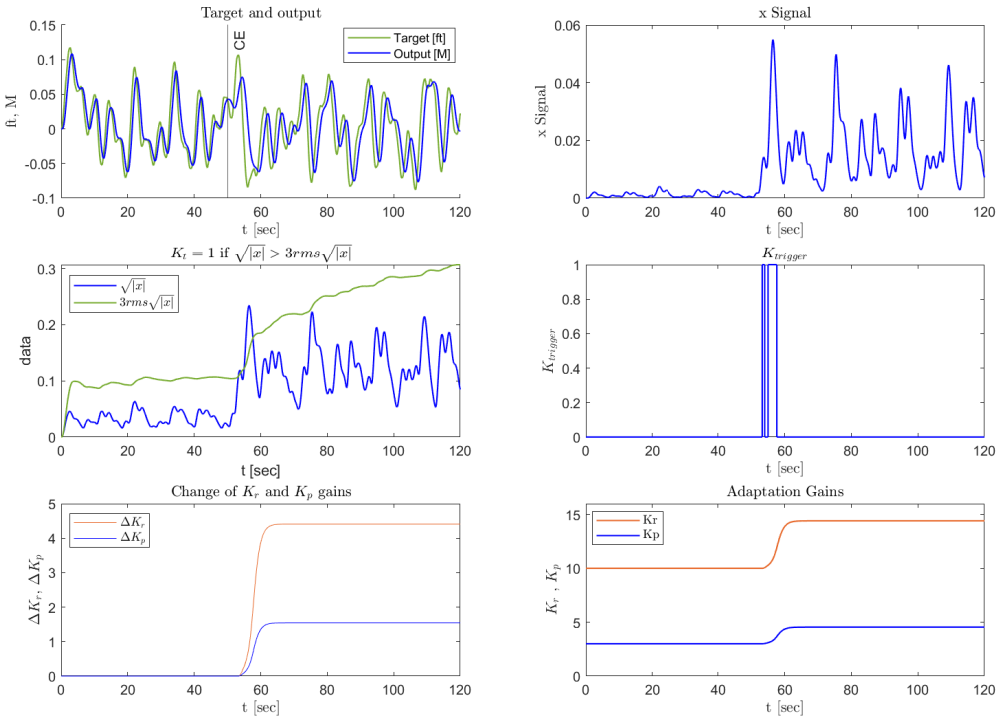

Figure 5.7: Interval over which CE dynamics change: DELT = 0.05 [sec]

Table 5.2: Summary of open-loop stability characteristics

DELT [sec]	K_r, K_p	Phase margin ϕ_m [deg]	Crossover frequency ω_c [rad/s]
0.05	$K_r = 14.4081$, $K_p = 4.5428$	60	1.0336
0.5	$K_r = 14.4079$, $K_p = 4.5427$	60.1299	1.0336
1	$K_r = 14.4068$, $K_p = 4.5424$	60.1336	1.0334
5	$K_r = 14.3966$, $K_p = 4.5388$	60.1742	1.0320
10	$K_r = 12.5561$, $K_p = 3.8946$	66.6658	0.7879
15	$K_r = 12.3949$, $K_p = 3.8382$	67.2345	0.7681

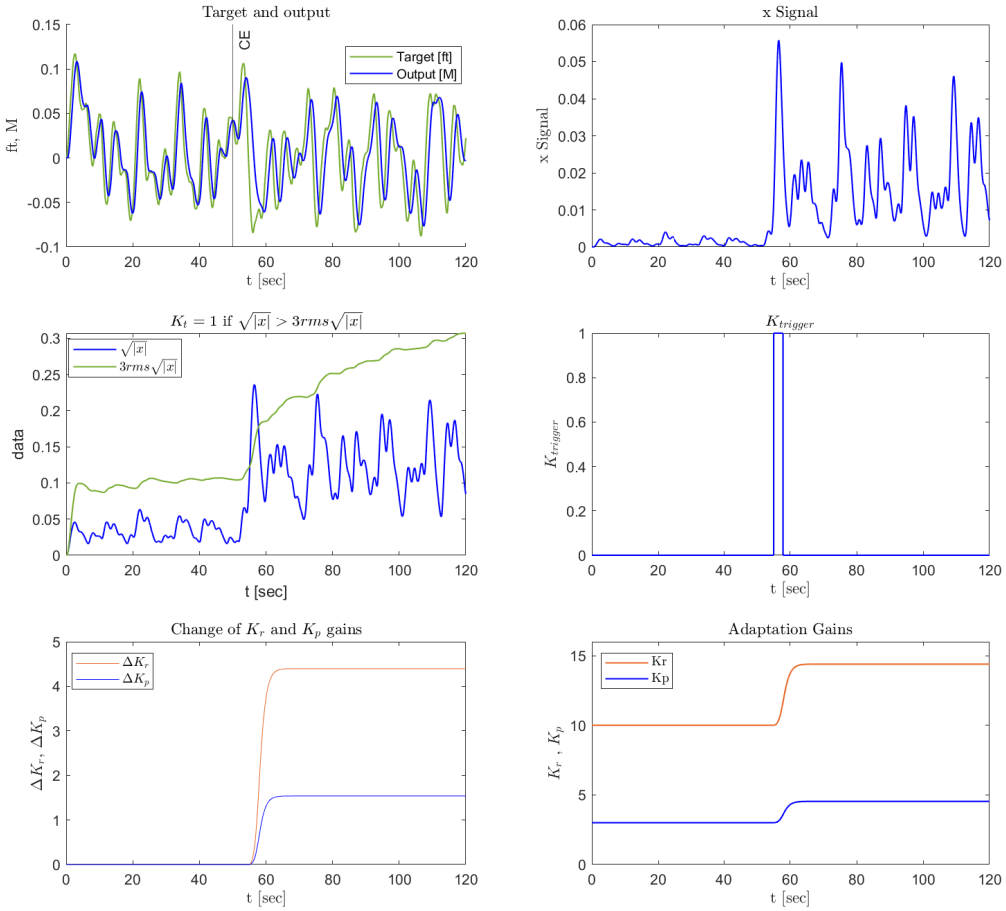

Figure 5.8: Interval over which CE dynamics change: DELT = 5 [sec]

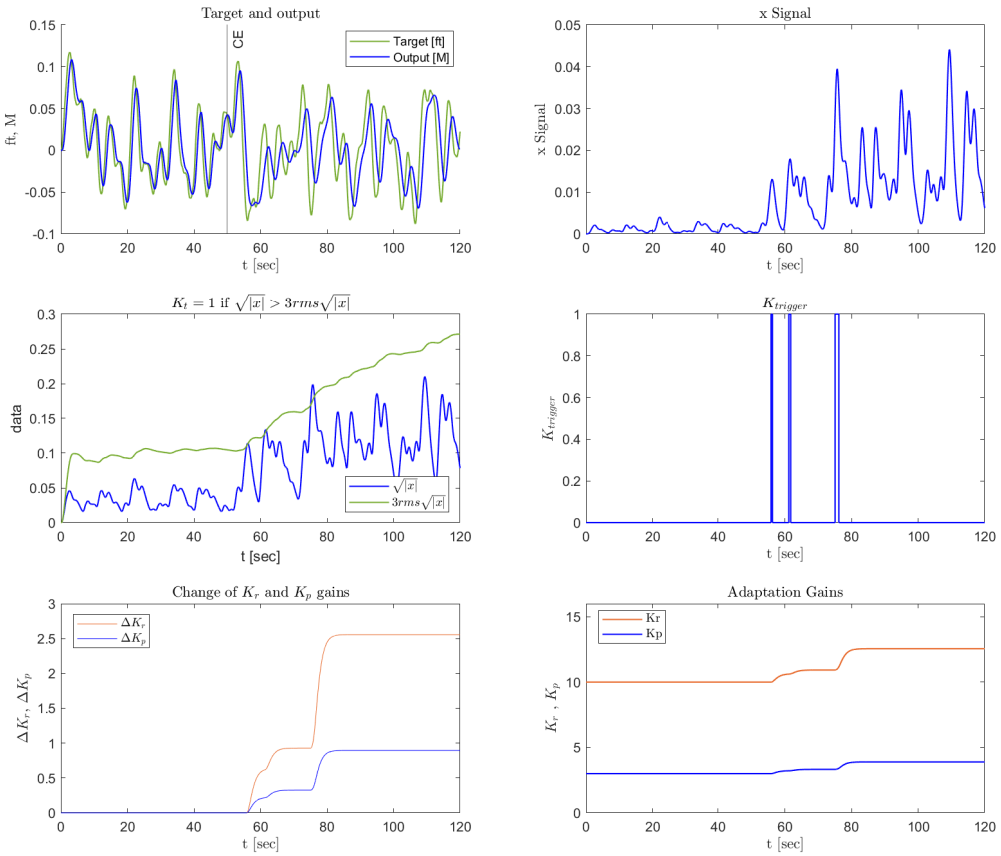

Figure 5.9: Interval over which CE dynamics change: DELT = 10 [sec]

6

Future Development

In this chapter, the next phases of the research project are discussed and outlined in Figure 6.1. From this figure, it can be observed that upcoming step is to compare the replicated model to existing experimental results; which have been performed at the section of Control and Simulation at TU Delft [40]. In order to do that, the experimental setup of the existing experiment needs to be used. This consists of the design of the forcing function, and time-varying CE dynamics which are defined in the sections below. Additionally, in order to compare the model to the existing experimental data, the parameters of the model need to be determined for the specific experimental setup used. Analysis of the results between the replicated model and existing experimental data would then lead to making modifications to the adaptive logic, conclusively yielding an improved framework for modeling the human adaptive process.

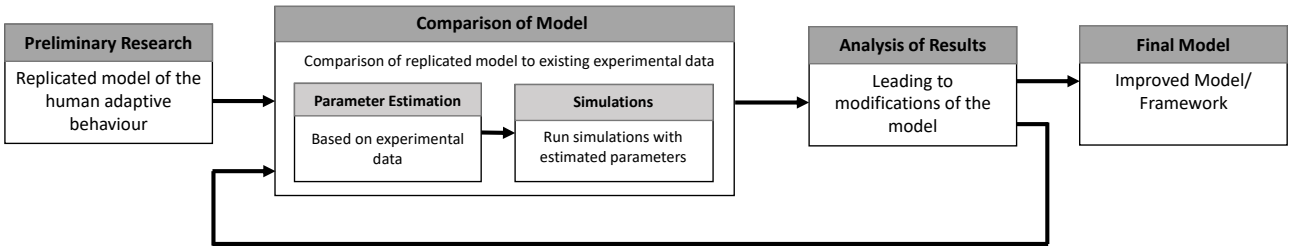

Figure 6.1: Flowchart of research progress

6.1. Parameter Estimation

The replicated model, introduced in Figure 3.6, has two parameters that have to be tuned in order to approximate the human operator for a nominal situation (pre-failure). These parameters are the gains values for K_r and K_p. A simple analysis can be made to determine what are the possible gain values for specific experimental set-up used. Figure 6.2 shows the range of values for the K_r and K_p gains in the pre-transition phase for the experimental-set up described in Chapter 4. Figure 6.2(a) shows possible combinations of K_r and K_p gains which lead to different values of the root mean square of the error (RMS(e)). Figure 6.2(b) shows possible combinations of K_r and K_p gains which lead to different root mean square values of the control activity u (RMS(u)). To lower the computation time, K_r ranged between 0 and 15 and K_p ranged between 0 and 5 with a step-time of 0.1. For combinations of K_r and K_p which lead to an unstable open-loop system, no data is shown in the figure. Moreover, from these figures it is evident that higher gain values lead to better performance until the system

becomes unstable (this cannot be seen in the figures due to the limited range of gains), however, better performance requires more control activity from the pilot. Therefore, a trade-off between the RMS(error) and RMS(u) values is necessary to determine suitable gain values.

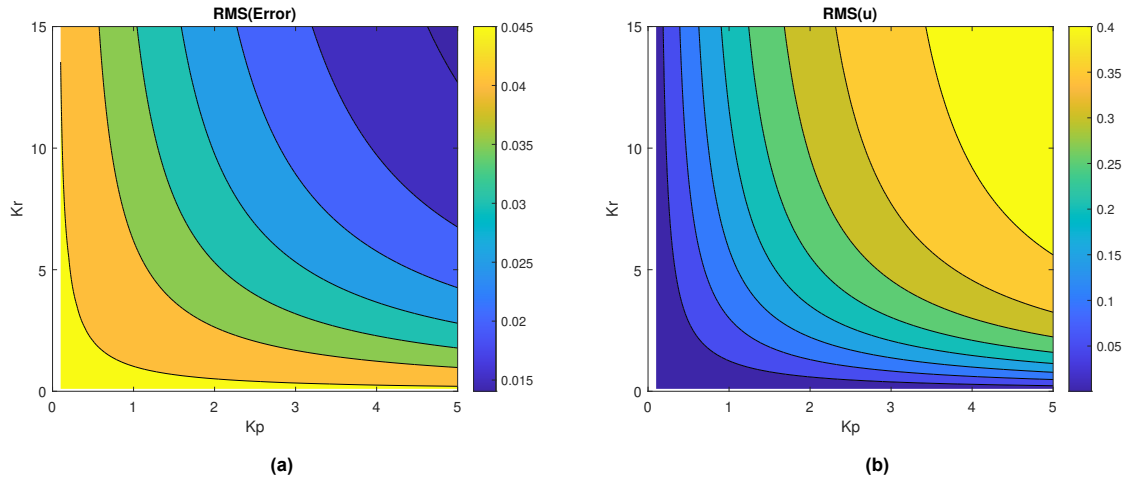

(a) (b)

Figure 6.2: K_r and K_p gain value combinations for RMS(error) (a) and RMS(u) (b)

Furthermore, as mentioned previously, Hess omitted the use of an effective time delay in his model. Therefore, an investigation needs to be conducted into analysing the effects of introducing an effective time delay which is an essential parameter of the human-describing function. Introducing a time delay term would also influence the initial parameters used for K_r and K_p, therefore, they would need to be re-determined.

Numerous techniques exists for estimating parameters of a pilot model from measurement data, these can be divided into parameter estimation in the time domain and in the frequency domain. The advantage of parameter estimation in the time domain is discussed by Zaal *et al.* in [41]. The vector $\theta = \begin{bmatrix} K_r & K_p & \tau \end{bmatrix}$ needs to be determined through an optimization problem (cost function). Where the difference between the model's controller output u_m, and the measured output of the human controller from the experimental data u_e is minimized.

6.2. Controlled Element Dynamics

To investigate the adaptation logic of Hess' model, it is necessary to examine how the model behaves with drastic changes in the CE dynamics. Moreover, in order to evaluate the results of the model, it is of importance to use CE dynamics which have been used in previous research on time varying control behaviour, such that the results can be evaluated. Previous research mainly focuses on a time-varying system that initially behaves like a single integrator, later transitioning to a double integrator and vice-versa [33],[40].

The structure of the CE dynamics is represented through the time-varying transfer function:

$$H_{c,w_b}(s) = \frac{K_c}{s(s+\omega_b)} \tag{6.1}$$

Where K_c represents the time-varying gain, and ω_b the time-varying break frequency. These time-varying parameters are implemented using the following sigmoid function:

$$P(t) = P_1 + \frac{P_2 - P_1}{1 + e^{(-G(t-M))}} \tag{6.2}$$

where P_1 and P_2 represent the initial and final values of the parameters K_c and ω_b. The value of G controls the speed of adaptation, which is kept a constant value of 100 s^{-1} in [40], this simulates step-like (instantaneous) changes. This parameter could interact with the adaptation of Hess' logic. Therefore, an investigation is needed to determine how this variable influences the model's adaptive logic, and whether a different constant is more suitable. Lastly, the parameter M represents the moment of maximum rate of change. This parameter will be equivalent to the one used in [40].

Table 6.1 shows the parameters which approximate single integrator dynamics $H_{c,si}$, and the double integrator dynamics $H_{c,di}$ in the region of the crossover frequency, while Figure 6.3 illustrates the frequency responses of the controlled elements.

Table 6.1: Controlled element dynamics

Symbol	Parameters	
	Kc [-]	$\omega_b[rad/s]$
$H_{c,si}$	90	6.0
$H_{c,di}$	30	0.2

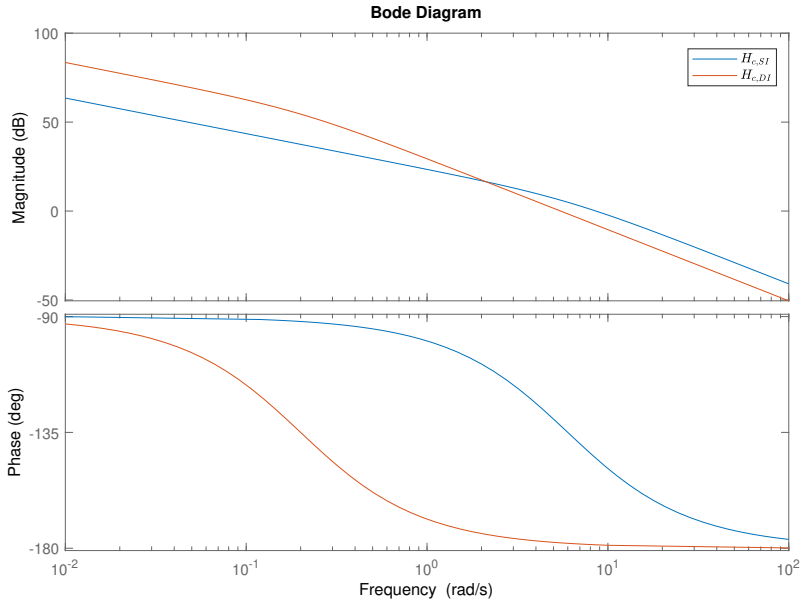

Figure 6.3: Frequency responses of the CE dynamics

6.3. Input Design - Forcing Functions

Input design is critically important to the results of the simulation, as research has shown that human pilots adapt their control strategy to the task they are exposed to [15]. Damveld *et al.* defined certain requirements that forcing functions must comply with. Forcing functions should not be predictable, and should appear to be random. If the pilot can anticipate the forcing function signal, then the pilot can adjust his/her response behavior accordingly. This means that the behavior needs to be modeled through a feedforward path, rather than a feedback system [42]. Furthermore, the forcing function should engage the pilot in order to prevent boredom, on the other hand, the signal should not be extremely difficult in order to avoid excessive workload.

In order to meet these requirements, forcing function signals are generally constructed as multisines which are a sum of sinusoids as shown in Equation (6.3) [21]. Single-sine inputs are not used as they

are predictable and would require multiple tests for a wide range of frequencies.

$$f_t(t) = \sum_{n=1}^{N} A_t[n] \sin\left(\omega_t[n]t + \phi_t[n]\right) \tag{6.3}$$

In this equation there are three important variables: $A_t[n]$, $\omega_t[n]$, and $\phi_t[n]$ which represent the amplitude, frequency, and phase shift of the n_{th} sine wave. N is the number of sine waves. The frequencies, ω_t, are integer multiples k of the fundamental measurement frequency ω_m, this is done in order to avoid spectral leakage [21].

While the total measurement time in the experimental set-up is $T = 90$ s, the signal is chosen to be periodic with three phases, meaning that the period is equal to $P = \frac{T_m}{3}$, therefore the forcing function has a period of 30 s. The advantage of having a periodic signal, is that the time traces can be directly compared across the three periods, and periodicity preserves the task difficulty meaning that the pilot is exposed to the same signal when transitioning from one dynamics to the other. Additionally, a run-in time of 5 sec was used.

The parameters values of the forcing function used in the experimental set-up as listed in Table 6.2 [40]. Note that two forcing functions are shown here, which can be distinguished through the phase shifts ϕ_t. The first forcing function, testing, will be used for parameter estimation. The second forcing function, validation, will be used for comparison of the replicated model to the experimental data results. Lastly, the crest factors were calculated in order to confirm that both forcing functions have similar values.

Table 6.2: Parameter values of forcing functions

			Testing	Validation
n [-]	ω_t [rad/s]	A_t [rad]	ϕ_t [rad]	ϕ_t [rad]
1	0.419	$2.905 \cdot 10^{-2}$	2.841	3.006
2	1.047	$1.961 \cdot 10^{-2}$	3.319	6.037
3	1.885	$1.020 \cdot 10^{-2}$	0.718	4.544
4	2.722	$6.032 \cdot 10^{-3}$	0.768	2.811
5	3.979	$3.356 \cdot 10^{-3}$	2.925	5.917
6	5.655	$1.983 \cdot 10^{-3}$	5.145	1.842
7	8.188	$1.230 \cdot 10^{-3}$	2.085	3.401
8	10.681	$9.331 \cdot 10^{-4}$	0.383	2.998
9	14.032	$7.541 \cdot 10^{-4}$	0.763	4.614
10	17.383	$6.674 \cdot 10^{-4}$	3.247	2.888

7

Conclusion

This preliminary report presents research which could have an important role in the improvement of safety in aviation. The goal of this project is to gain a better understanding of how pilots adapt their control strategy to maintain stability. Investigation into the pilot's adaptive behaviour would allow us to understand what *triggers* pilots to changes in the controlled element dynamics. The overarching goal of this thesis is to create a more complete mathematical model of the time-varying human adaptive behaviour, in the field of manual control.

Research in the field of manual control showed that the human adaptive behaviour should be considered in three phases: detection, identification, and modification. While a human adaptive model should capture these phases of adaptation, the detection phase would give more insight on what triggers the human pilot to adapt. According to the framework developed by Rasmussen which captures the nature of pilot control behaviour, detection is a skill-based behaviour which occurs unconsciously. In this behaviour, it is proposed that the CNS of the human pilot has an internal model of the task which is being performed. This internal model is constructed through experience from training and knowledge of the vehicle. Furthermore, research into different display models showed that the human pilot infers information differently depending on the nature of how it is presented. Since in a pursuit display the human pilot can recognize characteristics from the target signal and observe his/her own response, it is superior to the compensatory display.

Research in the current state-of-the-art models, which predict how humans adapt to changes in the system dynamics, showed that there are different way of creating these models. However, they are all based on the idea that humans have a reference model of the controlled system, also referred to as the internal model. This allows the human pilot to detect when a change in the system dynamics occurs from off-nominal tracking errors and error-rates in a compensatory tracking task, and outputs and output-rates in a pursuit tracking task. Some of the models presented can be re-created; therefore, one of the models was replicated in order to further investigate the human adaptive process.

The selected model for replication was the model developed by Ronald Hess, as there were several advantages of this model relative to the other models. Mainly, that this is the only model developed for a pursuit tracking task and it captures all phases of adaptation. This model is rule-based, where the adaptive logic is heuristically developed. Detection of changing CE dynamics is based on a trigger function, which, if activated, results in gain value variations in order to adapt to the rapidly changing vehicle dynamics. Comparison of the replicated model to the original model showed that there are slight differences in results; nevertheless, both models capture the essence of the adaptive human behaviour.

Moreover, a sensitivity analysis of varying the time at which CE dynamics changed showed that there were no significant changes in the pilot-model adaptation. However, this analysis revealed one of

the limitations of the model: the human pilot's control gains have no memory. In addition, another sensitivity analysis was conducted where the time interval over which CE dynamics change was varied. This analysis showed that adaptation is stronger for instantaneous change in CE dynamics compared to slow changes. However, one factor to consider is that the slow changes are implemented in a wider range of the forcing function (because their time period is larger) which also influences adaptation. Finally, the future developments of this research are presented, where the current replicated model will be compared to existing experimental data results. This will allow for validation of the model, which is currently lacking. Overall, the main goal is to create an improved framework for modeling the adaptive human process. This will be done by improving the model's adaptive logic and re-validating the model with experimental data in an iterative process.

References

[1] Drop F.M. *Control-Theoretic Models of Feedforward in Manual Control*. Vol. 46. Logos Verlag Berlin GmbH, 2016.

[2] Mulder, M., Pool, D.M., Abbink, D.A., Erwin R.B., Zaal, P.M.T., Frank M.D., van der El, K., van Paassen, M.M. "Manual control cybernetics: State-of-the-art and current trends". In: *IEEE Transactions on Human-Machine Systems* 48.5 (2017), pp. 468–485.

[3] McRuer, D.T. and Jex, H.R. "A review of quasi-linear pilot models". In: *IEEE transactions on human factors in electronics* 3 (1967), pp. 231–249.

[4] IATA. *Loss of Control In-flight (LOC-I)*. URL: https://www.iata.org/en/programs/safety/loss-of-control-inflight/.

[5] Tohidi, S.S. and Yildiz, Y. "Adaptive human pilot model for uncertain systems". In: *2019 18th European Control Conference (ECC)*. IEEE. 2019, pp. 2938–2943.

[6] Young, L.R., Green, D.M., Elkind, J.I., Kelly, J.A. "Adaptive Dynamic Response Characteristics of the Human Operator in Simple Manual Control". In: *IEEE Transactions on Human Factors in Electronics* HFE-5.1 (1964), pp. 6–13. DOI: 10.1109/THFE.1964.231648.

[7] Koppen, O.C. "Airplane Stability and Control from a Designer's Point of View". In: *Journal of the Aeronautical Sciences* 7.4 (1940), pp. 135–140.

[8] Stern, E. "Individual differences in the learning potential of human beings". In: *npj Science of Learning* 2.1 (2017), pp. 1–7.

[9] Young, L.R. "On adaptive manual control". In: *Ergonomics* 12.4 (1969), pp. 635–674.

[10] Rasmussen, J. "Skills, rules, and knowledge; signals, signs, and symbols, and other distinctions in human performance models". In: *IEEE transactions on systems, man, and cybernetics* 3 (1983), pp. 257–266.

[11] Vidal, F., Meckler, C., Hasbroucq, T. "Basics for sensorimotor information processing: some implications for learning". In: *Frontiers in Psychology* 6 (2015), p. 33. ISSN: 1664-1078. DOI: 10.3389/fpsyg.2015.00033. URL: https://www.frontiersin.org/article/10.3389/fpsyg.2015.00033.

[12] Henk, S.G., Johannsen, G., Moray, N. "Internal representation, internal model, human performance model and mental workload". In: *Automatica* 26.4 (1990), pp. 811–820. ISSN: 0005-1098. DOI: https://doi.org/10.1016/0005-1098(90)90057-O. URL: https://www.sciencedirect.com/science/article/pii/0005109890900570.

[13] Veldhuyzen, W. and Stassen, H.G. "The internal model concept: An application to modeling human control of large ships". In: *Human Factors* 19.4 (1977), pp. 367–380.

[14] Tustin, A. "The nature of the operator's response in manual control, and its implications for controller design". In: *Journal of the Institution of Electrical Engineers-Part IIA: Automatic Regulators and Servo Mechanisms* 94.2 (1947), pp. 190–206.

[15] Elkind, J.I. "Characteristics of simple manual control systems". In: (1956).

[16] McRuer, D.T. *Human pilot dynamics in compensatory systems*. Tech. rep. Systems Technology INC Hawthorne CA, 1965.

[17] National Research Council. *Aviation Safety and Pilot Control: Understanding and Preventing Unfavorable Pilot-Vehicle Interactions*. Washington, DC: The National Academies Press, 1997. ISBN: 978-0-309-05688-5. DOI: 10.17226/5469.

[18] Kleinman, D.L, Baron, S., Levison, W.H. "An optimal control model of human response part I: Theory and validation". In: *Automatica* 6.3 (1970), pp. 357–369. DOI: https://doi.org/10.

1016/0005-1098(70)90051-8. URL: https://www.sciencedirect.com/science/article/pii/0005109870900518.

[19] Xu, S., Tan, W., Efremov, A.V., Sun, L., and Qu, X. “Review of control models for human pilot behavior”. In: *Annual Reviews in Control* 44 (2017), pp. 274–291. ISSN: 1367-5788. DOI: https://doi.org/10.1016/j.arcontrol.2017.09.009. URL: https://www.sciencedirect.com/science/article/pii/S136757881730024X.

[20] Sweet, B.T. *The identification and modeling of visual cue usage in manual control task experiments*. Stanford University, 1999.

[21] van der El, K. “How humans use preview information in manual control”. In: (2018). DOI: https://doi.org/10.4233/uuid:cda9dd80-0a51-436e-9c70-ea174505692a.

[22] Chernikoff, R., Brimingham, H.P., Taylor, F.V. “A comparison of pursuit and compensatory tracking under conditions of aiding and no aiding.” In: *Journal of Experimental Psychology* 49.1 (1955), p. 55.

[23] Wasicko, R.J., McRuer, D.T., Magdaleno, R.E. *Human pilot dynamic response in single-loop systems with compensatory and pursuit displays*. Tech. rep. SYSTEMS TECHNOLOGY INC HAWTHORNE CA, 1966.

[24] Vos, M.C., Pool, D.M., Damveld, H.J., van Paassen, M.M., Mulder, M. “Identification of multimodal control behavior in pursuit tracking tasks”. In: *2014 IEEE International Conference on Systems, Man, and Cybernetics (SMC)*. IEEE. 2014, pp. 63–68.

[25] Allen, W.R., Jex, H.R. *An experimental investigation of compensatory and pursuit tracking displays with rate and acceleration control dynamics and a disturbance input*. Vol. 1082. National Aeronautics and Space Administration Washington, 1968.

[26] Mulder, M., Pool, D.M., Van der El, K., Drop, F.M., Van Paassen, M.M. “Manual Control with Pursuit Displays: New Insights, New Models, New Issues”. In: *IFAC-PapersOnLine* 52.19 (2019), pp. 139–144.

[27] Hess, R.A. “Modeling the pilot detection of time-varying aircraft dynamics”. In: *Journal of aircraft* 49.6 (2012), pp. 2100–2104.

[28] Stark, L. and Young, L.R. “Biological control system-a critical review and evaluation, developments in manual control”. In: (1965).

[29] Miller, D.C. and Elkind, J.I. “The adaptive response of the human controller to sudden changes in controlled process dynamics”. In: *IEEE Transactions on Human Factors in Electronics* 3 (1967), pp. 218–223.

[30] Phatak, A.V. and Bekey, G.A. “Model of the Adaptive Behavior of the Human Operator in Response to a Sudden Change in the Control Situation”. In: *IEEE Transactions on Man-Machine Systems* 10.3 (1969), pp. 72–80. DOI: 10.1109/TMMS.1969.299886.

[31] Phatak, A.V. “On the adaptive behavior of the human operator in response to a sudden change in the control situation”. PhD thesis. University of Southern California, 1968.

[32] Phatak, A.V. and Bekey, G.A. “Decision processes in the adaptive behavior of human controllers”. In: *IEEE Transactions on Systems Science and Cybernetics* 5.4 (1969), pp. 339–351.

[33] van Ham, J. “Predicting Adaptive Human Control Behavior to Changing Controlled Element Dynamics Based on Statistical Variations in Error and Error Rate”. In: (2021).

[34] Hess, R.A. “Modeling pilot control behavior with sudden changes in vehicle dynamics”. In: *Journal of Aircraft* 46.5 (2009), pp. 1584–1592.

[35] Hess, R.A. “A model for pilot control behavior in analyzing potential loss-of-control events”. In: *Proceedings of the Institution of Mechanical Engineers, Part G: Journal of Aerospace Engineering* 228.10 (2014), pp. 1845–1856.

[36] Hess, R.A. “Modeling human pilot adaptation to flight control anomalies and changing task demands”. In: *Journal of Guidance, Control, and Dynamics* 39.3 (2016), pp. 655–666.

[37] Proske, U. and Gandevia, S.C. “The proprioceptive senses: their roles in signaling body shape, body position and movement, and muscle force”. In: *Physiological reviews* (2012).

[38] Hess, R.A. ""Fast Simulation" in Evaluating Pilot/Aircraft Performance and Handling Qualities". In: *IFAC-PapersOnLine* 49.32 (2016). Cyber-Physical Human-Systems CPHS 2016, pp. 153–158. ISSN: 2405-8963. DOI: https://doi.org/10.1016/j.ifacol.2016.12.206. URL: https://www.sciencedirect.com/science/article/pii/S2405896316328786.

[39] Hess, R.A. "Simplified approach for modelling pilot pursuit control behaviour in multi-loop flight control tasks". In: *Proceedings of the Institution of Mechanical Engineers, Part G: Journal of Aerospace Engineering* 220.2 (2006), pp. 85–102.

[40] Terenzi, L. "Adaptive Motor Control: a Predictive Coding Approach". In: (2021).

[41] Zaal, P.M.T., Pool, D.M., Chu, Q.P., Van Paassen, M.M., Mulder, M. and Mulder, Jan A. "Modeling human multimodal perception and control using genetic maximum likelihood estimation". In: *Journal of Guidance, Control, and Dynamics* 32.4 (2009), pp. 1089–1099.

[42] Damveld, H. J. "A cybernetic approach to assess the longitudinal handling qualities of aeroelastic aircraft". In: (2009).

[43] Zaal, P.M.T. "Manual control adaptation to changing vehicle dynamics in roll–pitch control tasks". In: *Journal of guidance, control, and dynamics* 39.5 (2016), pp. 1046–1058.

A

Replicating Hess' Model

This chapter shows how the Hess' model was implemented in MATLAB and Simulink. Figure A.1 shows the main structure of the replicated model, while rest of the figures show the sub-systems.

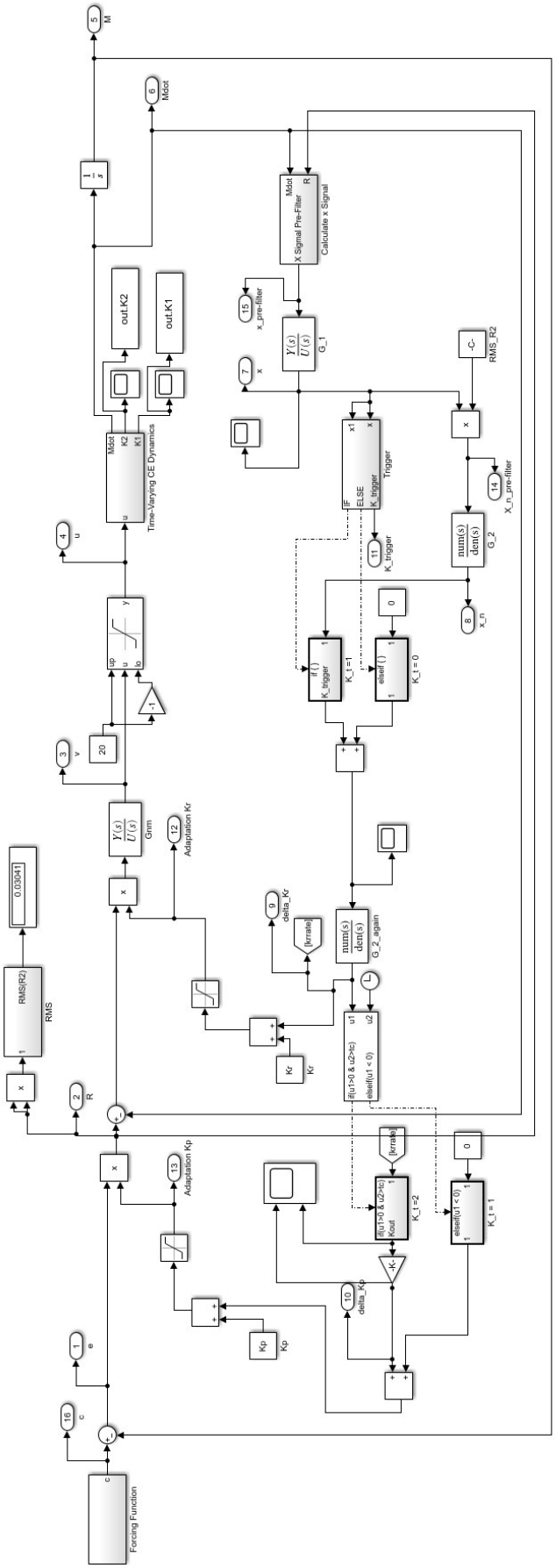

Figure A.1: Simulink Block Diagram of Hess' Model

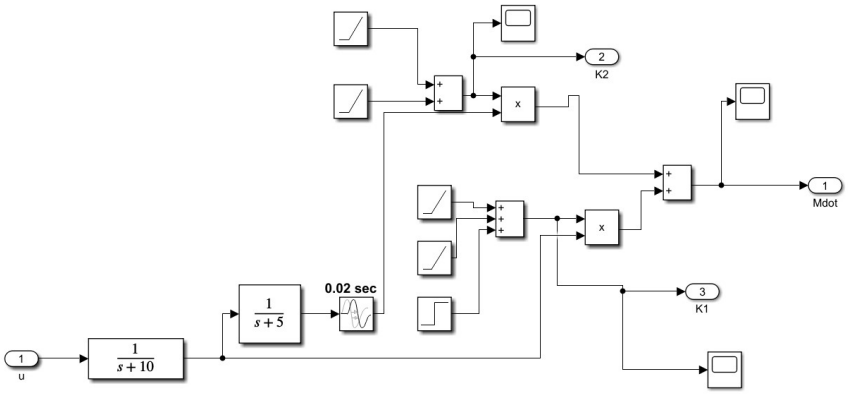

Figure A.2: Implementation of time-varying CE dynamics

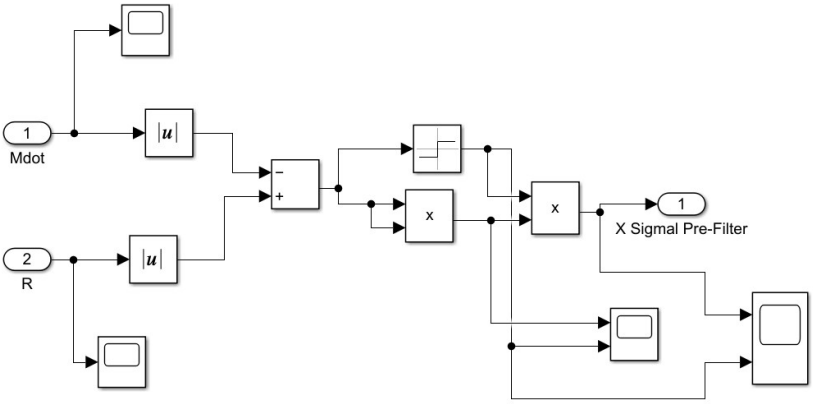

Figure A.3: Calculation of x signal

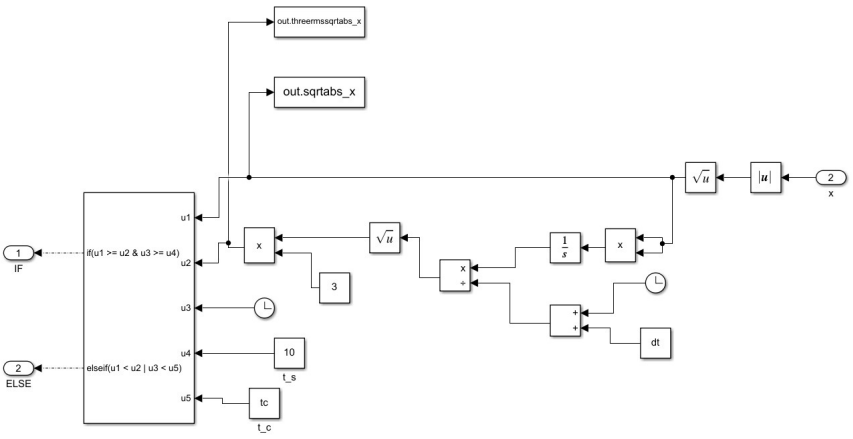

Figure A.4: Trigger Function

B

Investigation into Hess' Model

This chapter aims to understand how different parameters of the selected Hess model, in particular the gains K_r and K_p, are tuned for specific CE vehicle dynamics Y_c. The values of both K_r and K_p are dependent on a defined set of CE vehicle dynamics, Y_c. Therefore, in order to be able to use this model for different vehicle dynamics, it is important to tune these gains accordingly.

When describing the model of the human pilot control behaviour, Hess defines two methods which can be used to choose the value for the inner-loop gain K_r [39]. One method to select K_r is by creating a closed loop transfer function of the inner loop and choosing the gain K_r which corresponds to the minimum damping ratio of ζ_{min} = 0.15. Equation (B.1) demonstrates how the closed loop transfer function of the inner loop can be obtained. Equation (B.2) shows the general structure of a second-order transfer function, here ω_n and ζ represent the natural frequency and damping ratio, respectively.

$$\begin{aligned} Y_{OL}^{inner} &= K_r G_{nm} Y_c s \\ Y_{CL}^{inner} &= \frac{Y_{OL}^{inner}}{1 + Y_{OL}^{inner}} \end{aligned} \tag{B.1}$$

$$H(s) = \frac{\omega_n^2}{s^2 + 2\zeta s + \omega_n^2} \tag{B.2}$$

Alternately, Hess proposes another method to select K_r which is based on the Bode plot of the closed-loop inner-loop transfer function ($\frac{\dot{M}}{R}$). According to Hess, the gain K_r should be chosen such that it yields a 10 dB difference of magnitude between the neuromuscular peak and the mid-frequency of the transfer function, as visualized in Figure B.1.

Moreover, the outer-loop gain K_p should be chosen such that it provides a desired open-loop crossover frequency for the model. The selection of gain K_p is similar to the one from the theory of McRuer *et al.*, as discussed in Chapter 2. However, Hess does not disclose the reasoning behind the methods used to select values for K_r gain.

Therefore, it was decided to select the gains based on theory, such as the crossover model, which has been proved and validated. The theory of the crossover model, described in Chapter 2, is only validated for a compensatory display where the model is represented by a single loop as shown in Figure 2.2. Thus, in order to compare Hess' model to the crossover model, an investigation was made on whether Hess' model can be re-written into a single loop model. As mentioned in Section 3.1.4, Hess' original model is composed of an outer loop, representing the position, and an inner loop, representing the rate of change. Hess' original model was re-written into a single loop by combining the inner and the outer

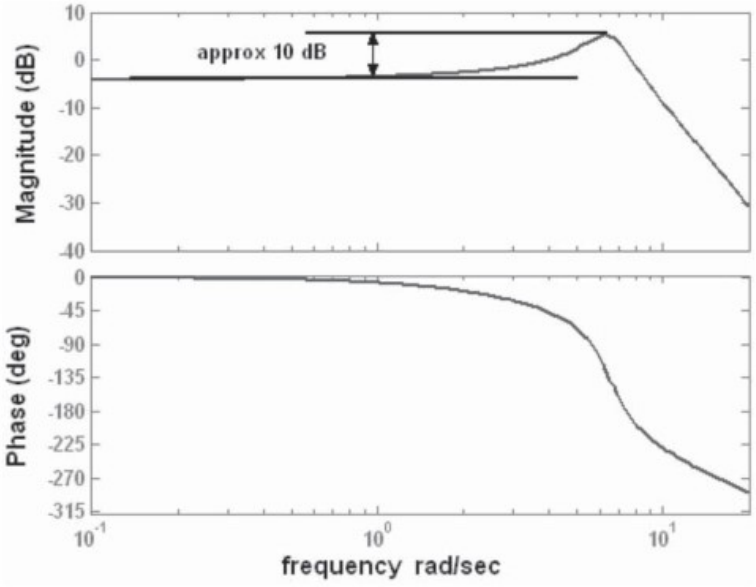

Figure B.1: Choosing K_r from the bode plot diagram of inner open-loop($\frac{\dot{M}}{R}$) [39]

loops, as shown in Figure B.2. The outcome of this model is similar to McRuer's model when comparing the pilot control dynamics $Y_p(s)$. Equation (B.3) gives the typical structure of the human-describing function proposed by McRuer where the limitations of neuromuscular systems are also present. Note that this human-describing function is a simplification of the McRuer *et al.* precision model [16], and is equivalent to the pilot control behaviour model used by Zaal [43].

$$Y_p(s) = \overbrace{K_p(1+T_L s)}^{\text{equalization}} \overbrace{e^{-j\omega\tau_e} G_{nm}}^{\text{limitations}} \tag{B.3}$$

The human-describing function can also be derived from the re-written single loop model shown in Figure B.2 and is given by Equation (B.4). Here, the equivalence with McRuer *et al.* model is evident, where the lead equalization parameter T_L is equivalent to the ratio of $\frac{K_r}{K_p}$. It can also be observed that in Equation (B.4) the effective time delay τ_e is not present as it is ommited in Hess' original model.

$$Y_p(s) = (K_p + K_r s)G_{nm} = K_p(1 + \frac{K_r}{K_p}s)G_{nm} \tag{B.4}$$

Then, depending on the controlled element dynamics $Y_c(s)$ of the vehicle, the parameters of the model can be computed using the verbal adjustment rules. The gain values K_r and K_p are obtained through Equation (B.5).

$$|Y_{OL}(j\omega)|_{\omega=\omega_c} = |Y_p(j\omega)Y_c(j\omega)|_{\omega=\omega_c} = 1 \tag{B.5}$$

However, further investigation into the re-written model and Hess' original model showed that these two models are not equivalent. This is because the original model contains an inner-loop feedback signal of the output rate $\dot{M}$, required for the computation of the signal x, which is proportional to the square of the inner-loop error signal. In the re-written model, the x signal cannot be computed as it is constructed using a PD controller ($K_r s$), which leads to a different signal. Using a PD controller makes the system respond faster due to the derivative on the tracking target signal C.

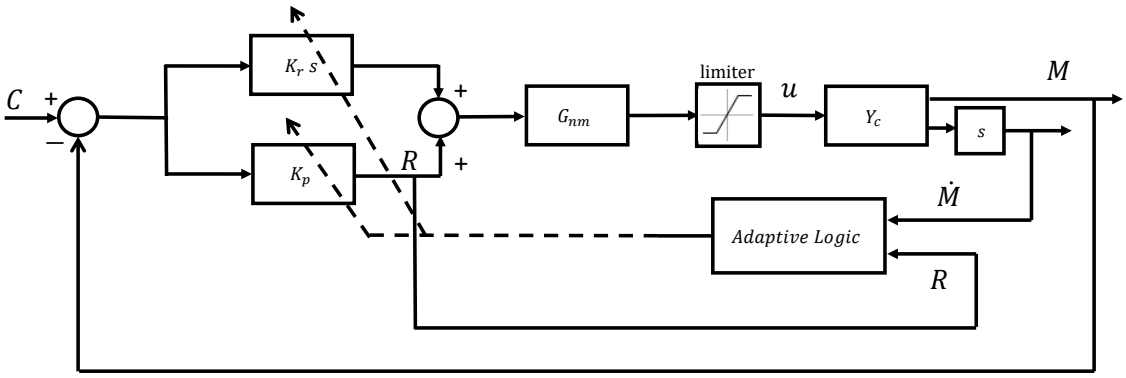

Figure B.2: Conversion to single loop of Hess' Model

The conclusion of this investigation is that the models are not equivalent and that Hess' model cannot be re-written using the structure of McRuer's model. It was also decided that the gain values K_r and K_p for a defined controlled element dynamics will be determined based on time-domain parameter estimation techniques. This will be accomplished using existing results from experimental data conducted at the Control and Simulation department at TU Delft [40].

C

Sensitivity Analysis Results (time of CE change)

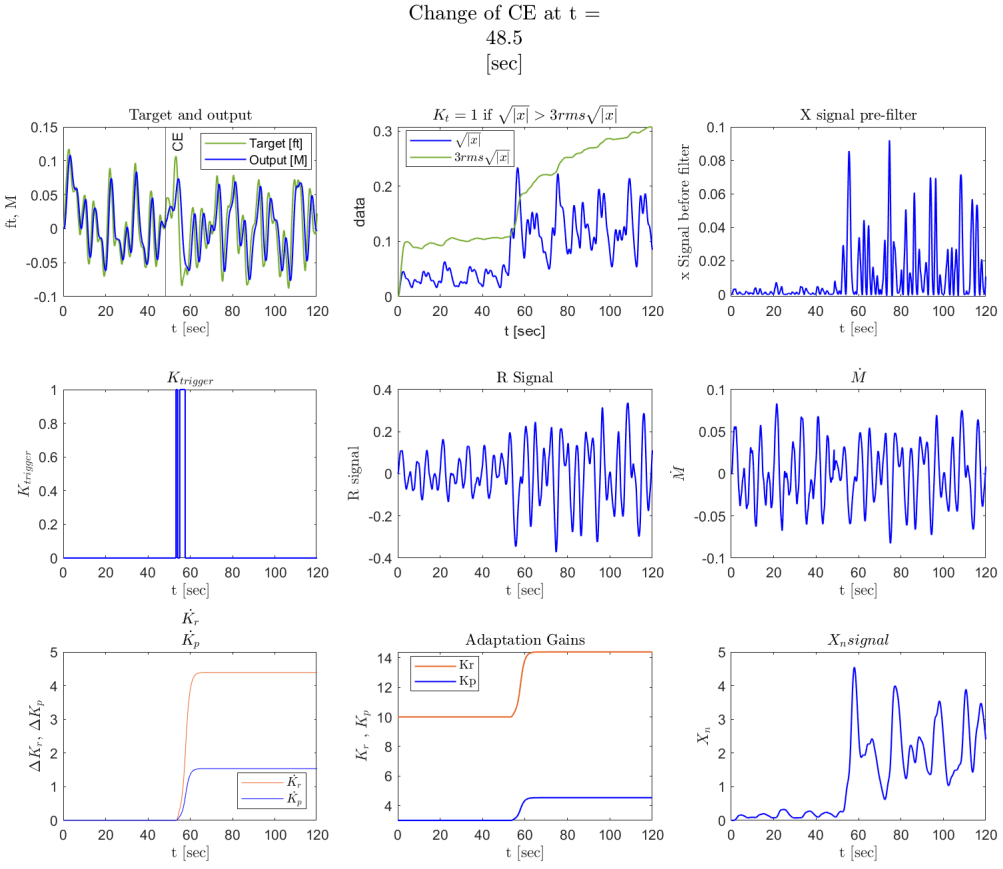

Change of CE at t = 48.5 [sec]

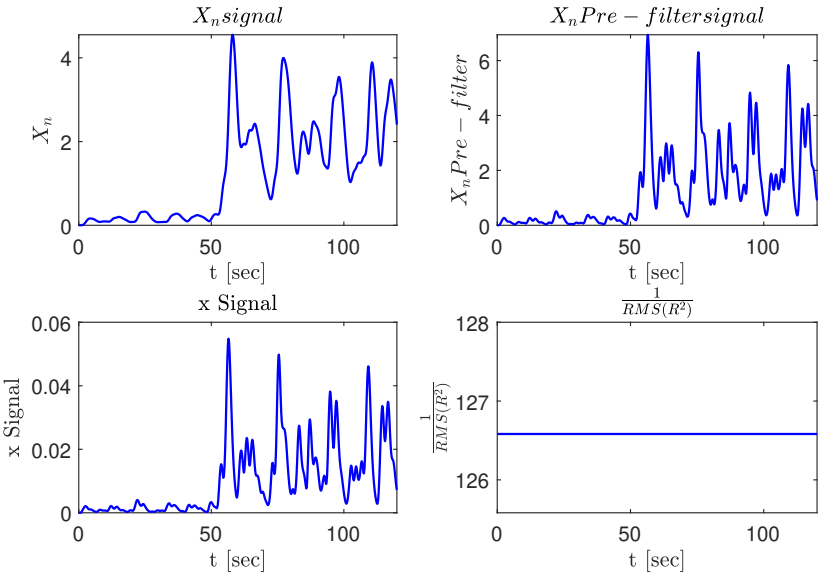

Change of CE at t = 49 [sec]

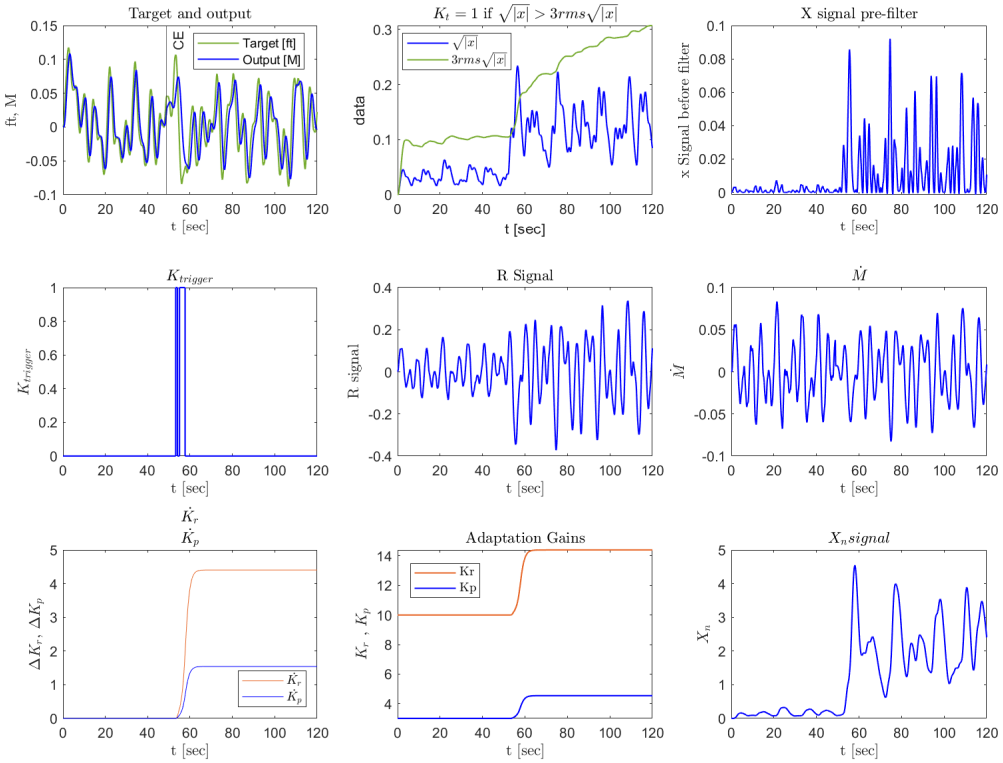

Change of CE at t = 49 [sec]

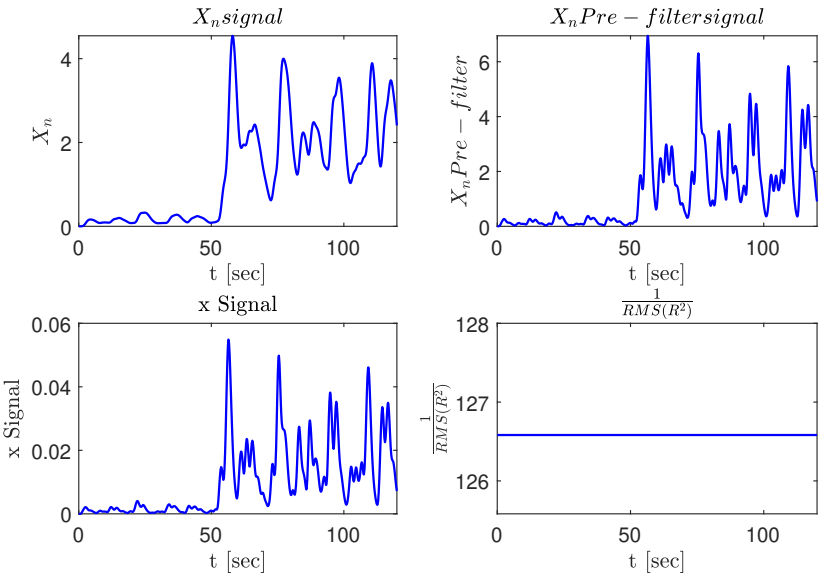

Change of CE at t = 49.5 [sec]

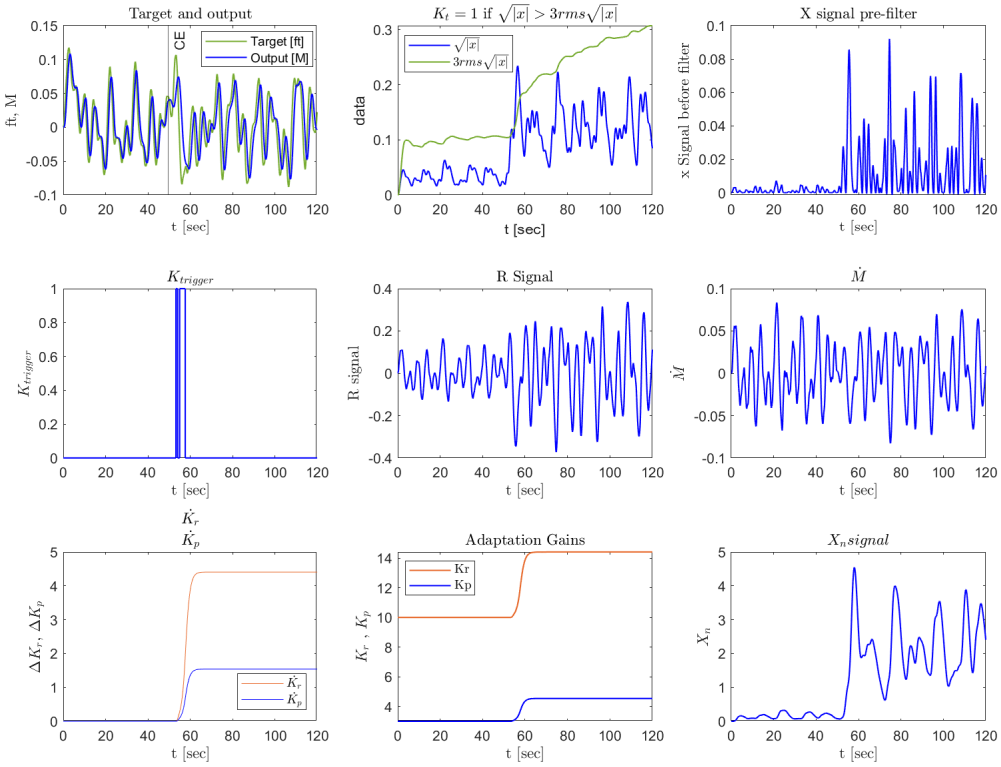

Change of CE at t = 49.5 [sec]

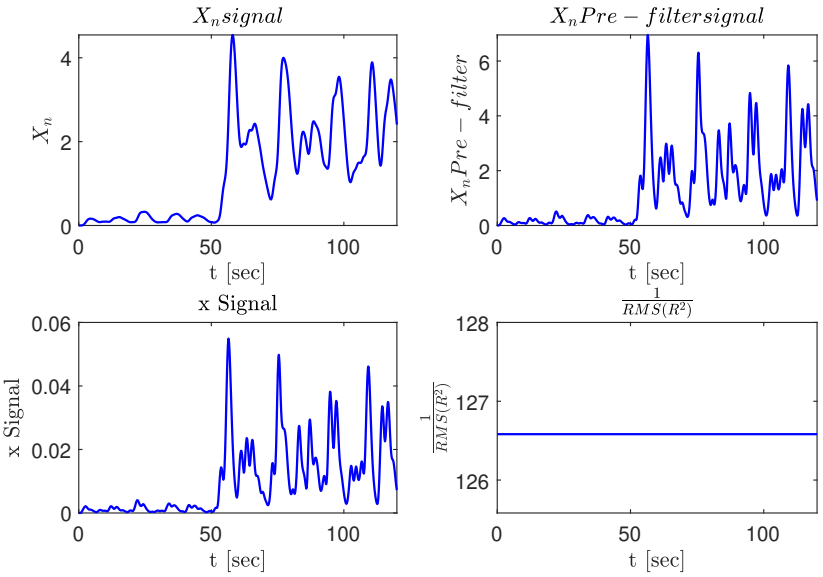

Change of CE at t = 50 [sec]

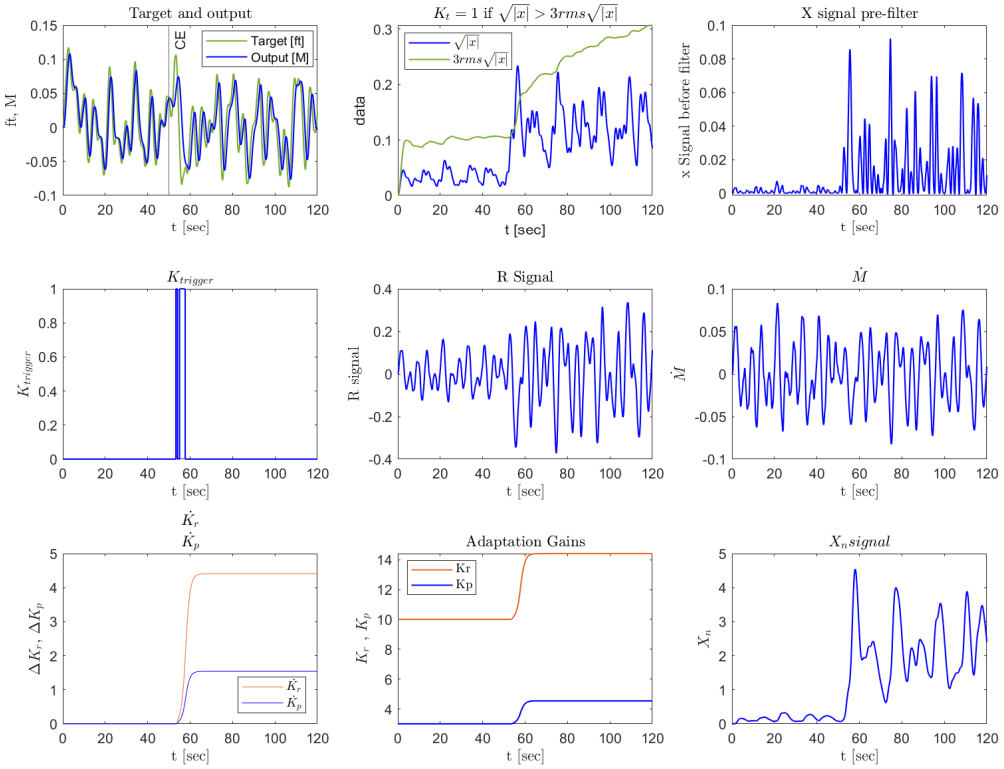

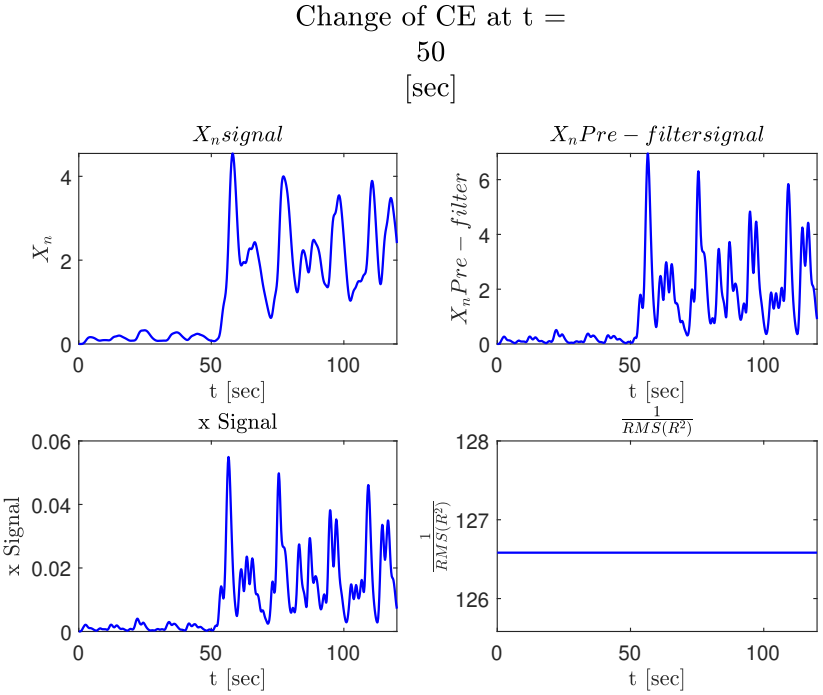
Change of CE at t = 50 [sec]
$X_n signal$
$X_n Pre-filter signal$
X_n
$X_n Pre-filter$
t [sec]
x Signal
$\frac{1}{RMS(R^2)}$

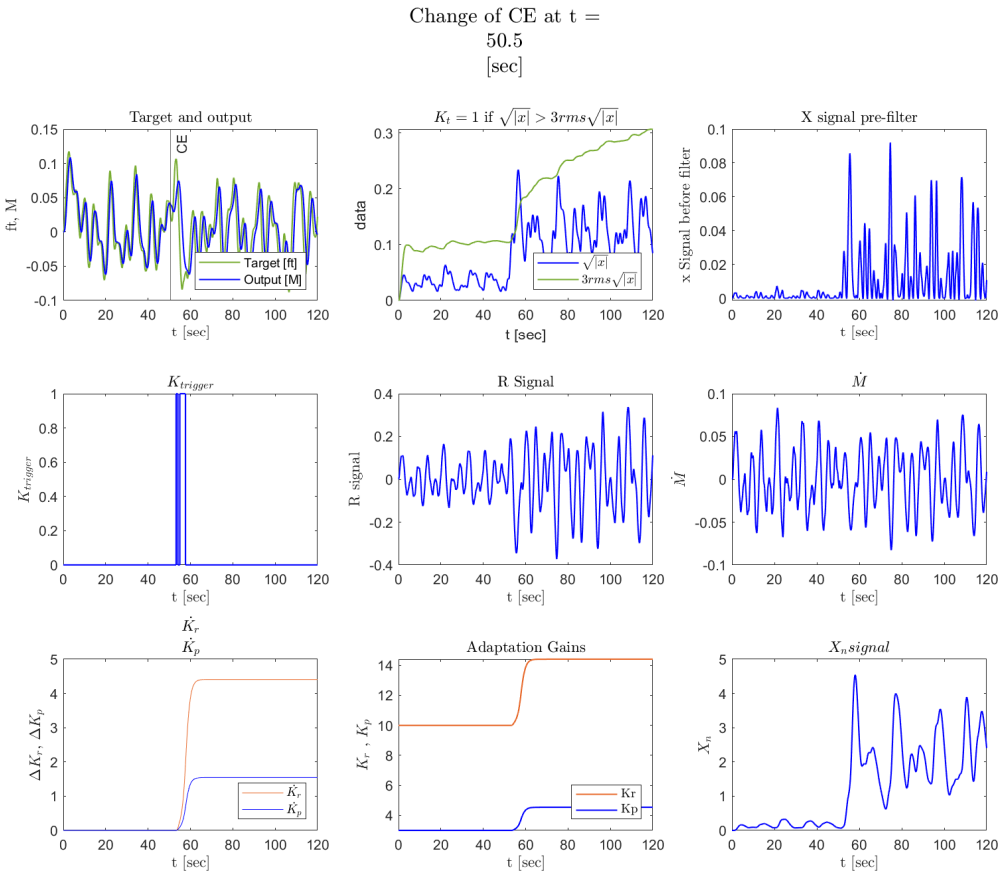
Change of CE at t = 50.5 [sec]
Target and output
$K_t = 1$ if $\sqrt{|x|} > 3rms\sqrt{|x|}$
X signal pre-filter
CE
Target [ft]
Output [M]
ft, M
data
x Signal before filter
$K_{trigger}$
R Signal
$\dot{M}$
R signal
$\dot{K}_r$
$\dot{K}_p$
Adaptation Gains
$\Delta\dot{K}_r$, $\Delta\dot{K}_p$
K_r, K_p
Kr
Kp
$X_n signal$
X_n
t [sec]

Change of CE at t = 50.5 [sec]

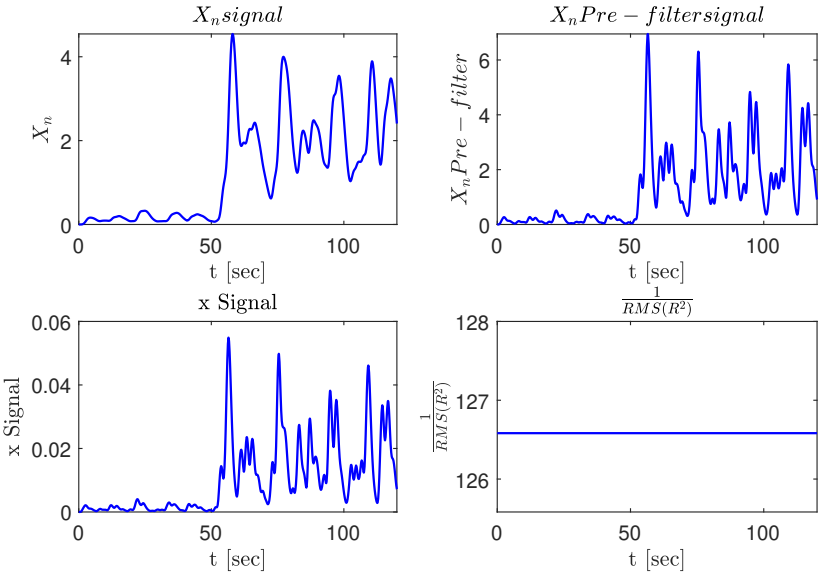

Change of CE at t = 51 [sec]

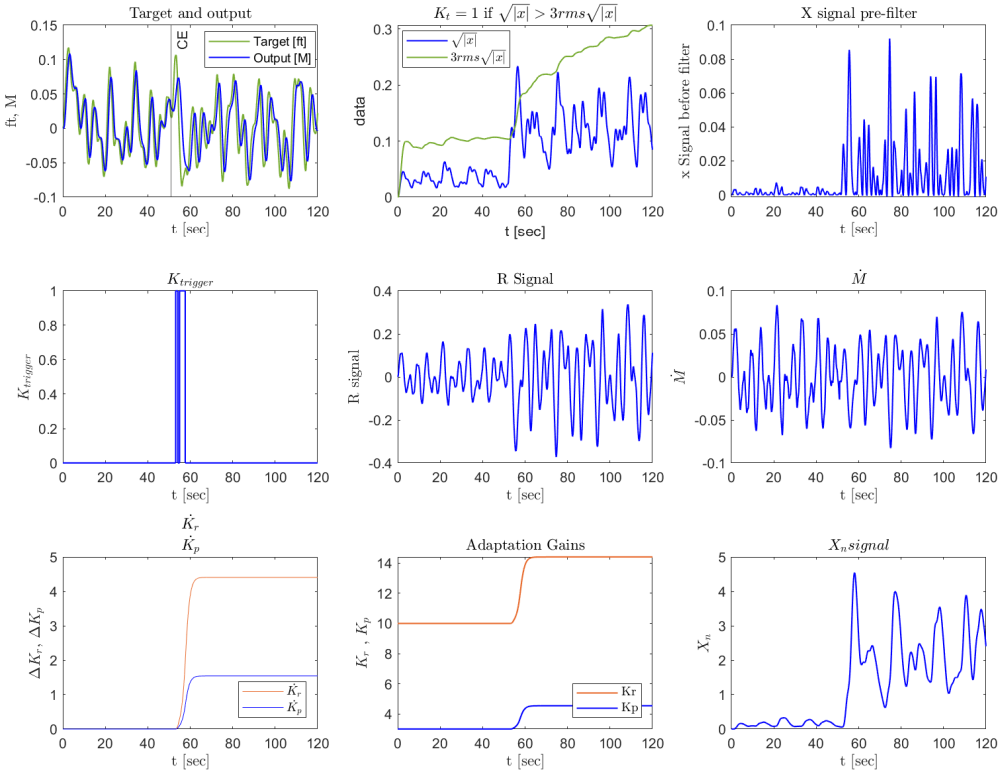

Change of CE at t =
51
[sec]

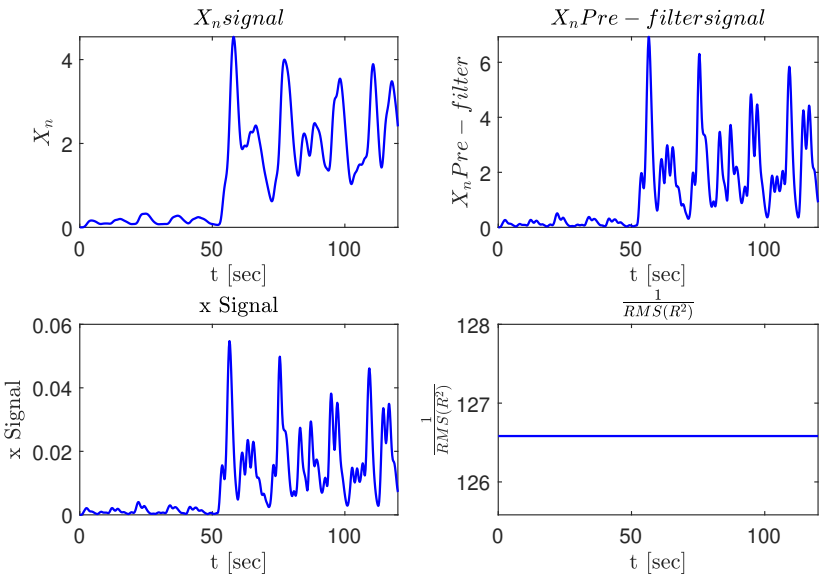

D

Sensitivity Analysis Results (interval of CE change)

Table D.1: Summary of open-loop stability characteristics

DELT [sec]	K_r, K_p	Phase margin ϕ_m	Crossover frequency ω_c
0.05	$K_r = 14.4081$, $K_p = 4.5428$	60	1.0336
0.5	$K_r = 14.4079$, $K_p = 4.5427$	60.1299	1.0336
1	$K_r = 14.4068$, $K_p = 4.5424$	60.1336	1.0334
5	$K_r = 14.3966$, $K_p = 4.5388$	60.1742	1.0320
10	$K_r = 12.5561$, $K_p = 3.8946$	66.6658	0.7879
15	$K_r = 12.3949$, $K_p = 3.8382$	67.2345	0.7681

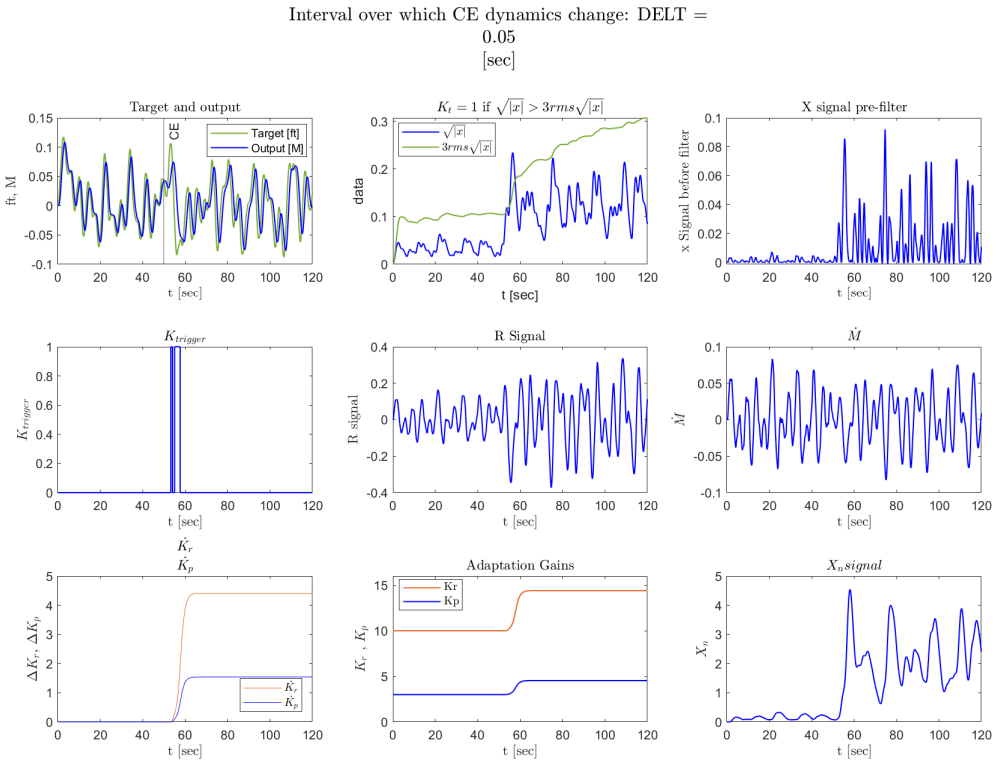

Interval over which CE dynamics change: DELT = 0.05 [sec]

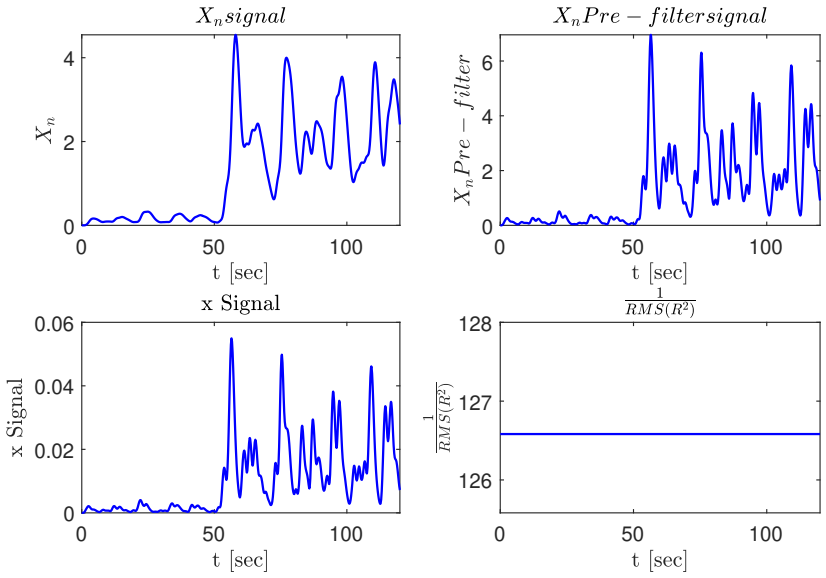

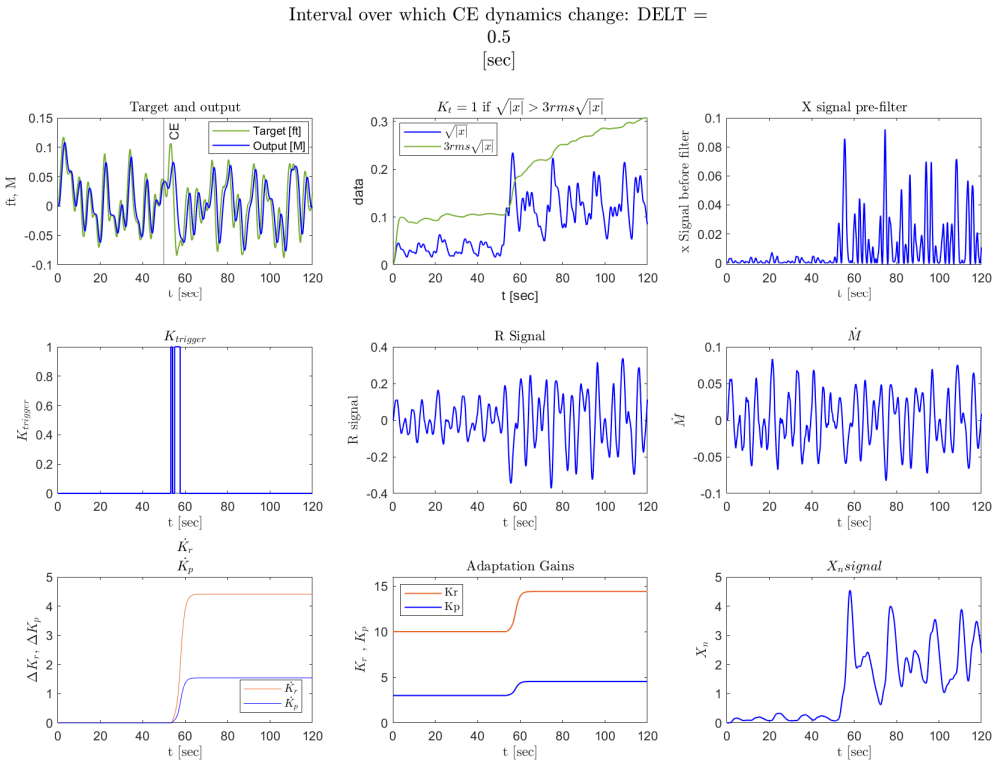

Interval over which CE dynamics change: DELT = 0.5 [sec]

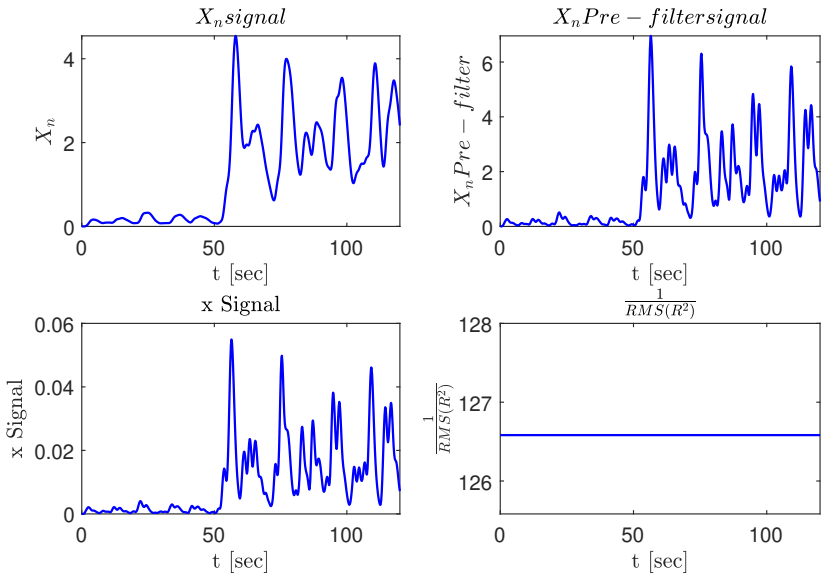

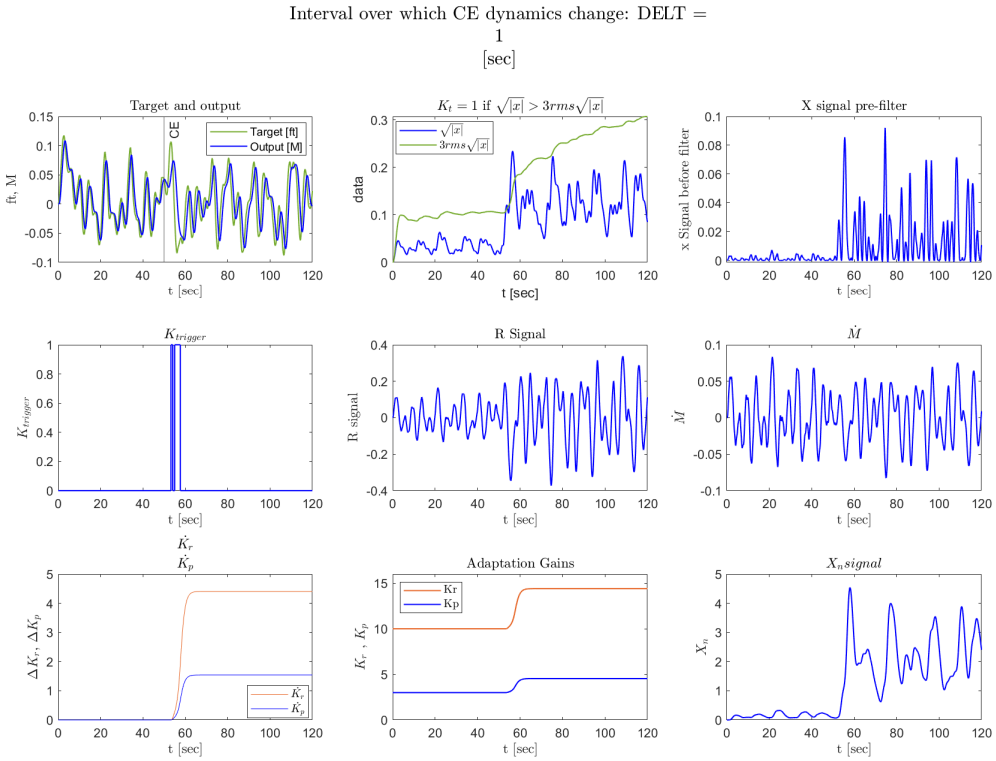
Interval over which CE dynamics change: DELT = 1 [sec]
Target and output
Target [ft]
Output [M]
CE
ft, M
t [sec]
$K_t = 1$ if $\sqrt{|x|} > 3rms\sqrt{|x|}$
$\sqrt{|x|}$
$3rms\sqrt{|x|}$
data
t [sec]
X signal pre-filter
x Signal before filter
t [sec]
$K_{trigger}$
$K_{trigger}$
t [sec]
R Signal
R signal
t [sec]
$\dot{M}$
$\dot{M}$
t [sec]
$\dot{K}_r$
$\dot{K}_p$
$\Delta\dot{K}_r$, $\Delta\dot{K}_p$
t [sec]
Adaptation Gains
Kr
Kp
K_r , K_p
t [sec]
$X_n signal$
X_n
t [sec]

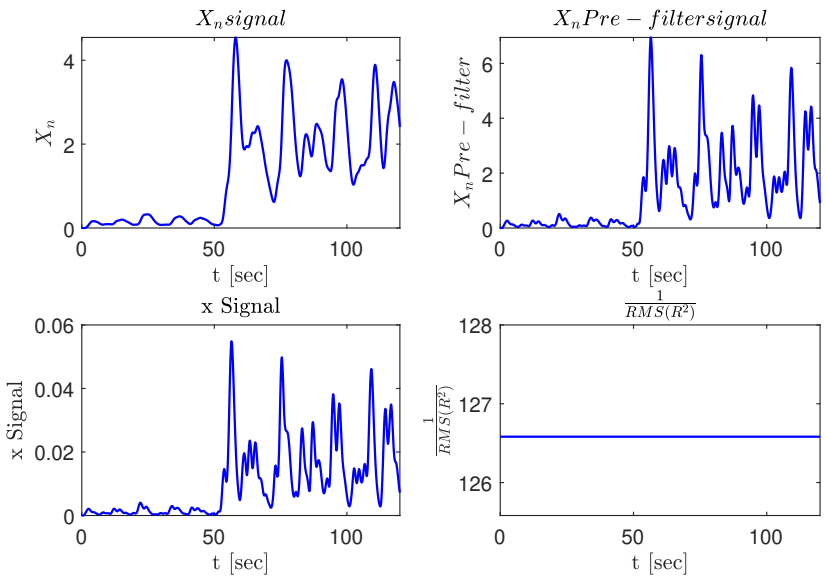
Interval over which CE dynamics change: DELT = 1 [sec]
$X_n signal$
X_n
t [sec]
$X_n Pre-filter signal$
$X_n Pre-filter$
t [sec]
x Signal
x Signal
t [sec]
$\frac{1}{RMS(R^2)}$
$\frac{1}{RMS(R^2)}$
t [sec]

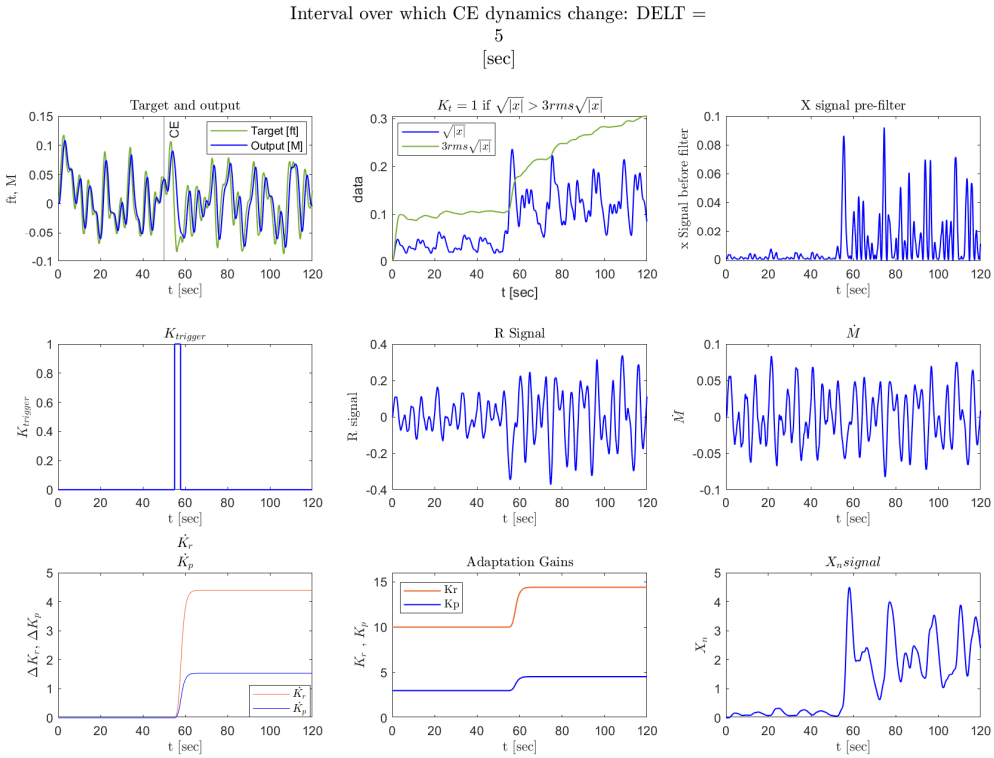

Interval over which CE dynamics change: DELT = 5 [sec]

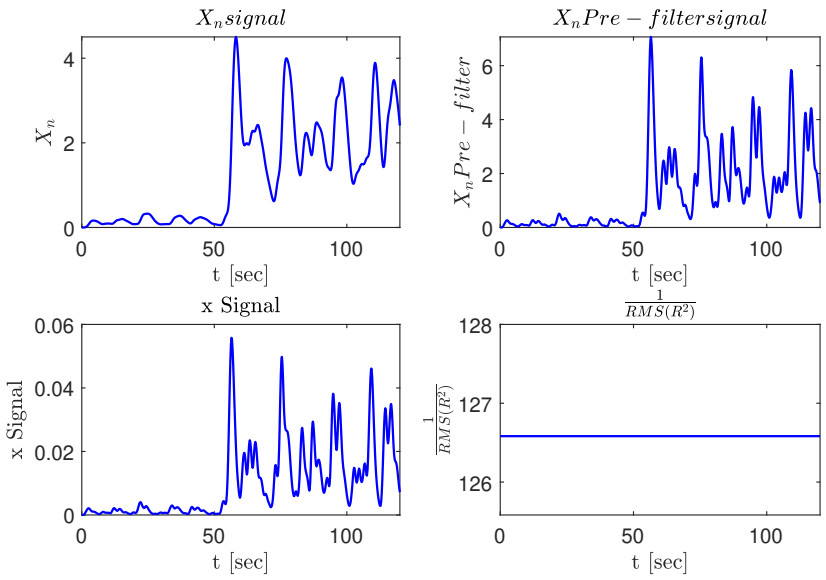

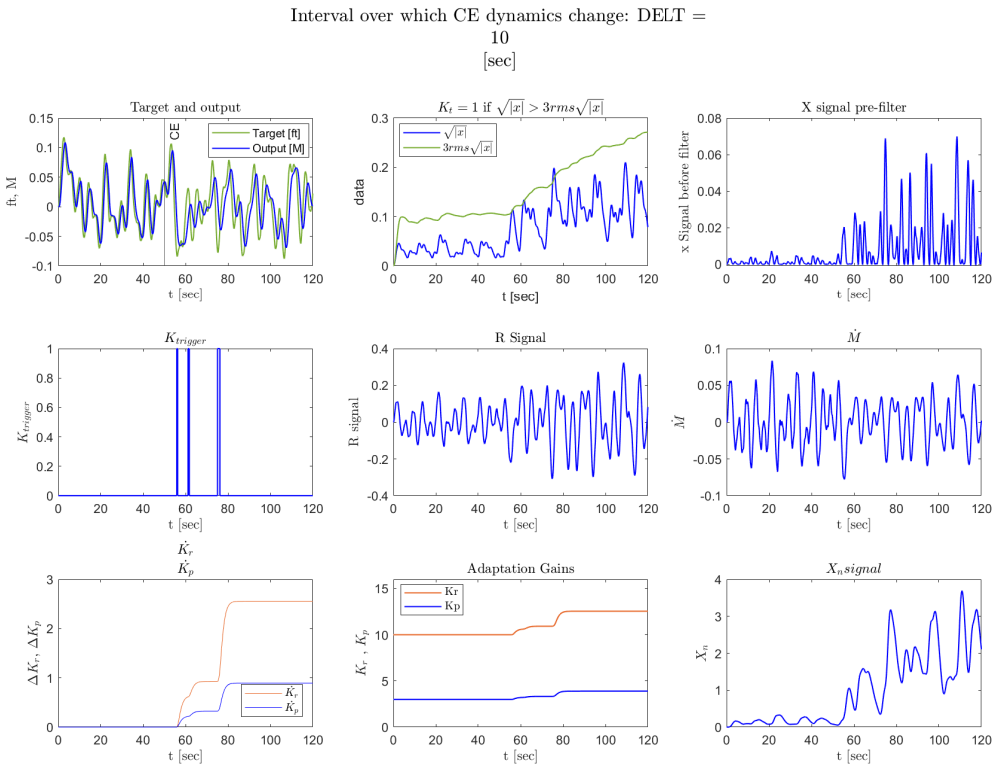

Interval over which CE dynamics change: DELT = 10 [sec]

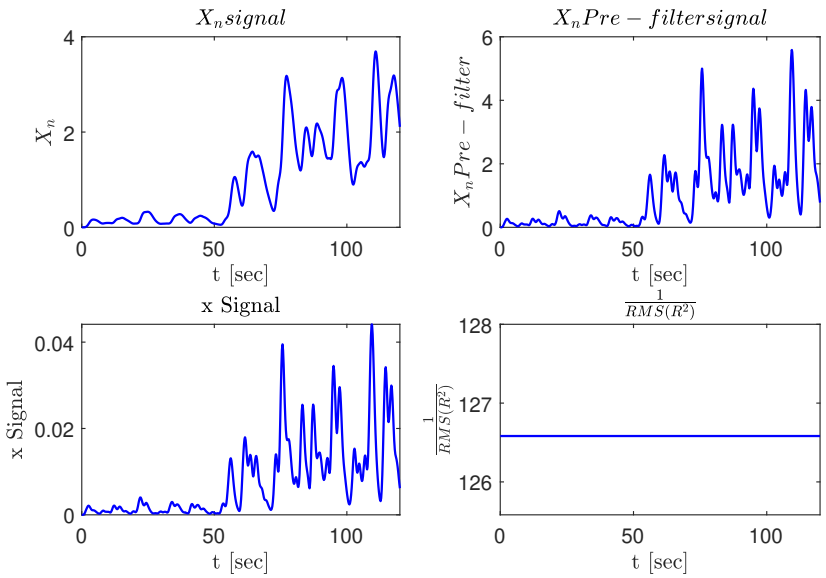

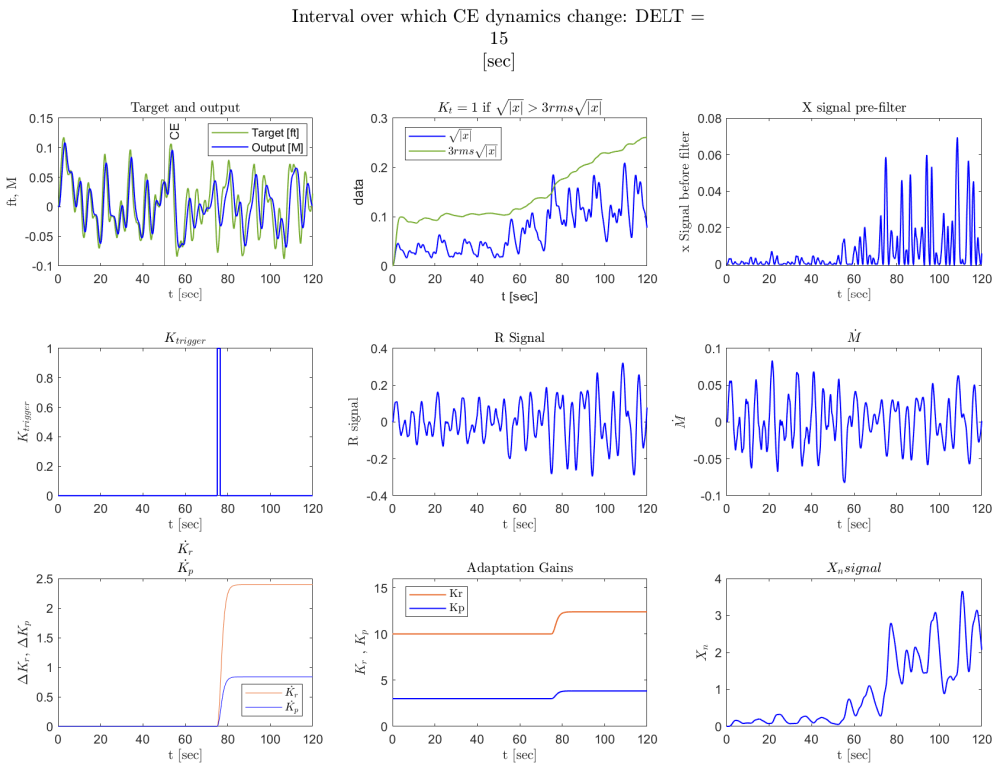
Interval over which CE dynamics change: DELT = 15 [sec]
Target and output
Target [ft]
Output [M]
CE
ft, M
t [sec]
$K_t = 1$ if $\sqrt{|x|} > 3rms\sqrt{|x|}$
$\sqrt{|x|}$
$3rms\sqrt{|x|}$
data
t [sec]
X signal pre-filter
x Signal before filter
t [sec]
$K_{trigger}$
$K_{trigger}$
t [sec]
R Signal
R signal
t [sec]
$\dot{M}$
$\dot{M}$
t [sec]
$\dot{K}_r$
$\dot{K}_p$
$\Delta\dot{K}_r$, $\Delta\dot{K}_p$
t [sec]
Adaptation Gains
Kr
Kp
K_r , K_p
t [sec]
$X_n signal$
X_n
t [sec]

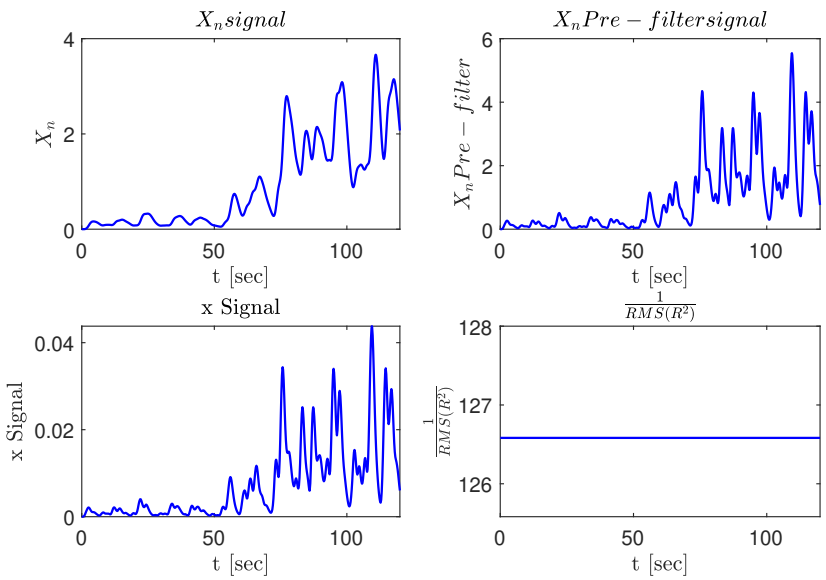
Interval over which CE dynamics change: DELT = 15 [sec]
$X_n signal$
X_n
t [sec]
$X_n Pre - filter signal$
$X_n Pre - filter$
t [sec]
x Signal
x Signal
t [sec]
$\frac{1}{RMS(R^2)}$
$\frac{1}{RMS(R^2)}$
t [sec]

Part III

Scientific Article Appendices

A

Tracking Performance and Control Activity Contour Plots

This appendix presents the results for both conditions DYN 1 and DYN 2, of the K_p and K_r gain combinations with varying time-delay τ_e = [0, 0.1, 0.2, 0.3] s. For both the DYN 1 and DYN 2 conditions, K_p ranged between 0 and 15 with a step size of 0.01, while K_r ranged between 0 and 0.15 with a step size of 0.01.

The figures below show the values of the human operator gains (horizontal and vertical axes), which lead to different values of the root mean square of the error (rms(e)) in figures labelled (a). Figures labelled (b) instead show the root mean square values of the control activity u (rms(u)). Additionally, for combinations of gain values which lead to an unstable open-loop system, no data is shown in the figures.

From these figures, it can be observed that as the time-delay τ_e increases, the optimal gain combinations decrease, as expected. Additionally, for each time-delay constant, when comparing the results for conditions DYN 1 and DYN 2, it can be expected that when the CE dynamics transition for DYN 12, K_p decreases, while K_r slightly increases. Thus, the opposite can be expected for the DYN 21 condition. These results are consistent for all time-delay τ_e cases.

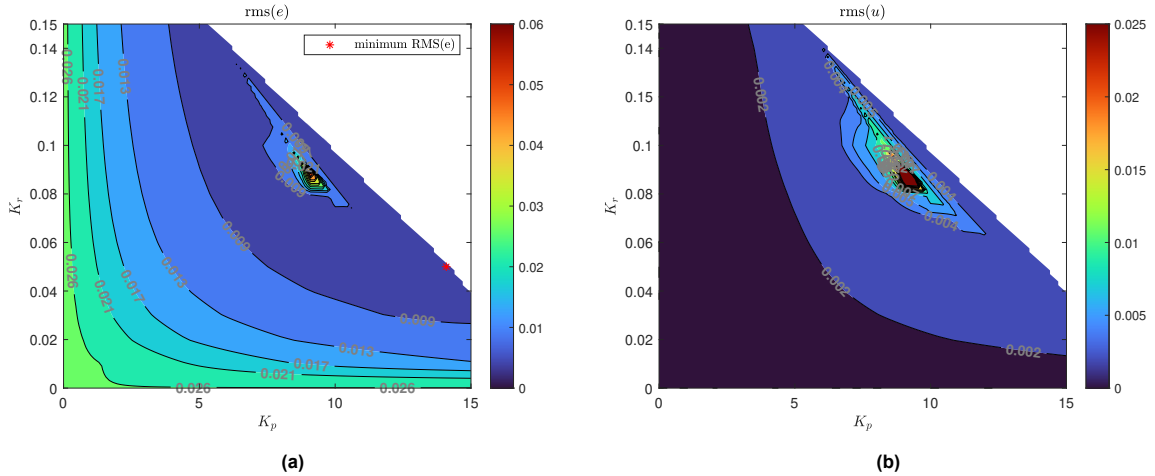

Figure A.1: Contour plots for the DYN 1 condition, τ_e = 0 s, showing how different combinations of K_p and K_r values lead to difference in (a) tracking performance - rms(e), (b) control activity - rms(u) (rms results in radians)

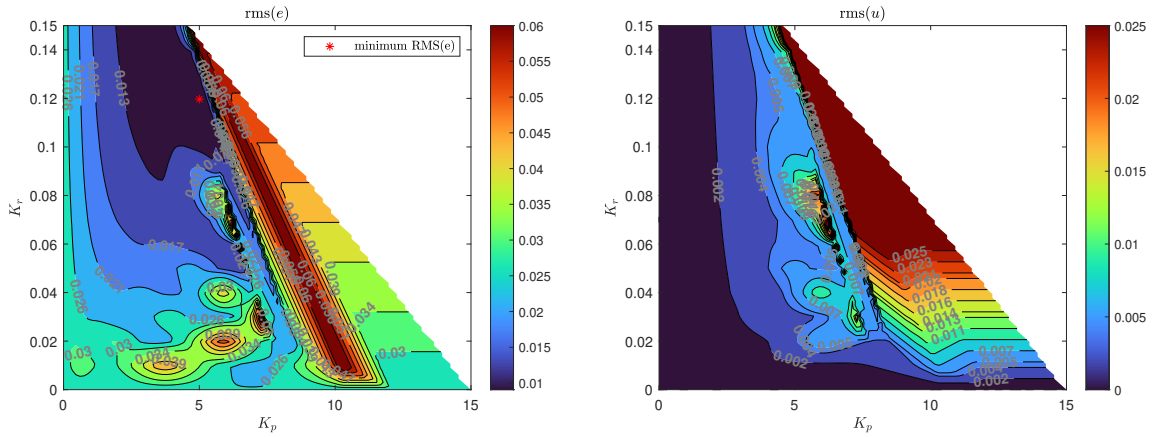

(a) (b)

Figure A.2: Contour plots for the DYN 2 condition, τ_e = 0 s, showing how different combinations of K_p and K_r values lead to difference in (a) tracking performance - rms(e), (b) control activity - rms(u) (rms results in radians)

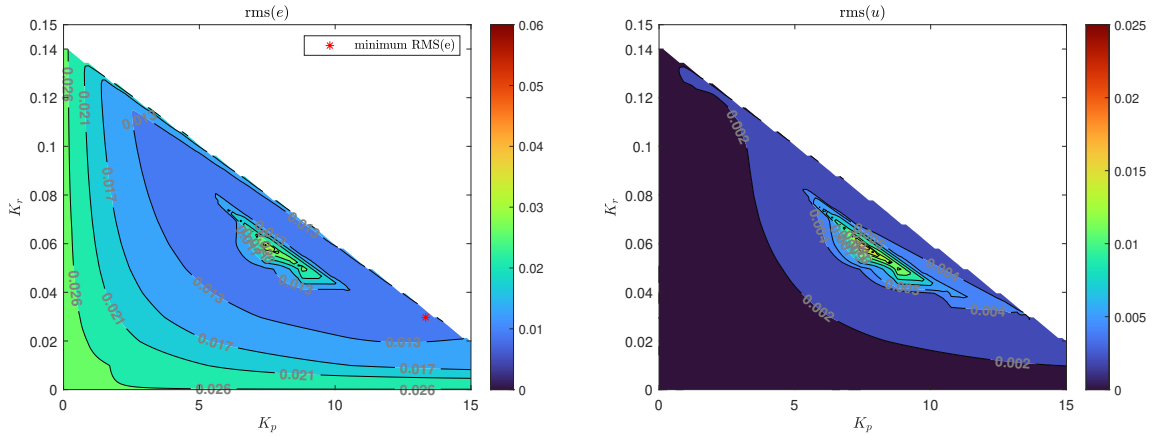

(a) (b)

Figure A.3: Contour plots for the DYN 1 condition, τ_e = 0.1 s, showing how different combinations of K_p and K_r values lead to difference in (a) tracking performance - rms(e), (b) control activity - rms(u) (rms results in radians)

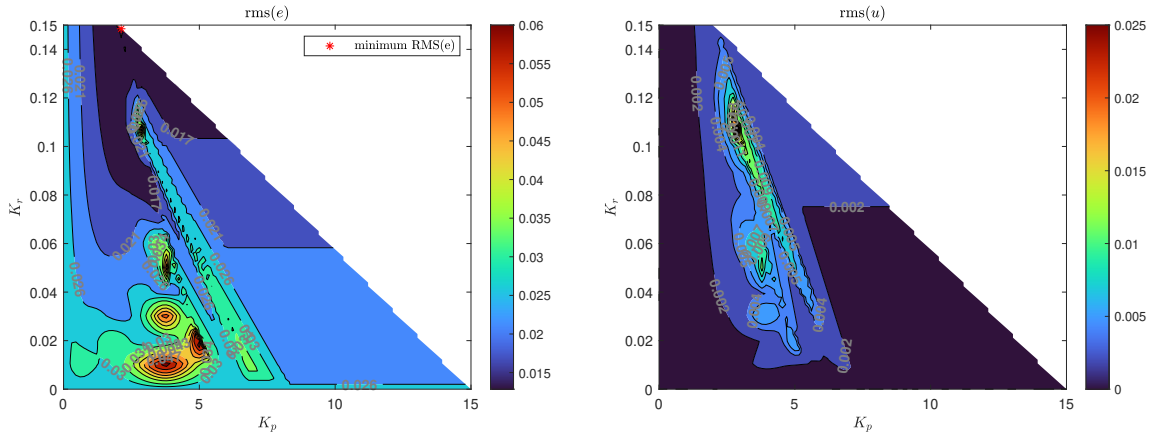

(a) (b)

Figure A.4: Contour plots for the DYN 2 condition, τ_e = 0.1 s, showing how different combinations of K_p and K_r values lead to difference in (a) tracking performance - rms(e), (b) control activity - rms(u) (rms results in radians)

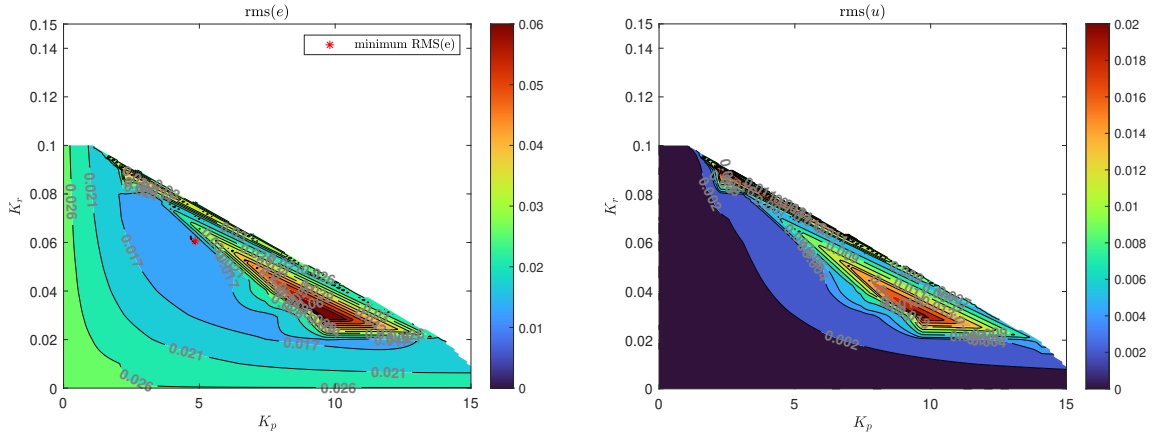

Figure A.5: Contour plots for the DYN 1 condition, τ_e = 0.2 s, showing how different combinations of K_p and K_r values lead to difference in (a) tracking performance - rms(e), (b) control activity - rms(u) (rms results in radians)

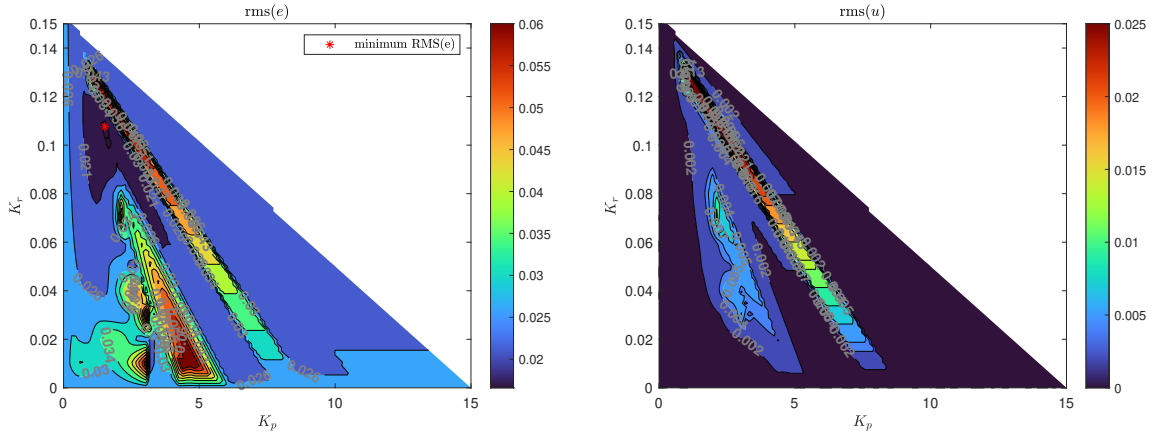

Figure A.6: Contour plots for the DYN 2 condition, τ_e = 0.2 s, showing how different combinations of K_p and K_r values lead to difference in (a) tracking performance - rms(e), (b) control activity - rms(u) (rms results in radians)

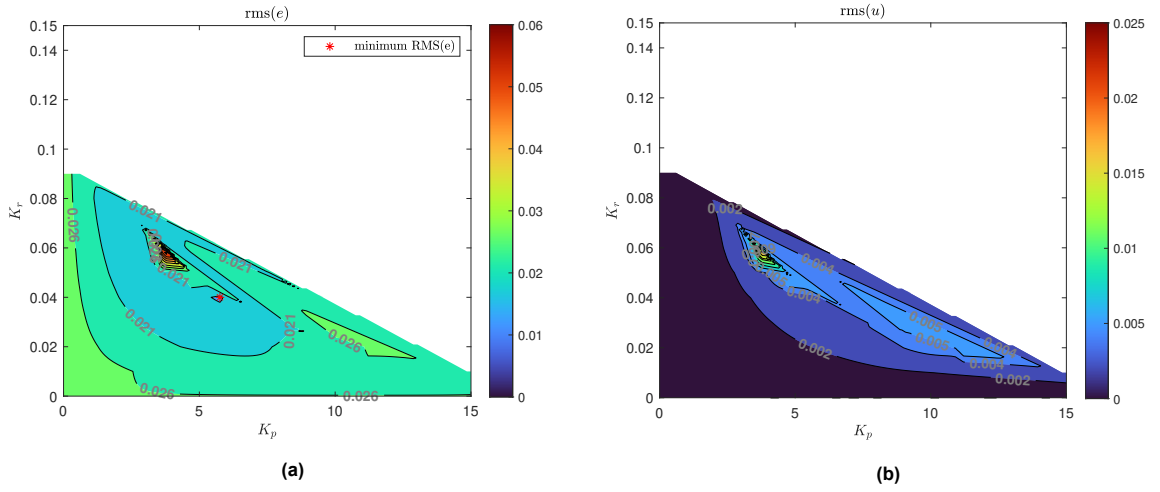

Figure A.7: Contour plots for the DYN 1 condition, τ_e = 0.3 s, showing how different combinations of K_p and K_r values lead to difference in (a) tracking performance - rms(e), (b) control activity - rms(u) (rms results in radians)

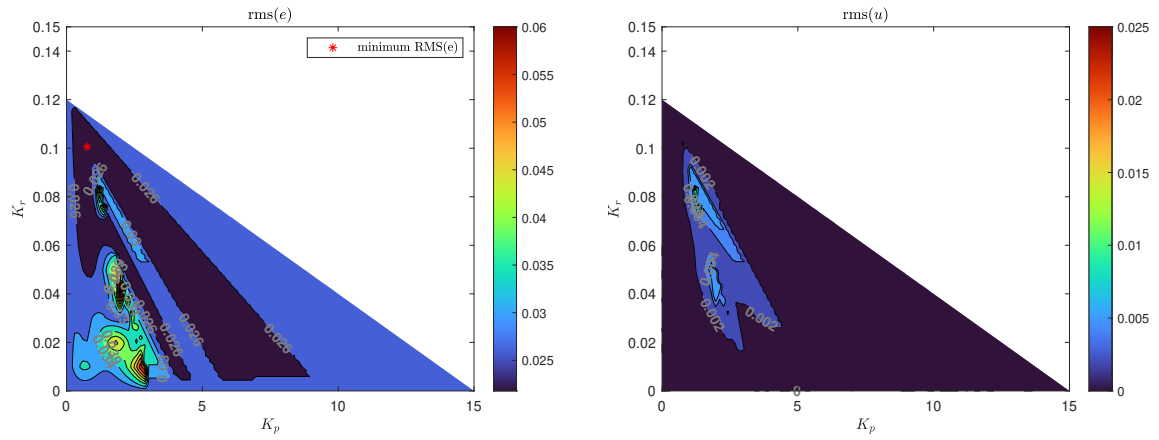

(a) (b)

Figure A.8: Contour plots for the DYN 2 condition, τ_e = 0.3 s, showing how different combinations of K_p and K_r values lead to difference in (a) tracking performance - rms(e), (b) control activity - rms(u) (rms results in radians)

B

Time Traces of Participants for condition DYN 12

This appendix provides the time-traces for all participants for DYN 12 for both the testing and validation data-sets. Additionally, for each participant the time-traces show the results with two settings for the $H(s)$ filter on the x signal. These two settings are: ω_{lp} = 1.5 rad/s and ω_{lp} = 3 rad/s. It can be observed that only for Subject06 the Triggering is activated when ω_{lp} = 1.5 rad/s. However, when the setting is increased, ω_{lp} = 3 rad/s, the Triggering logic is activated for more participants. This is the case for both the testing and validation data-sets.

Testing data-sets results

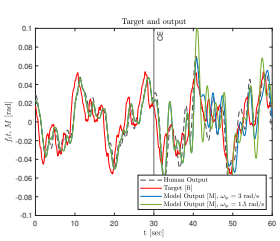

(a) Tracking Performance

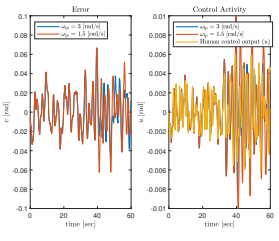

(b) Error e and control activity output u

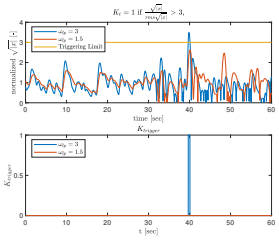

(c) Normalized $\sqrt{|x|}$ and Triggering logic

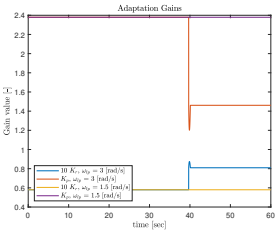

(d) K_p and K_r Human operator adaptive gains

Figure B.1: Results for condition DYN 12 for Subject00

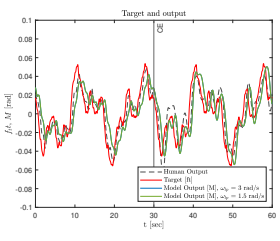

(a) Tracking Performance

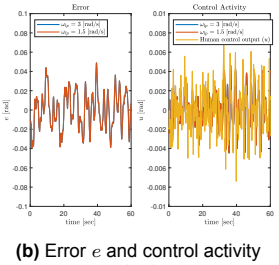

(b) Error e and control activity output u

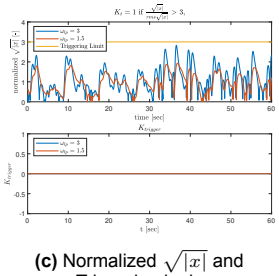

(c) Normalized $\sqrt{|x|}$ and Triggering logic

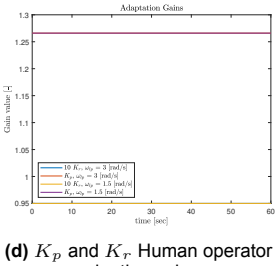

(d) K_p and K_r Human operator adaptive gains

Figure B.2: Results for condition DYN 12 for Subject01

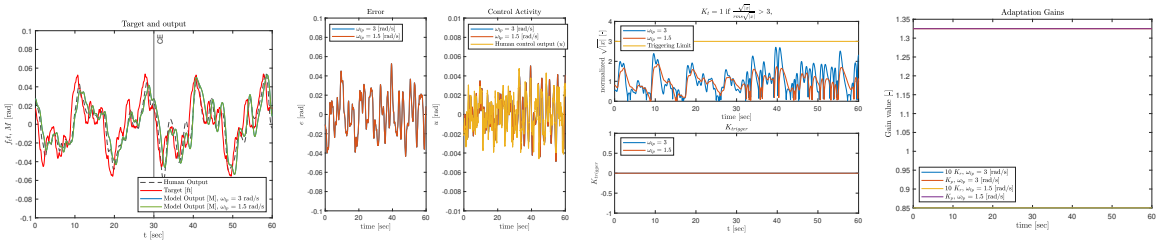

(a) Tracking Performance

(b) Error e and control activity output u

(c) Normalized $\sqrt{|x|}$ and Triggering logic

(d) K_p and K_r Human operator adaptive gains

Figure B.3: Results for condition DYN 12 for Subject03

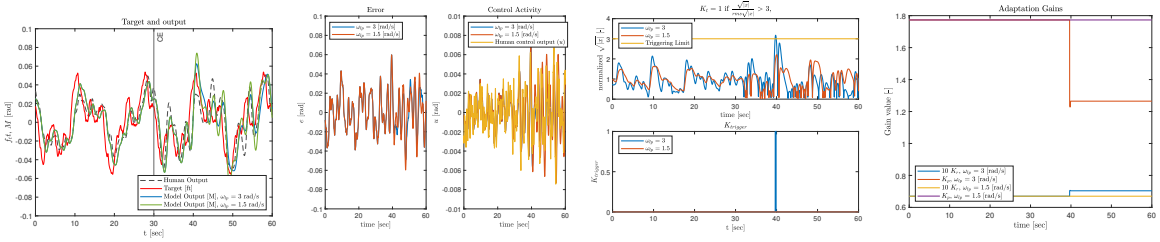

(a) Tracking Performance

(b) Error e and control activity output u

(c) Normalized $\sqrt{|x|}$ and Triggering logic

(d) K_p and K_r Human operator adaptive gains

Figure B.4: Results for condition DYN 12 for Subject04

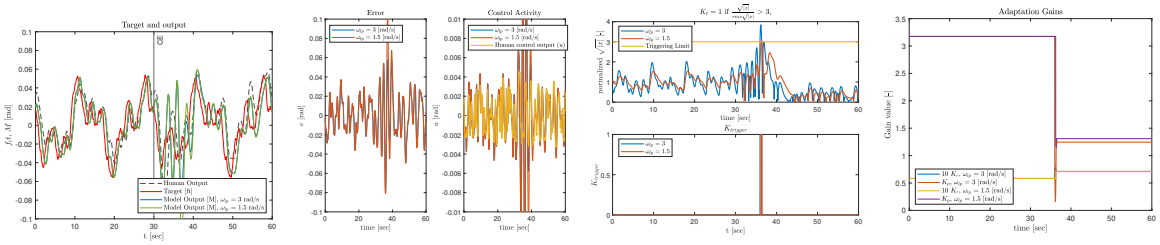

(a) Tracking Performance

(b) Error e and control activity output u

(c) Normalized $\sqrt{|x|}$ and Triggering logic

(d) K_p and K_r Human operator adaptive gains

Figure B.5: Results for condition DYN 12 for Subject06

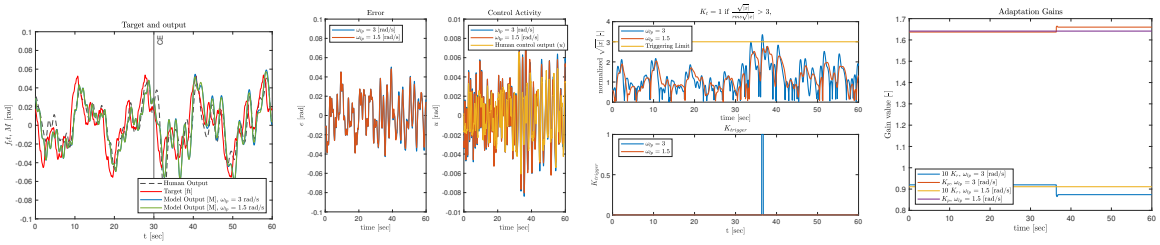

(a) Tracking Performance

(b) Error e and control activity output u

(c) Normalized $\sqrt{|x|}$ and Triggering logic

(d) K_p and K_r Human operator adaptive gains

Figure B.6: Results for condition DYN 12 for Subject08

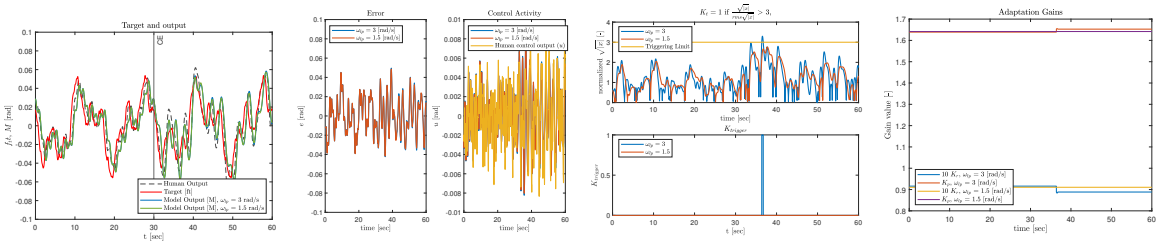

(a) Tracking Performance

(b) Error e and control activity output u

(c) Normalized $\sqrt{|x|}$ and Triggering logic

(d) K_p and K_r Human operator adaptive gains

Figure B.7: Results for condition DYN 12 for Subject09

Validation data-sets results

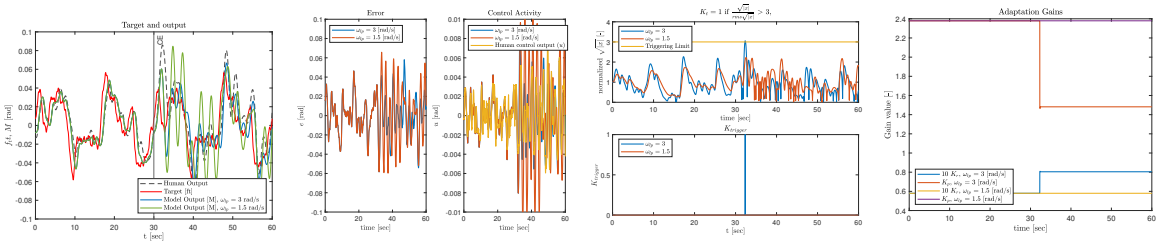

(a) Tracking Performance

(b) Error e and control activity output u

(c) Normalized $\sqrt{|x|}$ and Triggering logic

(d) K_p and K_r Human operator adaptive gains

Figure B.8: Results for condition DYN 12 for Subject00

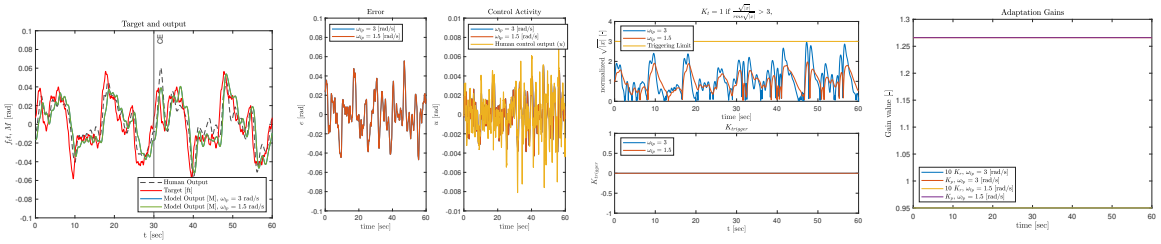

(a) Tracking Performance

(b) Error e and control activity output u

(c) Normalized $\sqrt{|x|}$ and Triggering logic

(d) K_p and K_r Human operator adaptive gains

Figure B.9: Results for condition DYN 12 for Subject01

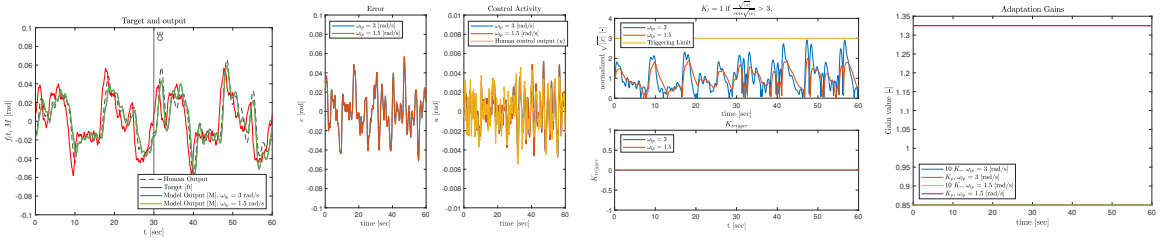

(a) Tracking Performance

(b) Error e and control activity output u

(c) Normalized $\sqrt{|x|}$ and Triggering logic

(d) K_p and K_r Human operator adaptive gains

Figure B.10: Results for condition DYN 12 for Subject03

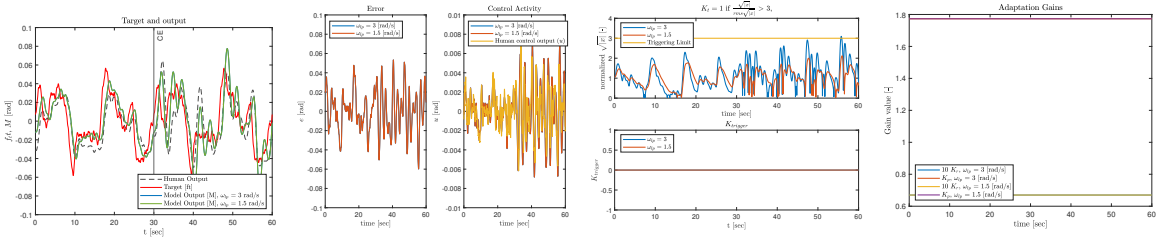

(a) Tracking Performance

(b) Error e and control activity output u

(c) Normalized $\sqrt{|x|}$ and Triggering logic

(d) K_p and K_r Human operator adaptive gains

Figure B.11: Results for condition DYN 12 for Subject04

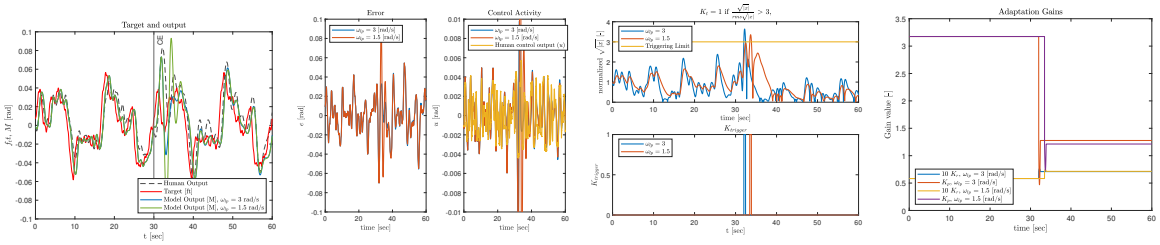

(a) Tracking Performance

(b) Error e and control activity output u

(c) Normalized $\sqrt{|x|}$ and Triggering logic

(d) K_p and K_r Human operator adaptive gains

Figure B.12: Results for condition DYN 12 for Subject06

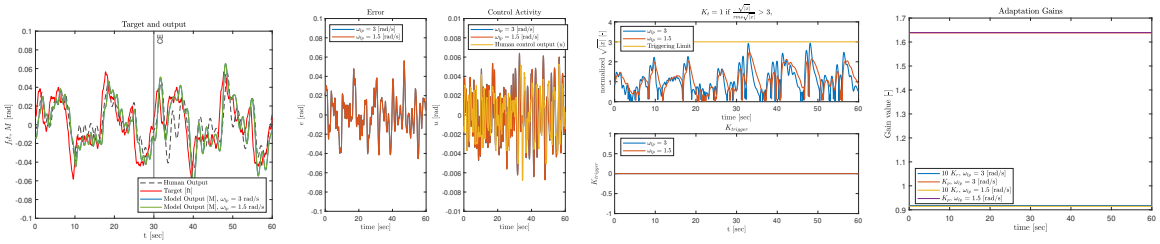

(a) Tracking Performance

(b) Error e and control activity output u

(c) Normalized $\sqrt{|x|}$ and Triggering logic

(d) K_p and K_r Human operator adaptive gains

Figure B.13: Results for condition DYN 12 for Subject08

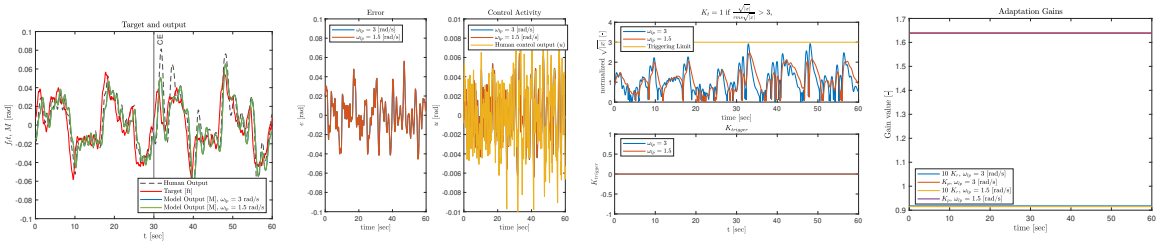

(a) Tracking Performance

(b) Error e and control activity output u

(c) Normalized $\sqrt{|x|}$ and Triggering logic

(d) K_p and K_r Human operator adaptive gains

Figure B.14: Results for condition DYN 12 for Subject09

C

Testing vs Validation Data-sets for condition DYN 12

This appendix presents the results of the Trigger logic activation for both the testing and validation data-sets for Subject04, Subject08, Subject09. In Part I it was shown that while the adaptive logic was triggered for the testing data-sets, when the CE dynamics transitioned at M = 30 s, there was no triggering for the validation data-sets.

A Monte Carlo analysis was conducted to investigate whether the forcing function influences the triggering logic of the model. Additionally, the results show two settings for the $H(s)$ filter on the x signal, which are ω_{lp} = 1.5 rad/s and ω_{lp} = 3 rad/s. From the figures it can be observed that more trigger activations occur when ω_{lp} = 3 rad/s. In fact, for participant S04 no Trigger activations were observed when ω_{lp} = 1.5 rad/s. Therefore, this result is not shown. Additionally, for the testing and validation data-sets of participants S08 and S09 the triggering mechanism was activated for 14 % and 20 % of the total M_1 transitions respectively, when ω_{lp} = 1.5 rad/s. However, when ω_{lp} = 3 the trigger mechanism activations increased to 53 % and 74 % respectively.

Lastly, since S08 and S09 have the same initial human operator gains, the same results can be observed for both participants.

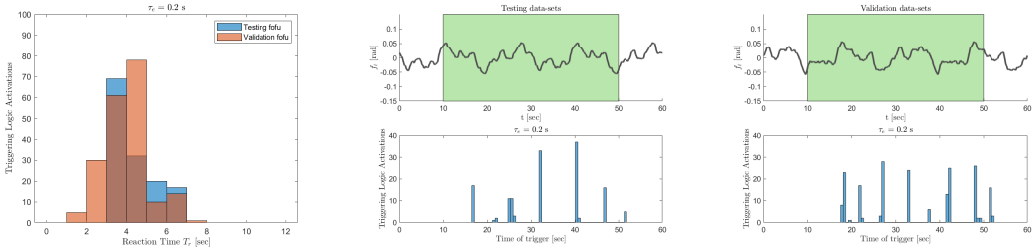

(a) Reaction Time T_r [s] **(b)** Time of trigger for testing data-set **(c)** Time of trigger for validation data-set

Figure C.1: Results for Subject08, ω_{lp} = 1.5 rad/s

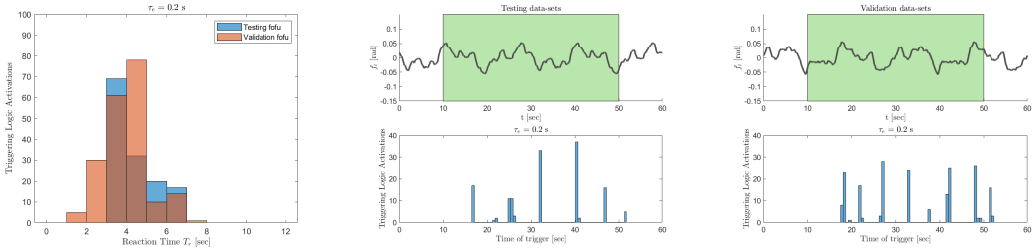

(a) Reaction Time T_r [s] **(b)** Time of trigger for testing data-set **(c)** Time of trigger for validation data-set

Figure C.2: Results for Subject08, ω_{lp} = 1.5 rad/s

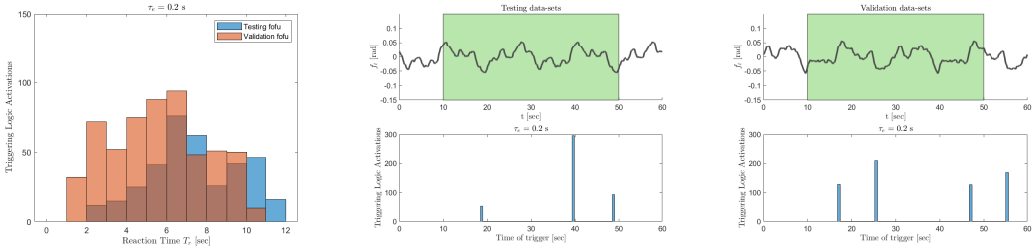

(a) Reaction Time T_r [s] **(b)** Time of trigger for testing data-set **(c)** Time of trigger for validation data-set

Figure C.3: Results for Subject04, ω_{lp} =3 rad/s

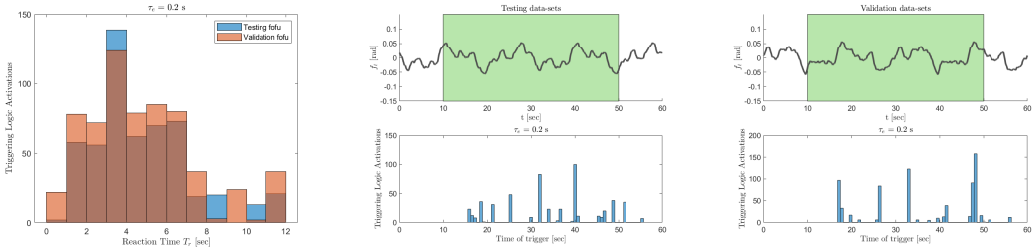

(a) Reaction Time T_r [s] **(b)** Time of trigger for testing data-set **(c)** Time of trigger for validation data-set

Figure C.4: Results for Subject08, ω_{lp} = 3 rad/s

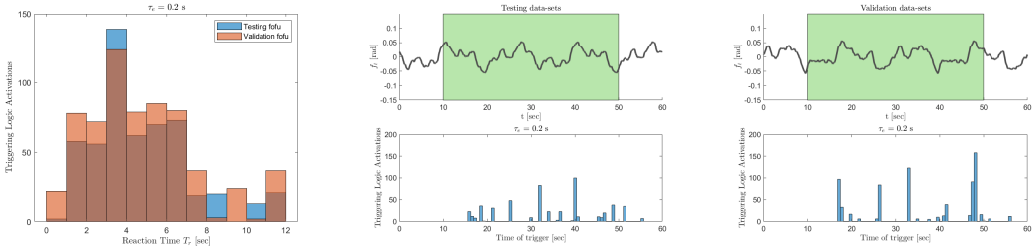

(a) Reaction Time T_r [s] **(b)** Time of trigger for testing data-set **(c)** Time of trigger for validation data-set

Figure C.5: Results for Subject09, ω_{lp} = 3 rad/s

D

Time Traces of Participants for condition DYN 21

This appendix provides the time-traces for all participants for condition DYN 21 for both the testing and validation data-sets. From these figures it can be observed that the Triggering logic is not activated for any of the participants, therefore, the human operator gains remain constant even when the controlled system dynamics transition.

Testing Data-sets results

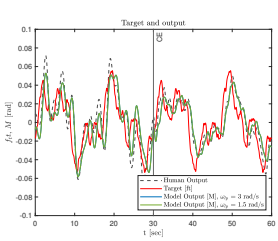

(a) Tracking Performance

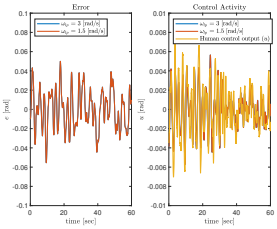

(b) Error e and control activity output u

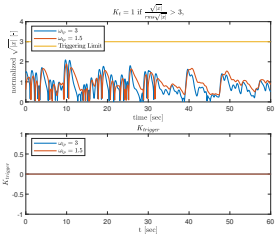

(c) Normalized $\sqrt{|x|}$ and Triggering logic

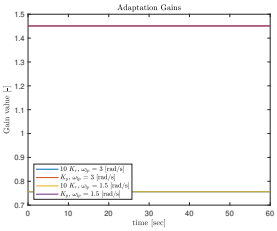

(d) K_p and K_r Human operator adaptive gains

Figure D.1: Results for condition DYN 21 for Subject00

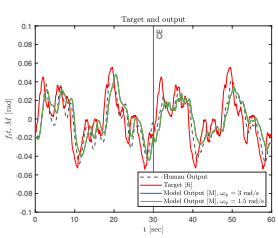

(a) Tracking Performance

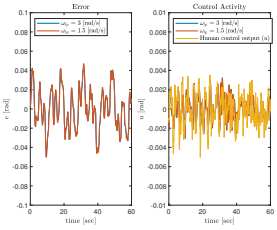

(b) Error e and control activity output u

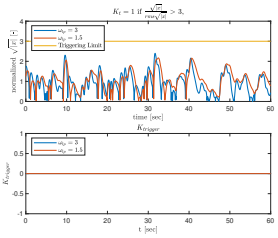

(c) Normalized $\sqrt{|x|}$ and Triggering logic

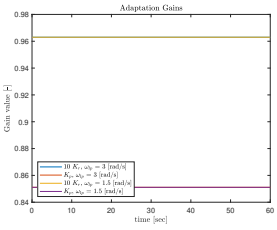

(d) K_p and K_r Human operator adaptive gains

Figure D.2: Results for condition DYN 21 for Subject03

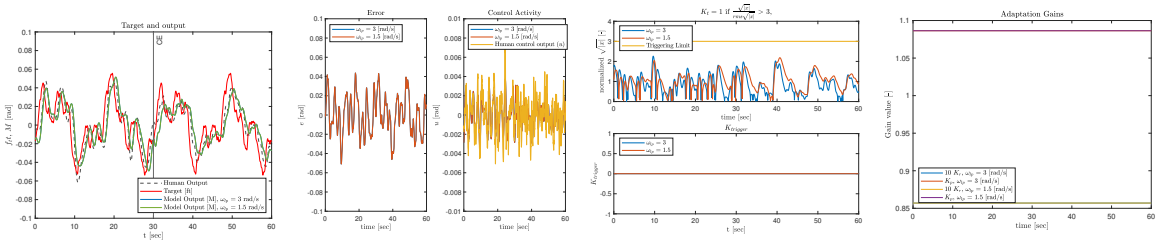

(a) Tracking Performance

(b) Error e and control activity output u

(c) Normalized $\sqrt{|x|}$ and Triggering logic

(d) K_p and K_r Human operator adaptive gains

Figure D.3: Results for condition DYN 21 for Subject04

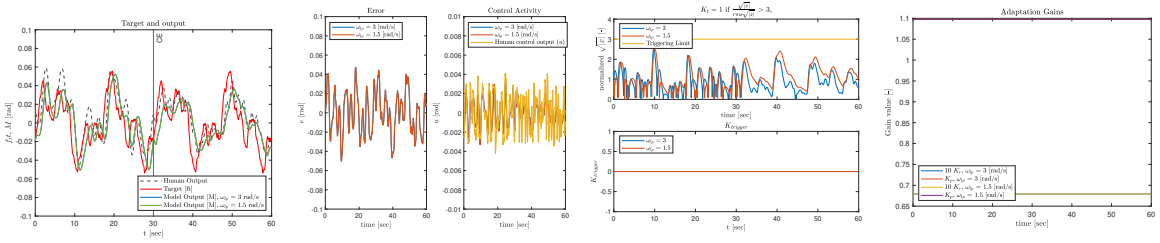

(a) Tracking Performance

(b) Error e and control activity output u

(c) Normalized $\sqrt{|x|}$ and Triggering logic

(d) K_p and K_r Human operator adaptive gains

Figure D.4: Results for condition DYN 21 for Subject06

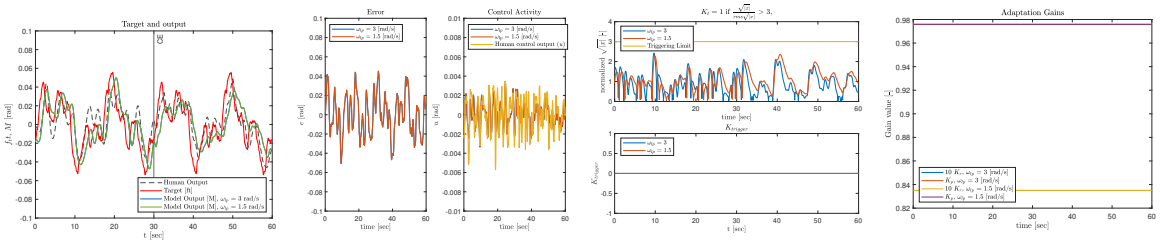

(a) Tracking Performance

(b) Error e and control activity output u

(c) Normalized $\sqrt{|x|}$ and Triggering logic

(d) K_p and K_r Human operator adaptive gains

Figure D.5: Results for condition DYN 21 for Subject08

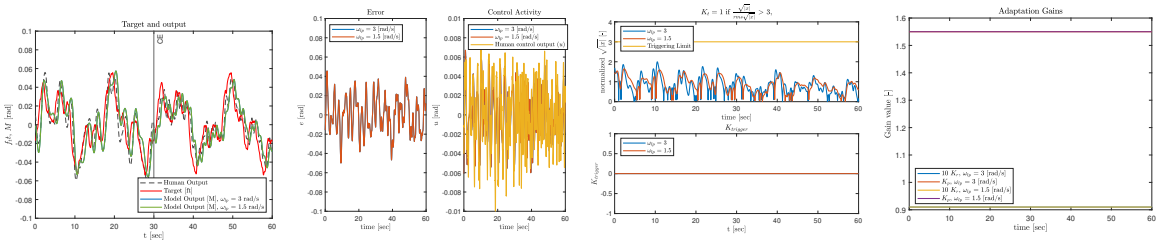

(a) Tracking Performance

(b) Error e and control activity output u

(c) Normalized $\sqrt{|x|}$ and Triggering logic

(d) K_p and K_r Human operator adaptive gains

Figure D.6: Results for condition DYN 21 for Subject09

Validation data-sets results

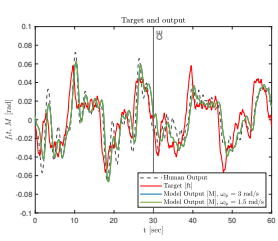

(a) Tracking Performance

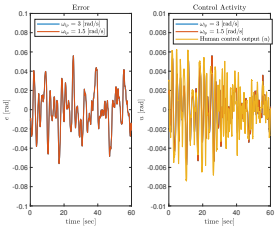

(b) Error e and control activity output u

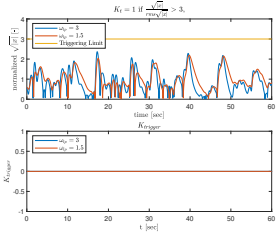

(c) Normalized $\sqrt{|x|}$ and Triggering logic

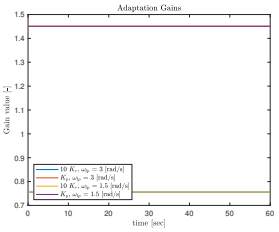

(d) K_p and K_r Human operator adaptive gains

Figure D.7: Results for condition DYN 21 for Subject00

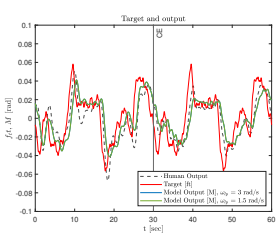

(a) Tracking Performance

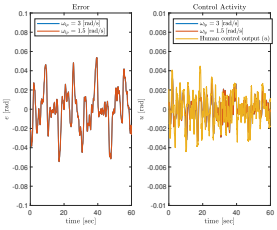

(b) Error e and control activity output u

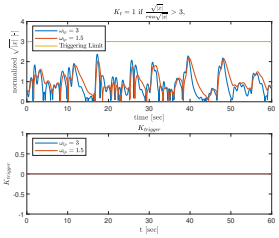

(c) Normalized $\sqrt{|x|}$ and Triggering logic

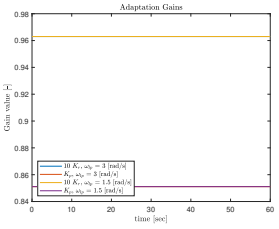

(d) K_p and K_r Human operator adaptive gains

Figure D.8: Results for condition DYN 21 for Subject03

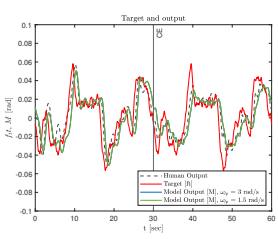

(a) Tracking Performance

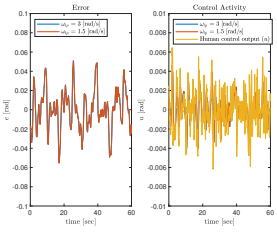

(b) Error e and control activity output u

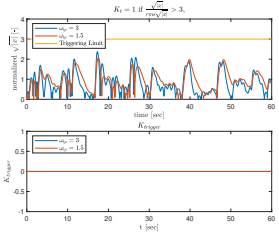

(c) Normalized $\sqrt{|x|}$ and Triggering logic

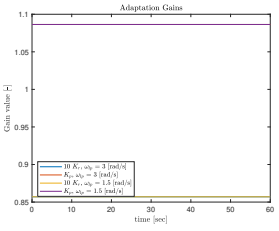

(d) K_p and K_r Human operator adaptive gains

Figure D.9: Results for condition DYN 21 for Subject04

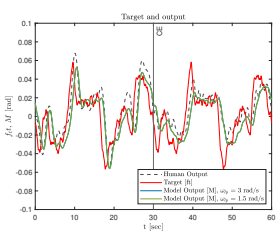

(a) Tracking Performance

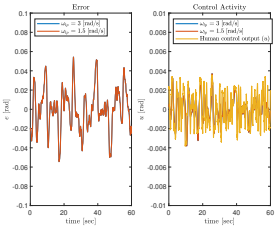

(b) Error e and control activity output u

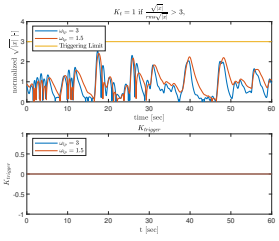

(c) Normalized $\sqrt{|x|}$ and Triggering logic

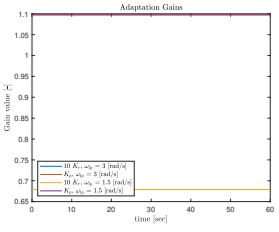

(d) K_p and K_r Human operator adaptive gains

Figure D.10: Results for condition DYN 21 for Subject06

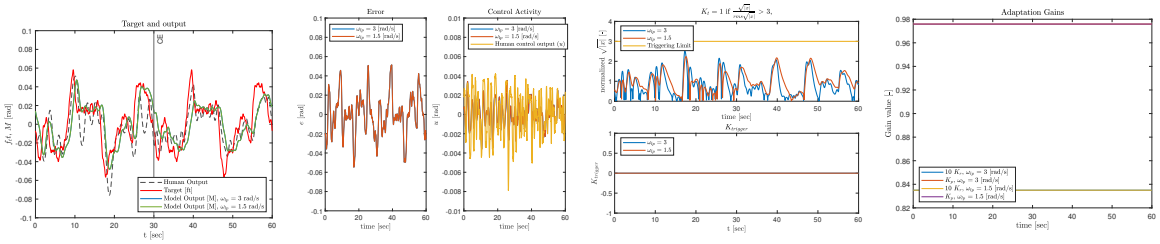

(a) Tracking Performance

(b) Error e and control activity output u

(c) Normalized $\sqrt{|x|}$ and Triggering logic

(d) K_p and K_r Human operator adaptive gains

Figure D.11: Results for condition DYN 21 for Subject08

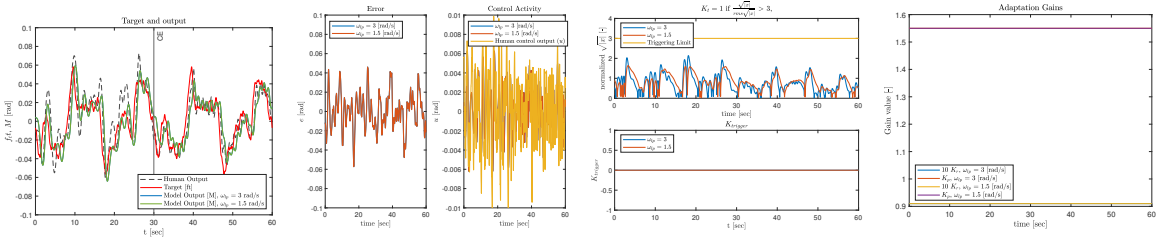

(a) Tracking Performance

(b) Error e and control activity output u

(c) Normalized $\sqrt{|x|}$ and Triggering logic

(d) K_p and K_r Human operator adaptive gains

Figure D.12: Results for condition DYN 21 for Subject09